Integrating the concepts of optimization and reliability in the design of agricultural machines

Abd Al-Kareem Abo Al-Kheer

Année 2010

Ecole doctorale SPMII

Thèse

Présentée à

L'Institut National des Sciences Appliquées de Rouen

Pour obtenir le grade de Docteur de l'Institut National des Sciences Appliquées de Rouen

Spécialités : Génie mécanique

Intégration des concepts d'optimisation et de fiabilité dans la conception des machines agricoles

Par

Abd Al-kareem ABO AL-KHEER

Soutenue le 19 novembre 2010 devant la commission d'examen composée de :

A. CHATEAUNEUF	Rapporteur	Professeur à l'Université Blaise Pascal
F. GUERIN	Rapporteur	Professeur à l'Université d'Angers
G. KHARMANDA	Examinateur	Professeur à l'Université d'Alep
A.M. MOUAZEN	Examinateur	Professeur à l'Université de Cranfield
Y. AOUES	Examinateur	Maître de Conférence à l'INSA de Rouen
M. EID	Examinateur	Professeur à l'INSA de Rouen
A. EL HAMI	Directeur de thèse	Professeur à l'INSA de Rouen

Laboratoire de Mécanique de Rouen (LMR) Institut National des Sciences Appliquées de Rouen
LMR / INSA de Rouen / Technopole du Madrillet, Avenue de l'Université,
76801 Saint Etienne du Rouvray cedex France

Rouen National Institute of Applied Sciences

Mechanical Engineering Laboratory

Doctoral school SPMII

Integrating the concepts of optimization and reliability in the design of agricultural machines

A Thesis submitted for the degree of Doctor in

Mechanical Engineering

By

Abd Al-kareem Abo Al-kheer

November 2010

Abstract

Agricultural machines should be designed to be optimal, reliable and have the capacity to resist failure by fatigue. Although, the deterministic design approach does not guarantee these requirements, it is traditionally applied in the design of agricultural machines. This is due to the difficulties to model the stochastic nature of the forces acting on agricultural machines, especially the forces acting on tillage machines which work in irregular environment and under varying conditions. Therefore, the main objective of this dissertation is to develop a general framework for the design of agricultural machines by integrating the optimization, the reliability and the fatigue tools. We aim to provide an alternative to the traditional deterministic design one. First, this dissertation proposes methods and models for modeling the variability in tillage forces considering both the variability in tillage system parameters and the soil failure. Second, based on the available methods in reliability-based design optimization and fatigue analysis approaches, it proposes methodologies for the design of agricultural machines. Throughout the dissertation, the developed approaches are applied to the design of the shack of a chisel plough.

Keywords: variability; tillage system parameters; soil failure; tillage forces; tillage machines; reliability; optimization; fatigue analysis.

Résumé

Les machines agricoles doivent être conçues pour être optimales, fiables et résistantes à la rupture par fatigue. L'approche déterministe de la conception ne garantit pas ces exigences, elle est néanmoins traditionnellement appliquée pour la conception de machines agricoles. Cela est dû à la difficulté de modéliser la nature stochastique des forces agissant sur les machines agricoles, en particulier les machines de labour, car elles fonctionnent dans un environnement irrégulier et dans des conditions de fonctionnement variables. Le principal objectif de cette thèse est de développer un cadre général pour la conception de machines agricoles, en intégrant les outils d'optimisation, de fiabilité et de fatigue. En cela, nous visons à proposer une alternative à l'approche déterministe. Tout d'abord, cette thèse propose des méthodes et des modèles pour modéliser la variabilité des forces durant le labour en prenant en compte à la fois la variabilité des paramètres du système de labour et de rupture du sol. Deuxièmement, sur la base des méthodes d'optimisation fiabiliste et d'analyse de la fatigue, nous proposons des méthodologies pour la conception de machines agricoles. Tout au long de la thèse, les approches développées sont appliquées à la conception de la dent d'un chisel.

Mots-clés: variabilité; paramètres du système de labour; rupture du sol; forces de labour; machines de labour; fiabilité; optimisation; analyse de la fatigue.

To my family

Acknowledgments

First, I would like to express my sincere gratitude to my advisor, Prof. A. El-hami, for his support and encouragement during my stay at the Rouen Mechanics Laboratory. He gave a lot of freedom in my course and research work, and has been understanding at all times.

I would thank the committee members: Prof. A. Chateauneuf and Prof. F. Guerin. I would like to express my gratitude to Prof. G. Kharmanda, Dr. A. Mouazen, Prof. M. Eid, and Dr. Y. Aoues for helping me in my research activities and for valued contributions at this work. Thanks are due to Dawn Hallidy, from LeHavre university, for proofreading the paper “Probabilistic analysis of soil tillage forces“.

I would like to extend my thanks to the staff of the Rouen Mechanics Laboratory and the mechanical department in the National Institute of Applied Sciences and especially to Dr. F. Barbe, Dr. B. Vieille, Dr. A. Guillet, Dr. L. Khalij and Dr. E. Pagnacco for their constructive comments and assistance. Many thanks go to D. Blanchard and A. Lépine for administrative support.

I wish to acknowledge the financial support from the Aleppo University, which enabled me to carry out the research activities.

I would also like to thank my colleges in the Rouen Mechanics Laboratory; S. Meftah, J. Rojas, S. Lambert, A. Makhloufi, J. Aucher, C. Kpodekon, I. Nistea, N. Benmeziane, A. Tahimi and A. Belattar.

Last but not the least; I thank each member of my family and all my friends for their moral support and unending encouragement.

Publications

The following papers were produced from this work and are incorporated in this Thesis.

A. Abo Al-kheer, M.G. Kharmanda, A. El-Hami. *Probabilistic design of agricultural machines*. International Conference on Non-convex Programming, Rouen, France, 2007.

A. Abo Al-Kheer, M.G. Kharmanda, A. El-Hami. *Probabilistic analysis of soil tillage forces*. 18th Triennial ISTRO Congress, Izmir, Turkey, 2009.

A. Abo Al-Kheer, M.G. Kharmanda, A. El-Hami. *Intégration des incertitudes de propriétés mécaniques du sol pour l'analyse de conception de machines agricoles*. 19ème Congrès Français de Mécanique, Marseille, France, 2009.

A. Abo Al-Kheer, M.G. Kharmanda, A. El-Hami. *Application of reliability methods for the safety assessment of soil tillage machines*. International Congress for Applied Mechanics, Marrakech, Morocco, 2010.

A. Abo Al-Kheer, Y. Aoues, A. El-Hami. *Integrating the reliability constraints into the design optimization of tillage machines*. International symposium on aircraft materials, Marrakech, Morocco, 2010.

A. Abo Al-Kheer, A. El Hami, M. G. Kharmanda, A. M. Mouazen. *Reliability-based design for soil tillage machines.* Journal of Terramechanics, 2011, Issue 1, Vol. 48, pp. 57-64.

A. Abo Al-Kheer, Y. Aoues, A. El-Hami. *Integration of economical requirements into probabilistic approach for the design of agricultural machines.* In "Proceedings of the Tenth International Conference on Computational Structures Technology", Civil-Comp Press, Stirlingshire, UK, Paper 177, 2010. doi:10.4203/ccp.93.177

A. Abo Al-Kheer, Y. Aoues, A. El-Hami, M. Eid. *Reliability-based design optimization of soil tillage machines while considering fatigue life performance*. In "Proceedings of the Tenth International Conference on Computational Structures Technology", Civil-Comp Press, Stirlingshire, UK, Paper 176, 2010. doi:10.4203/ccp.93.176.

A. Abo Al-Kheer, M. G. Kharmanda, A. M. Mouazen, A. El Hami. *Estimating the variability of tillage forces on a chisel plough shank by modeling the variability of tillage system parameters.* Article submitted to the International Journal of Computers and Electronics in Agricultural.

A. Abo Al-Kheer, M. Eid, Y. Aoues, A. El-Hami, A. M. Mouazen. *Modeling the spatial variability in tillage forces for fatigue analysis of tillage machines.* Article submitted to Journal of Terramechanics.

Table of contents

List of figures

List of tables

Extended French summary

Cette partie présente la synthèse des travaux réalisés, qui sont ensuite détaillés en version anglaise.

1 Introduction (Chapitre 1)

Le sol est une structure hétérogène et discontinue. Toutefois, il est considéré comme le facteur prépondérant pour la conception des machines agricoles. Les verrous de la conception des machines agricoles sont liés à la détermination du comportement du sol sous les chargements mécaniques et le calcul des forces agissant sur les outils de labour. Pour cela, cette conception est généralement basée sur des règles issues des observations expérimentales.

Toutefois, au cours des six dernières décennies, des recherches ont déterminé les formes de la rupture du sol sous différentes conditions de fonctionnement et ils ont proposé des modèles pour estimer les forces agissant sur les outils de labour. Le premier modèle a été proposé par Reece en 1965 basé sur les travaux de Terzaghi. Aujourd'hui des efforts considérables ont été accomplis dans ce domaine, toutefois, il n'existe pas de modèle général permettant de prévoir l'interaction entre le sol et l'outil de labour.

La démarche déterministe de la conception des machines agricoles est basée sur la mesure des forces agissant sur les machines dans différentes conditions de fonctionnement afin de déterminer leurs valeurs nominales. Ensuite, des facteurs de sécurité empiriques sont appliqués afin d'assurer une marge de sécurité entre les contraintes appliquées et la résistance limite du matériau.

La démarche déterministe de la conception basée sur les coefficients de sécurité ne garantit pas une conception fiable. Puisque, la forte variabilité des propriétés mécanique du sol et des conditions de fonctionnement des machines agricoles peut conduire à des écarts imprévisibles des performances réelles et espérées. Par conséquent, la conception de ces structures doit être placée dans un contexte aléatoire.

La démarche rationnelle de la conception des machines agricoles consiste à considérer la propagation des incertitudes dans l'analyse en s'appuyant sur une modélisation probabiliste des propriétés mécaniques du sol, les paramètres de conception des outils de labour et les conditions de fonctionnement. La théorie des probabilités offre

un cadre global pour la considération des incertitudes et des variabilités des données dans la modélisation mécanique.

L'optimisation de la conception basée sur les critères de fiabilité propose de tenir compte des incertitudes dans la recherche de la conception optimale des structures. Cette approche datant du début des années 70 vise à trouver le meilleur compromis entre les coûts de la conception et la fiabilité d'un dimensionnement. Aujourd'hui, une variété d'approches d'optimisation fiabiliste sont développées afin de relever le défi de la conception des structures complexes. En outre, ces méthodes ont été appliquées dans plusieurs domaines industriels, par exemple l'automobile, les systèmes micro-électro-mécaniques, l'aéronautique, et le formage des matériaux.

Ces développements (fiabilité des structures, optimisation fiabiliste, analyse de fatigue) n'ont pas été appliqués à la conception des machines agricoles. Cela est principalement dû aux difficultés liées à la modélisation de la variabilité des forces agissant sur les outils de labour. Par conséquent, l'objectif principal de ce travail de thèse est de proposer une approche destinée à la modélisation de la variabilité des forces agissant sur l'outil de labour. Ensuite, d'utiliser l'approche de l'optimisation fiabiliste pour la recherche de la conception optimale des machines agricoles. Finalement, une approche de modélisation de la variabilité spatiale des forces de labour est proposée pour l'analyse de fatigue des machines agricoles.

2 Objectifs du travail (Chapitre 1)

Cette thèse propose des méthodologies pour l'intégration des approches de la fiabilité des structures, de l'optimisation fiabiliste et de l'analyse de fatigue dans la conception des machines agricoles. L'objectif principal est de développer un cadre probabiliste pour la conception des machines agricoles en considérant la variabilité des forces de labour. Ainsi, l'approche probabiliste développée peut être considérée par les concepteurs comme une alternative à l'approche déterministe. Les objectifs de ce travail sont les suivants:

1- Proposer une approche probabiliste pour la modélisation de la variabilité des forces de labour résultant de la variabilité des paramètres du système de labour (les propriétés mécaniques du sol, les paramètres de conception de l'outil de labour et les conditions de fonctionnement).
2- Développer une méthodologie d'optimisation fiabiliste pour les machines de labour.

3- Développer un nouveau modèle pour décrire la variabilité spatiale des forces totales de labour.
4- Analyse du comportement en fatigue des machines de labour afin de calcul la durée de vie en tenant en compte de la variabilité spatiale des forces de labour.

3 Synthèse du travail de thèse réalisé (Chapitre 1)

La variabilité des forces de labour peut résulter de deux sources distinctes: d'une part la variabilité des paramètres du système de labour qui ont des effets globaux, d'autre part, la variabilité des formes de la rupture du sol qui ont des effets locaux. Par conséquent, nous appelons les forces de labour liées aux paramètres du système de labour par les forces globales de labour et celles liées à la rupture du sol par les forces locales de labour.

La variabilité des paramètres du système de labour résulte de la variabilité des propriétés mécaniques du sol, de la variabilité des paramètres de conception de l'outil de labour et de la variabilité des conditions de fonctionnement. La variabilité des propriétés mécaniques du sol reflète l'hétérogénéité et la discontinuité du sol. La variabilité des paramètres de conception de l'outil de labour est due aux processus de fabrication. Par contre, la variabilité des conditions de fonctionnement est due au fait que ces paramètres ne sont pas complètement contrôlée pendant l'opération de labour.

L'organigramme de ce travail est présenté en Figure 1. Premièrement, la variabilité des forces globales de labour résultant de la variabilité des paramètres du système de labour est modélisée et intégrée dans l'optimisation fiabiliste afin d'avoir des machines optimales et fiables. Deuxièmement, la variabilité de la rupture du sol est ajoutée à la variabilité des paramètres du système de labour et la variabilité des forces totales de labour est prise en compte dans l'analyse de fatigue pour estimer la durée de vie des machines de labour.

La variabilité des forces locales de labour est négligée lors de l'analyse d'optimisation fiabiliste, pour plusieurs raisons. D'une part, elle n'a aucun effet significatif sur la variabilité des forces totales de labour, et d'autre part, pour des raisons de simplicité et de réduction du temps de calcul. Par contre, la variabilité des forces locales de labour est prise en compte dans l'analyse de fatigue car celle-ci a un caractère cyclique qui affecte de manière significative la durée de vie des machines de labour.

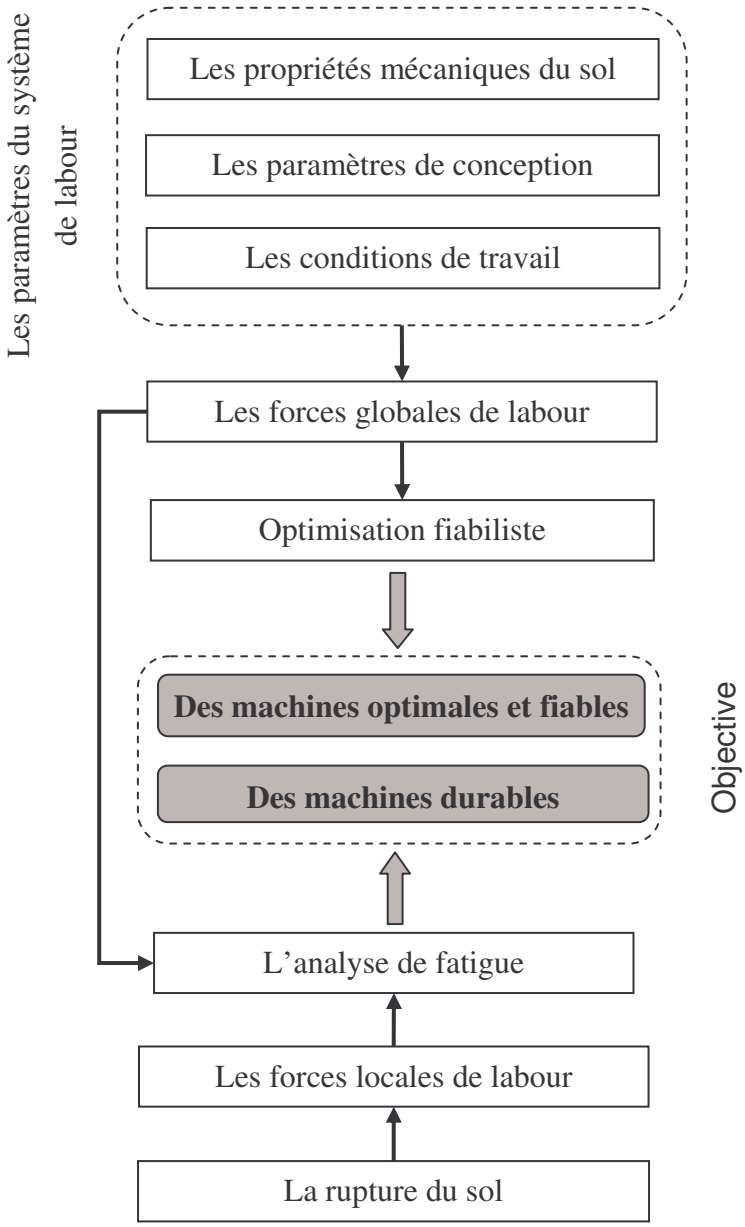

Figure 1 : Organigramme du plan du travail

4 Modélisation de la variabilité des forces de labour (Chapitre 2)

Ce chapitre propose une approche probabiliste pour la modélisation de la variabilité des forces de labour résultant de la variabilité des paramètres du système de labour. Cette approche est composée de quatre étapes, telles qu'illustrées en Figure 2. La première étape vise à estimer les forces de labour en utilisant le model de McKyes et Ali et de déterminer les principaux paramètres du système de labour (propriétés mécaniques du sol, les paramètres de conception d'outil de labour et les conditions de fonctionnement), qui affectent les forces de labour.

La deuxième étape vise à modéliser la variabilité des propriétés mécaniques du sol en utilisant des techniques graphiques et quantitatives et de proposer des hypothèses pour modéliser la variabilité des paramètres de conception de l'outil de labour et des conditions de fonctionnement.

La troisième étape vise à déterminer les effets de dispersion des paramètres du système de labour sur les forces de labour. A ce stade, nous allons négliger la variabilité des paramètres du système de labour qui n'a aucun effet significatif sur les forces de labour afin de simplifier la modélisation et de réduire le temps de calcul.

La dernière étape consiste à estimer la variabilité des forces de labour en prenant en compte la variabilité des paramètres du système de labour. La méthodologie proposée s'appuie sur la technique de MCS (les simulations de Monte Carlo).

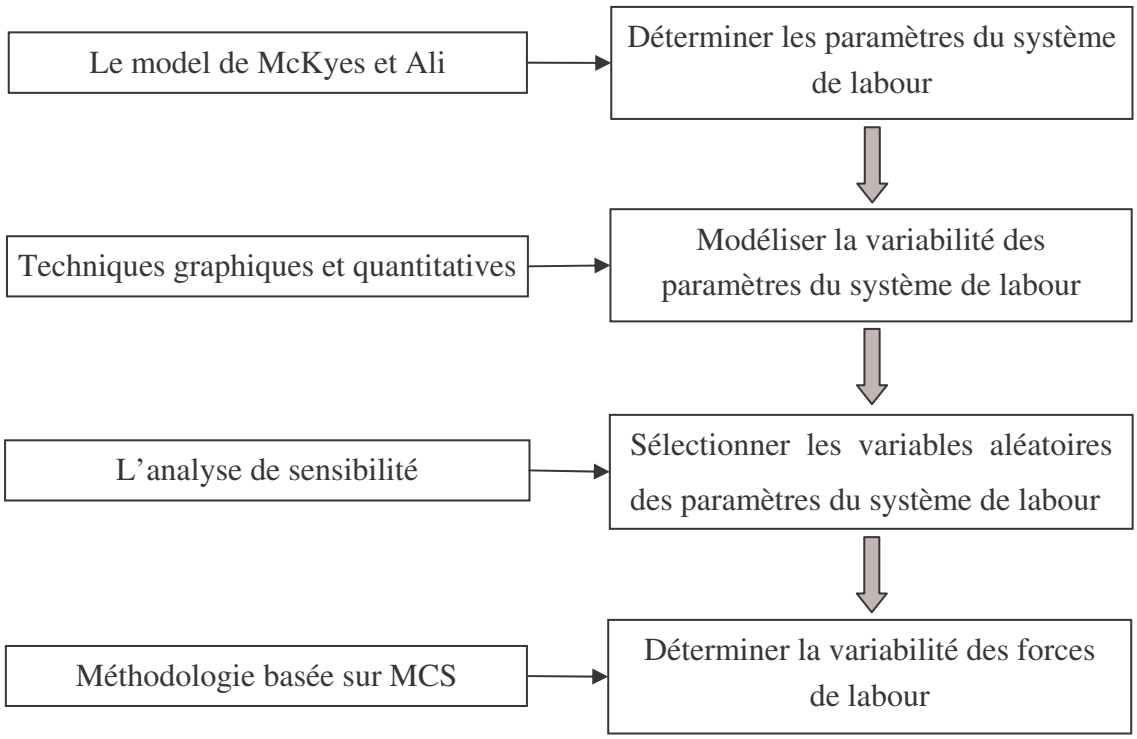

Figure 2 : Organigramme de la modélisation de la variabilité des forces de labour

Cette approche est appliquée à la modélisation de la variabilité des forces horizontale et verticale de labour pour la dent d'un chisel (Figures 3 et 4). Nous avons utilisé 57 échantillons pour modéliser la variabilité des propriétés mécaniques du sol. En plus, Nous avons utilisé les lois normale et uniforme pour représenter la variabilité des paramètres de conception et des conditions de fonctionnement. Les histogrammes et les fonctions de

densité de probabilité des forces horizontale et verticale sont présentés en Figure 5. Les résultats obtenus montrent que les deux forces suivent la loi log-normal et leur caractéristiques probabilistes sont $\mu = 0.872, \xi = 0.449$ et $\mu = 0.004, \xi = 0.447$ respectivement. Le coefficient de corrélation entre les forces horizontale et verticale est de $\rho(P_H, P_V) = 0.93$. Ces résultats montrent que les dispersions des forces de labour sont importantes et nous devons les prendre en compte dans l'analyse de fiabilité.

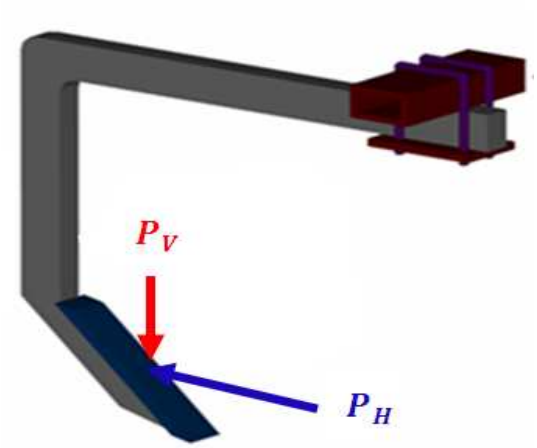

Figure 3 : Illustration de la dent d'un chisel avec les forces de labour

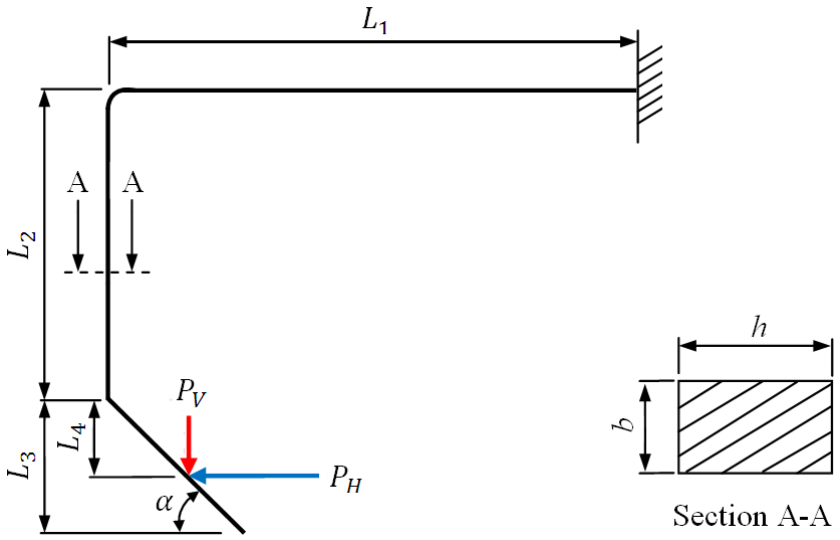

Figure 4 : Illustration schématique de la dent avec les forces horizontale et verticale

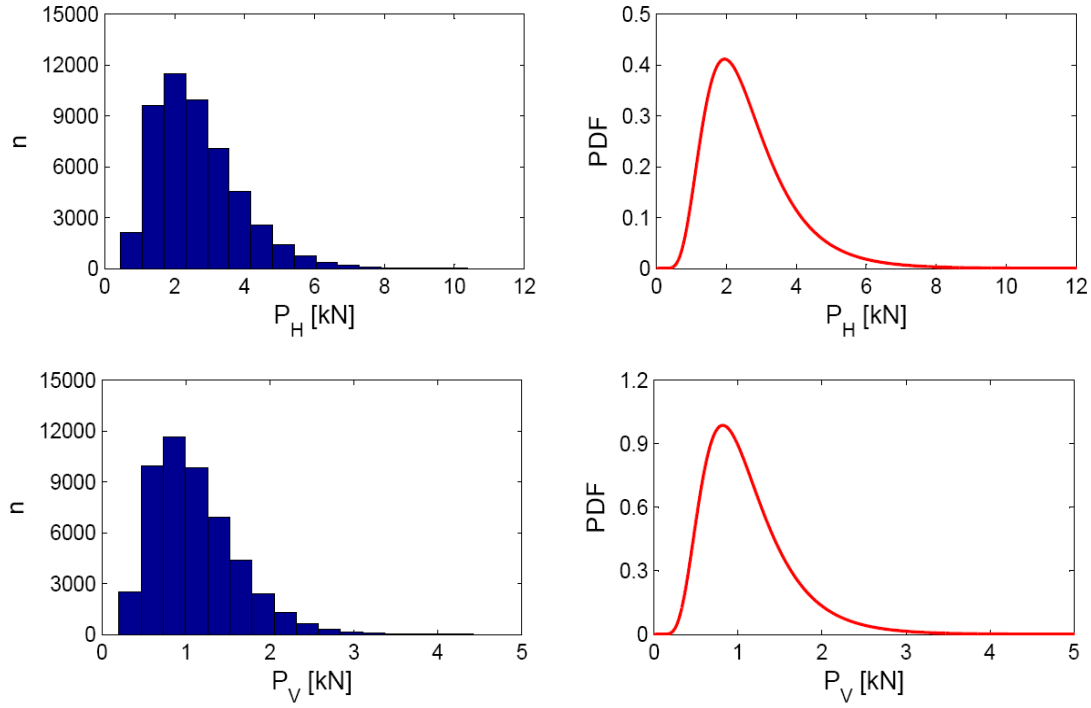

Figure 5 : Les histogrammes et les fonctions de densité de probabilité des forces horizontales et verticales

5 Optimisation fiabiliste des machines de labour (Chapitre 3)

L'approche proposée pour la conception des machines de labour s'appuie sur les outils de conception probabiliste et les méthodes d'optimisation fiabiliste. Cette approche se compose de quatre étapes principales, comme illustré en Figure 6.

La première étape de cette approche consiste à déterminer les fonctions d'état limite selon les scénarios de défaillance. Pour les machines de labour, deux fonctions d'état limite peuvent être considérées. La première fonction d'état limite est liée à la résistance mécanique des machines et la seconde fonction d'état limite à la qualité de l'opération de labour.

Les fonctions d'état limite déterminées dans la première étape sont fonctions des variables d'entrée. Ces variables n'ont pas la même variabilité et la même influence sur la probabilité de défaillance. Par conséquent, l'analyse des sensibilités est appliquée pour déterminer les vecteurs de variables déterministes et aléatoires.

La troisième étape consiste à utiliser la technique de MCS et la méthode FORM pour calculer la probabilité de défaillance selon les fonctions d'état limite déterminées dans la première étape. La technique de MCS est utilisée directement pour estimer la probabilité

de défaillance, lorsque les deux fonctions d'état limite sont impliquées dans l'analyse de fiabilité. Lorsque la méthode FORM est utilisée, un indice de fiabilité est calculé pour chaque fonction d'état limite. En suite, la défaillance du système est estimée par la méthode de Ditlevsen.

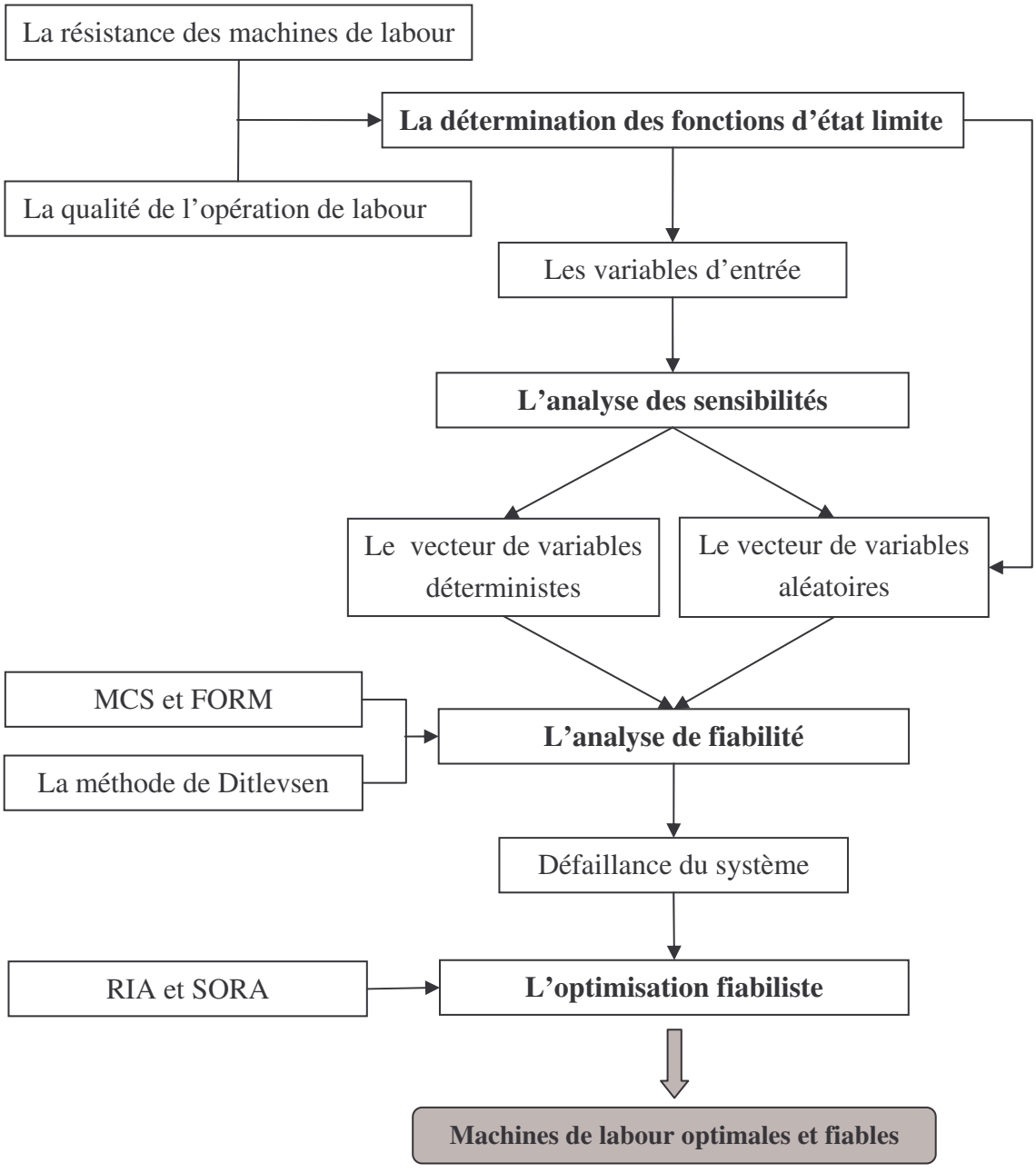

Figure 6 : Organigramme de la l'approche proposée pour la RBDO des machines de labour

La quatrième étape a pour objectif de rechercher la conception optimale et fiable des machines de labour. Deux approches de l'optimisation fiabiliste sont utilisées, d'une part, l'approche classique de l'optimisation fiabiliste souvent appelée RIA (Reliability index approach), et d'autre part, la méthode SORA (Sequential optimization and reliability assessment). La comparaison des deux méthodes est réalisée à travers les solutions optimales obtenues est les performances numériques des deux approches.

Les résultats de l'analyse de fiabilité montrent que la méthode FORM peut être utilisée pour calculer la probabilité de défaillance en considérant seulement la première fonction d'état limite et la présence de la corrélation entre les forces de labour. Cette simplification conduit à une estimation moins couteuse en temps de calcul de la probabilité de défaillance. De plus, cette simplification n'altère pas la précision des résultats.

Les méthodes RIA et SORA sont appliquées pour déterminer le volume minimum de la dent d'un chisel tout en vérifiant un indice de fiabilité cible de $\beta^T = 3$. La méthode RIA a convergé au volume minimal de $f^* = 1.95 \times 10^6\ mm^3$ correspondant à la conception optimale de $\{\mathbf{d}\}^* = [25.96\ mm, 64.90\ mm]$. Par contre, la méthode SORA a convergé au volume minimal de $f^* = 1.96 \times 10^6\ mm^3$ correspondant à la conception optimale de$\{\mathbf{d}\}^* = [26.02\ mm, 65.05\ mm]$, Figure 7.

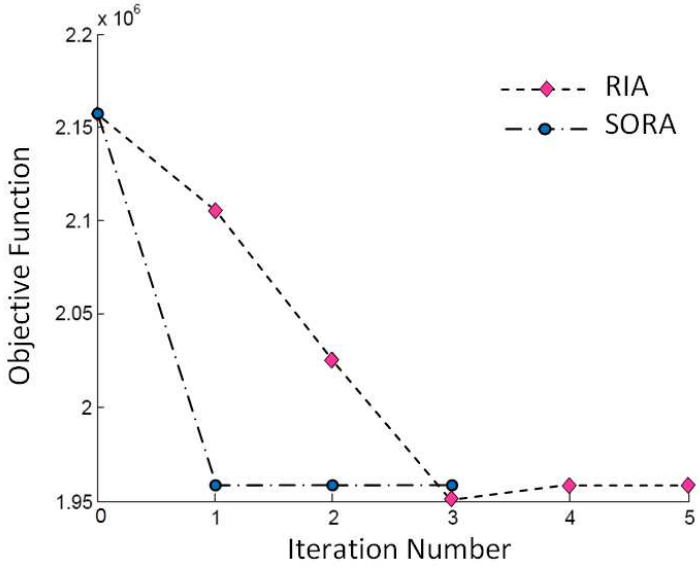

Figure 7 : L'historique de la fonction objective

Les solutions optimales obtenues par les deux méthodes sont pratiquement identiques. Cependant, la méthode RIA nécessite 1100 évaluations du modèle d'éléments finis. En revanche, la méthode SORA exige 397 évaluations seulement. D'un point de vue

numérique, la méthode SORA est plus efficace que la méthode RIA. Par conséquent, la méthode SORA peut être adoptée pour résoudre le problème de la RBDO des machines de labour.

La méthode SORA est utilisée pour la recherche du niveau optimum de fiabilité cible permettant de minimiser le coût total composé du coût initial (coût de construction) et du coût de défaillance. La Figure 8 montre que le niveau optimum de fiabilité cible de $\beta_{Opt} = 3.105$ permet de vérifier l'équilibre entre le coût initial et le coût de défaillance. En effet, ce niveau optimum de fiabilité correspondant à un indice optimal de fiabilité cible est différent de l'indice cible utilisé au début de ce travail. En d'autres termes, la recherche de l'indice de fiabilité optimal cible doit être intégrer dans une procédure de la RBDO afin de vérifier le meilleur compromis entre le coût total et le niveau de fiabilité souhaitée.

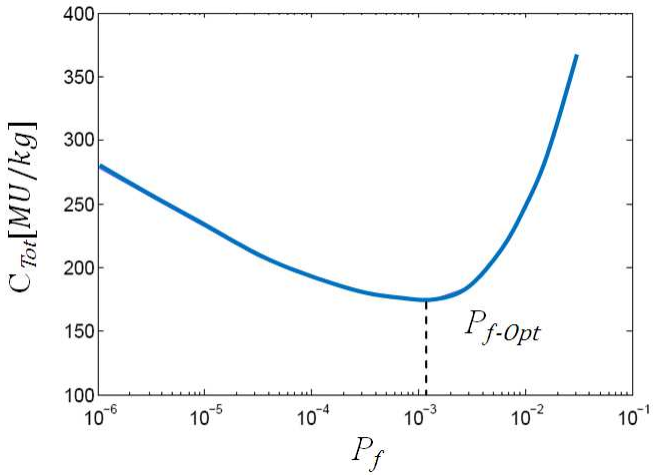

Figure 8 : La relation entre le coût total et le niveau de fiabilité

6 Modélisation de la variabilité spatiale des forces de labour (Chapitre 4)

Ce chapitre vise à proposer un nouveau modèle pour la modélisation de la variabilité spatiale des forces de labour, en tenant compte de la variabilité des forces de labour résultant de la variabilité des paramètres du système de labour (la variabilité des forces globales de labour) et de la variabilité des forme de défaillance du sol (la variabilité des forces locales de labour).

Le modèle proposé repose sur deux hypothèses fondamentales, qui sont les suivantes: 1) la variabilité spatiale des forces globales est aléatoire, reflétant la variabilité des sols agricoles, les incertitudes des paramètres de conception de l'outil de labour, les fluctuations des conditions de fonctionnement qui sont généralement immaîtrisables

pendant l'opération de labour, 2) la variabilité spatiale des forces locales de labour est cyclique reflétant la formation répétitive des blocs du sol devant l'outil de labour.

La variabilité spatiale des forces globales de labour est combinée à la variabilité spatiale des forces locales de labour en tenant compte de l'hypothèse que les forces locales sont proportionnelles aux forces globales. Par conséquent, la variabilité spatiale des forces de labour peut être représentée par les cinq paramètres suivants $P_{HG}, P_{VG}\, S_1, S_2$ et τ telle que illustrée en Figure 9. Où, P_{HG} est la force globale horizontale, P_{VG} est la force globale verticale, S_1 est la distance entre deux changements successifs des forces globales, S_2 est la durée du cycle des forces locales et τ est le pourcentage de proportionnalité entre les forces locales et les forces globales de labour.

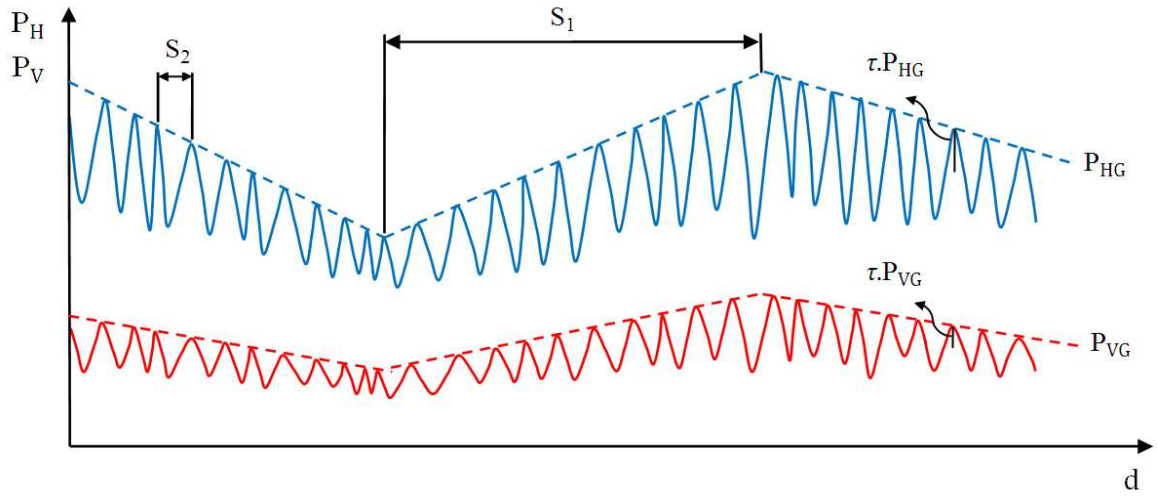

Figure 9 : Illustration de la variabilité spatiale des forces horizontale et verticale

Figure 10 montre la variabilité spatiale des forces horizontale et verticale pour la dent d'un chisel à travers 1000 m de distance.

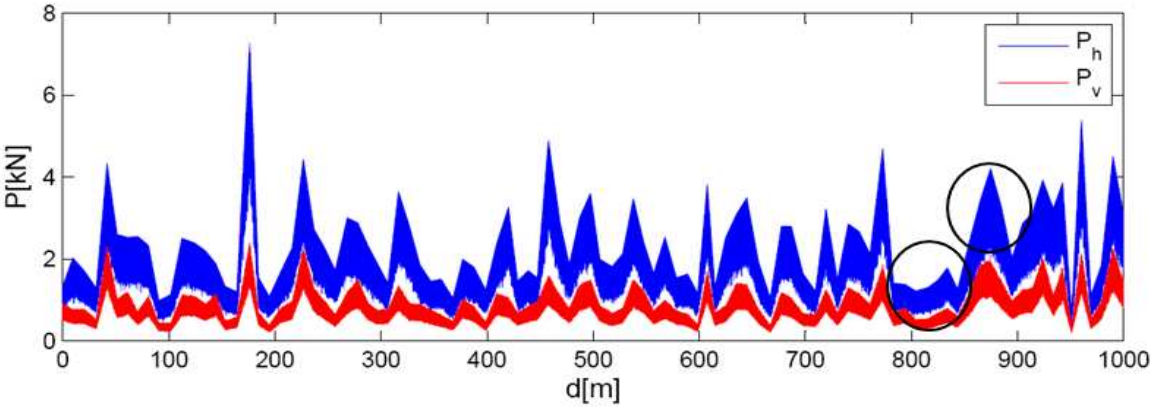

Figure 10 : La variabilité spatiale des forces horizontale et verticale de la dent

7 L'analyse de fatigue des machines de labour (Chapitre 5)

Les machines de labour sont soumises à des contraintes multiaxiales provoquées par la variabilité des forces de labour. La défaillance du sol crée des chargements cycliques sur les machines qui peuvent avoir des effets sur la durée de vie de ces machines. Pour cette raison, nous avons étudié les effets de la variabilité des forces de labour sur la durée de vie des machines de labour. Les étapes principales de cette analyse sont présentées en Figure 11.

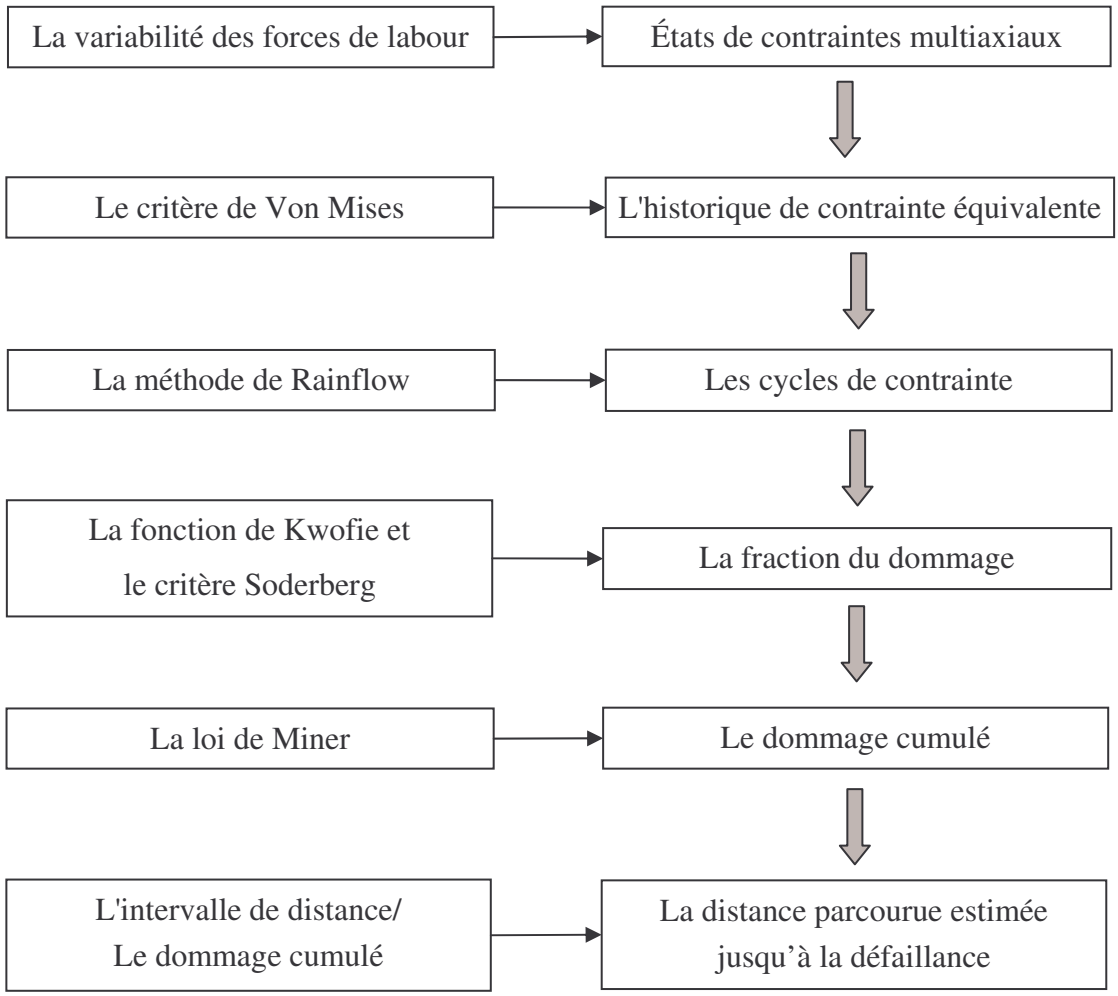

Figure 11 : Organigramme de l'analyse de fatigue des machines de labour

La contrainte équivalente générée par les contraintes multiaxiales est calculée selon le critère de Von Mises dans un intervalle de distance bien déterminée. L'algorithme de Rainflow est utilisé pour extraire les cycles de contrainte et de déterminer leurs moyennes et leurs amplitudes. La fraction du dommage causé par chaque cycle de contrainte est calculée par la fonction de Kwofie et le critère de Soderberg. Le choix de la fonction de Kwofie et le critère de Soderberg est basé sur l'hypothèse de la linéarité des déformations.

En d'autres termes, les contraintes appliquées sur les machines de labour sont toujours dans le domaine élastique du matériau. Ainsi, le dommage cumulé causé par tous les cycles est calculé selon la loi de Miner. Enfin, la distance parcourue estimée jusqu'à la défaillance est calculée en divisant l'intervalle de distance par le dommage cumulé.

Le dommage total calculé sur l'intervalle de distance de $(d_o = 1000m)$ est égal à $D = 1.212 \times 10^{-6}$. La distance parcourue estimée jusqu'à la défaillance est égale à $d_f = 0.825 \times 10^6\ km$. Malgré que la contrainte équivalente soit inférieure à la limite élastique, la défaillance se produit après une certaine distance d_f. En suite, nous avons utilisé des valeurs différentes de h et b pour calculer la distance parcourue estimée jusqu'à la défaillance, comme illustre la Figure 12. Les résultats montrent que la variation de la distance parcourue jusqu'à la défaillance en fonction des dimensions (b, h) est très importante $\left(d_{f\ min} = 2.004 \times 10^4\ km,\ d_{f\ max} = 9.213 \times 10^8\ km\right)$.

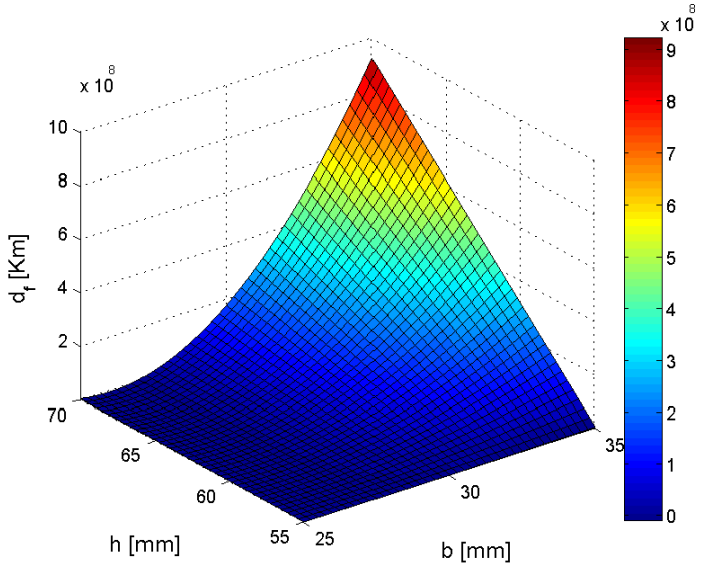

Figure 12 : La distance parcourue estimée à la défaillance en fonction de b et h

Nous avons également étudié l'effet du pourcentage (τ) sur la distance d_f, voir Figure 13. En effet, une augmentation de τ de 0,1 à 0,4 provoque une réduction de d_f de $1.2 \times 10^5\ km$. Cela signifie que la réduction de d_f en raison de l'augmentation de τ est très importante. Par conséquent, nous conseillons d'effectuer l'opération de labour lorsque l'humidité du sol est autour de la limite de liquidité. Cela peut améliorer considérablement la distance parcourue jusqu'à la défaillance et augmenter la durée de vie des machines de labour.

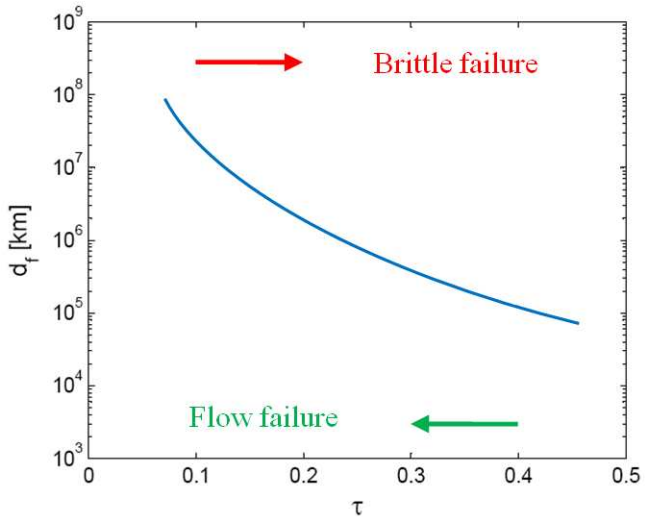

Figure 13 : La relation entre τ et d_f

8 Conclusions et perspectives (Chapitre 6)

Le principal objectif de cette thèse est de proposer une alternative à l'approche déterministe de la conception des machines agricoles, cela en intégrant les approches de fiabilité des structures, d'optimisation fiabiliste et d'analyse de fatigue. L'approche probabiliste proposée dans la Section 5 nous a permis de modéliser la variabilité de forces de labour résultant de la variabilité des paramètres du système de labour. La modélisation de la variabilité des forces de labour a permis ensuite d'effectuer l'optimisation fiabiliste des machines agricoles. Cela dans l'objectif de concevoir des machines de labour fiables et économiques. Le modèle proposé dans la Section 7 associe la variabilité de forces de labour résultant de la rupture du sol et la variabilité de forces de labour résultant de la variabilité des paramètres du système de labour, cette combinaison a permis de modéliser la variabilité de forces totales de labour. Ainsi, le modèle développé est utilisé dans l'analyse de fatigue présentée dans la Section 8. Cette analyse nous a conduit à étudier la sensibilité de la distance parcourue jusqu'à la défaillance par rapport aux paramètres de la conception et par rapport au paramètre de proportionnalité entre les forces locales et les forces globales de labour.

Afin d'améliorer l'estimation de la variabilité des propriétés mécaniques du sol, un nombre élevé d'échantillons doit être employé et les inter-corrélations entre ces propriétés devraient être étudiées. Des observations expérimentales peuvent être utilisées pour améliorer les estimations de la variabilité des paramètres de conception et des conditions de fonctionnement. Des recherches supplémentaires sont nécessaires pour étudier les

corrélations entre les forces globales et locales de labour (P_{HG}, P_{VG}) et la variabilité des paramètres (S_1, S_2, τ) du modèle présenté en Section 7. La distance parcourue estimée jusqu'à la défaillance est calculée sur 1000 m ne suffit pas pour représenter la variabilité spatiale des forces de labour. En effet, l'analyse de fatigue sur une distance plus longue doit être réalisée afin d'obtenir une estimation plus précise de la distance parcourue jusqu'à la défaillance. De plus, la génération de plusieurs trajectoires spatiales des forces de labour permettra d'utiliser les simulations de Monte Carlo afin d'estimer la distribution de probabilité de la distance parcourue jusqu'à la défaillance.

Chapter 1

Introduction and objectives

1.1 Introduction

In the design of agricultural machines, the soil heterogeneity and discontinuous structure should be taken into account. Given the difficulties related to the determination of soil failure patterns under mechanical loads and the calculation of the relevant forces, the design of agricultural machines is far from being a deterministic science. However, in the last six decades, researchers have worked to determine the patterns of soil failure under different operational conditions and propose models to estimate the acting forces. The first model was proposed by Reece in 1965 and was based on the work of Terzaghi. From there on, immense efforts have been made in this area, but there is still no well-defined generalised model to predict the behaviour of soil-tool interactions.

Because of to these drawbacks in the design analysis of agricultural machines, designers maintain the classical design approach, i.e. the deterministic design approach. In this approach, the designers measure the forces acting on machines in different field conditions in order to determine their maximum values. Then, safety factors are applied so as to assure that the stresses resulted by the applied forces are smaller than the resistance of the materials used in manufactory processes.

In the early 70's, reliability-based design optimization was proposed to account for the uncertainty of design variables in the optimization design approach in order to overcome the drawbacks of deterministic design approach. Nowadays, a variety of reliability-based design optimization methods is available to meet the challenge of design analysis of complex structural systems. Furthermore, these methods have been applied in several industrial fields, e.g. automotive, micro-electro-mechanical systems, aircraft, and metal forming.

In the 19th century, remarkable research was done by August Wöhler to investigate the effects of cycle loading on structures. This phenomenon, so-called fatigue, has become

more and more well-known and understood. Fatigue mechanism for the most commonly used materials has been well-defined and four main fatigue analysis approaches have been developed, according to fatigue phases, in order to estimate the life time of structures and to prevent failure by fatigue.

All these developments in the reliability-based design optimization approaches and the fatigue analysis approaches haven't been applied yet for the design of agricultural machines. This is mainly due to the difficulties related to the modeling of the variability in forces involved, especially the forces acting on tillage machines.

Therefore, the main focus of this work is to model the variability in the acting forces and to use appropriate methods available in reliability-based design optimization and fatigue analysis approaches. Special attention has been given to tillage machines that work in irregular environment and under variable conditions.

1.2 Overview of the work

The variability in tillage forces can be generated by two main sources: the variability in tillage system parameters which has a global effect on tillage forces and the variability in soil failure patterns which has a local effect on tillage forces. Therefore, we call the tillage forces related to the tillage system parameters as global tillage forces and those related to the soil failure as local tillage forces.

The variability in tillage system parameters is caused by the variability in soil engineering properties, in tool design parameters and in operational conditions. The variability in soil engineering properties reflects the heterogeneity and the discontinuity of agricultural soils. The variations in tool design parameters are due to the manufacturing processes, while the variations in operational conditions are due to the fact that these parameters are not completely controlled during tillage operation. The variability in soil failure patterns can be attributed to the variations of mechanical behaviour of soil under mechanical loads.

An overview of this work is illustrated in Figure 1-1. Firstly, the variability in global tillage forces derived from the variability in tillage system parameters were modelled and integrated in the reliability-based design optimization analysis in order to achieve optimum and reliable machines. Secondly, the variability in soil failure was added to the variability in tillage system parameters and the total variability in tillage forces were considered in the fatigue analysis for the object of calculating the live time of tillage machines.

The variability in local tillage forces was omitted during the reliability-based design optimization analysis for several reasons. Firstly, it has no significant effects on the variability of total tillage forces. Secondly, we wanted to simplify the calculation procedures and reduce the computational cost. This variability was considered in the fatigue analysis because it has a cyclic nature that affects significantly the life time of tillage machines.

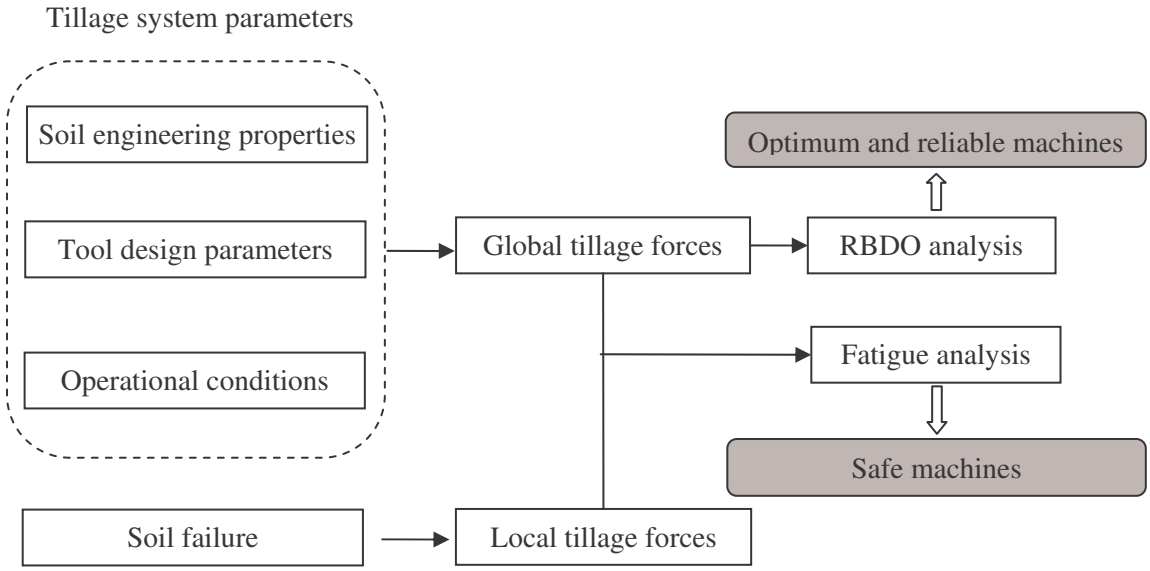

Figure 1-1 : Overview of the work

1.3 Research objectives

This dissertation investigates and develops formulations and methodologies for integrating the optimization, reliability and fatigue in the design of agricultural machines. The main focus is to develop a general framework for the design of agricultural machines in order to provide an alternative to traditional deterministic design methods by considering the variability in tillage forces. The research objectives were:

1- Proposing a probabilistic approach for modeling the variability in tillage forces due to the variability of tillage system parameters (soil engineering properties, tool design parameters and operational conditions).

2- Implementing a reliability-based design optimization framework for tillage machines based on existing probabilistic design tools and reliability-based design optimization methods.

3- Developing a new model to describe the variability in both global and local tillage forces.

4- Investigating the existing fatigue analysis methods and select those which are appropriate for calculating the life time of tillage machines when considering the spatial variability in tillage forces.

1.4 Outline of the dissertation

In Chapter 2, the objectives of tillage and their implements are presented, followed by an overview of the soil failure patterns according to the tillage depth/tool width ratio. Next, the soil-tillage tool forces are determined and different approaches used to estimate the forces needed to cut the soil are presented. The probabilistic approach proposed to model the variability in tillage forces derived from the variability in tillage systems parameters is then described. This is followed by modeling the variability in tillage forces for a chisel plough shank by means of 57 samples of soil engineering properties.

Chapter 3 begins with the types of uncertainties encountered during the design of structural systems and the necessity to consider the uncertainties of design variables in the design analysis. A general formulation of the deterministic design optimization and its drawbacks are then presented. Next, structural reliability methods used to estimate the failure probability of a structure is discussed, followed by a brief description of the reliability-based design optimization methods. A reliability-based design optimization approach for tillage machines is detailed. At the end of this chapter, a numerical application demonstrates the interest of using this approach for tillage machines.

In Chapter 4, the soil failure mechanism and its effect on the total tillage forces are presented. Next, a new model for describing the spatial variability in tillage forces when considering both the variability in tillage system parameters and soil failure is presented. This model is then applied to model the spatial variability of the shank of chisel plough across a distance of 1000 m.

Chapter 5 explains the fatigue phenomenon and presents the main approaches proposed to deal with it according to its phases. More details on the stress-based fatigue life approach are given in this chapter. The methods used to calculate the life time of tillage machines, i.e. expected travel distance to failure, are presented and applied with considering the results obtained in Chapter 4.

Chapter 6 presents a summary of this dissertation, conclusions concerning the results and recommendations for future work.

Chapter 2

Modeling variability in tillage forces

2.1 Introduction

This chapter consists of four sections. The first one provides a general overview of the soil-tillage tool interactions. This section begins with an introduction to the definition of a tillage operation, their objectives and their implements. Soil failure patterns, according to the tillage depth/tool width ratio, are then presented. This is followed by presenting the soil-tillage tool force components and the three approaches (analytical, numerical and empirical approaches) used to estimate the forces needed to cut the soil.

The second section describes the main steps of the proposed approach for modeling the variability in tillage forces. This section starts by determining the tillage system parameters (soil engineering properties, tool design parameters and operations conditions) involved in the calculations of the tillage forces. Then, the methodology proposed for modeling the variability in soil engineering properties and assumptions about the variability in tool design parameters and operational conditions are presented. After that, a method for determining the dispersion effects of tillage system parameters on tillage forces is introduced. This section finishes by the methodology proposed for determining the variability in tillage forces.

The third section presents an illustration application of the proposed approach for modeling the variability in tillage forces on the shank of a chisel plough. A total of 57 soil samples were considered for modeling the variability in soil engineering properties (soil density, soil cohesion, internal friction angle, soil-tool friction angle and soil-tool adhesion). Uniform and normal distributions were used to present the variability in tool design parameters (tool width and rake angle) and operations conditions (tool working depth, surcharge pressure at the soil surface and tool speed), because no data are available for these parameters. This chapter is concluded by some conclusions of the realized work.

2.2 Soil-tillage tool interactions

2.2.1 Introduction

"Tillage" may be defined as the mechanical manipulation of soil for any purpose, but usually for cultivating crops. The objectives of soil tillage can be resumed as: 1) to develop a desirable soil structure for a seedbed or a root-bed, 2) to control weeds or remove unwanted crop plant, 3) to manage plant residues, 4) to minimize soil erosion, 5) to establish specific surface configurations, 6) to incorporate and mix fertilizers, manure, … into the soil and 7) to accomplish segregation which may involve moving soil from one layer to another, removal of rocks and undesired objects or root harvesting [1]. In order to achieve these objectives, different types of tillage implements provided with different types of tillage tools have been developed.

A tillage tool, also called the working part, is an individual soil-working element, such as a plow bottom, a disk blade or a cultivator shovel. The working part, receiving energy from the tractor or other sources, works the soil and changes its state and properties [2]. A tillage implement consists of a single tool or a group of tools, together with the associated frame, wheels, control and protection devices, and any other structural and power transmission components [3].

Tillage implements can be classified according to their tasks into five main categories: primary tillage implements, secondary tillage implements, cultivating tillage implements, combined primary tillage implements and combined secondary tillage implements [1] [4] [5]. Primary tillage implements are used after harvest and it is normally designed to reduce soil strength, cover plant materials, and rearrange the aggregates, e.g. moldboard plows and subsoilers. Secondary tillage implements are used to break down large clods and to prepare an ideal seedbed, e.g. spring tooth harrows and rotary hoes. Cultivating tillage implements perform shallow post-plant tillage to aid the crop by loosening the soil and/or by mechanical eradication of undesired vegetation, e.g. row crop cultivators and rotary tillers-strip type. Combination primary tillage implements perform primary tillage functions and utilize two or more dissimilar tillage components as integral parts of the implement. Combination secondary tillage implements perform secondary tillage functions by using two or more dissimilar tillage components as integral parts of the implement, e.g. roller harrow with dual folding wings.

2.2.2 Soil failure patterns

The cutting of the soil involves the failure (or the rupture) of the soil which usually occurs in the shear mode along internal rupture surfaces, and often at the boundary between soil and tillage tool surface [4]. For a simple tillage tool, shown in Figure 2-1, the soil failure pattern can be similar to that shown in Figure 2-2.

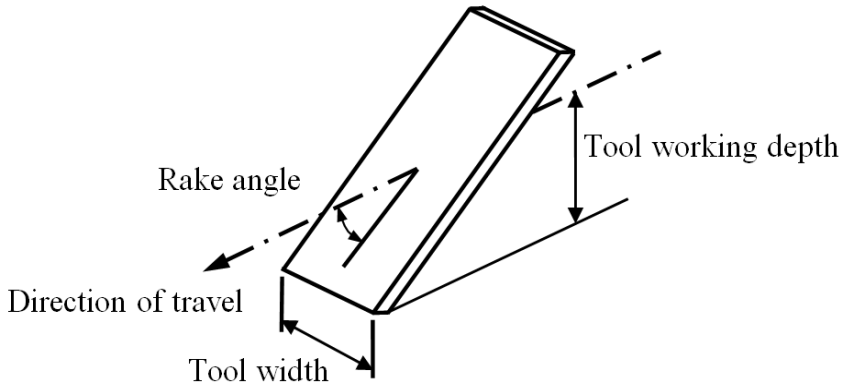

Figure 2-1 : Basic tillage tool geometry

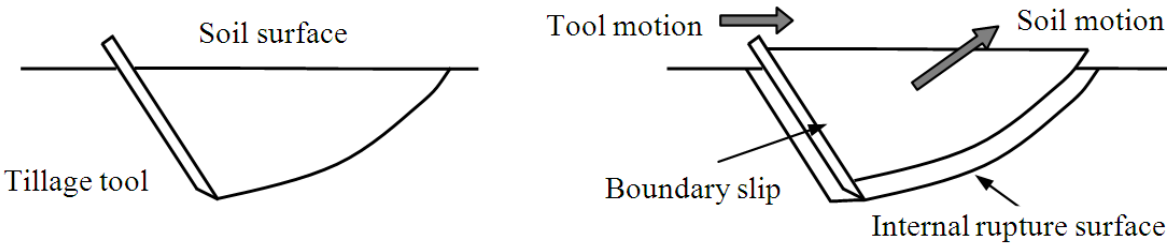

Figure 2-2 : Internal and boundary soil failure during cutting

Godwin and O'Dogherty [6] reported that soil failure patterns are significantly affected by the depth (d) / width (w) ratio of a tillage tool. They subdivided tillage tools, depending on their d/w ratio, into the following three categories:

- Wide tines for which $d/w < 0.5$.
- Narrow tines for which $1 < d/w < 6$.
- Very narrow tines for which $d/w > 6$.

Wide and narrow tines with d/w ratios less than 5 and rake angles less than $(90°)$ tend to produce the patterns shown in Figure 2-3 (a) and (b). This type of upward and forward failure tends to loosen the soil in a crescent manner. As the d/w ratio increases, the soil failure changes to that shown in Figure 2-3 (c), where there is a small crescent close to the soil at depth which is forced laterally to produce a slot.

The transition from one type to another occurs at a critical depth d_c. Therefore, knowledge of d_c is required to determine the tine force components [6]. Godwin and Spoor [7] determined the critical depth for a narrow tine by minimizing the horizontal force. Determining the critical depth in this way requires the rupture distance ratio (forward rapture distance/critical depth). Therefore, they plotted the rupture distance ratio for different tine rake angles, experimentally.

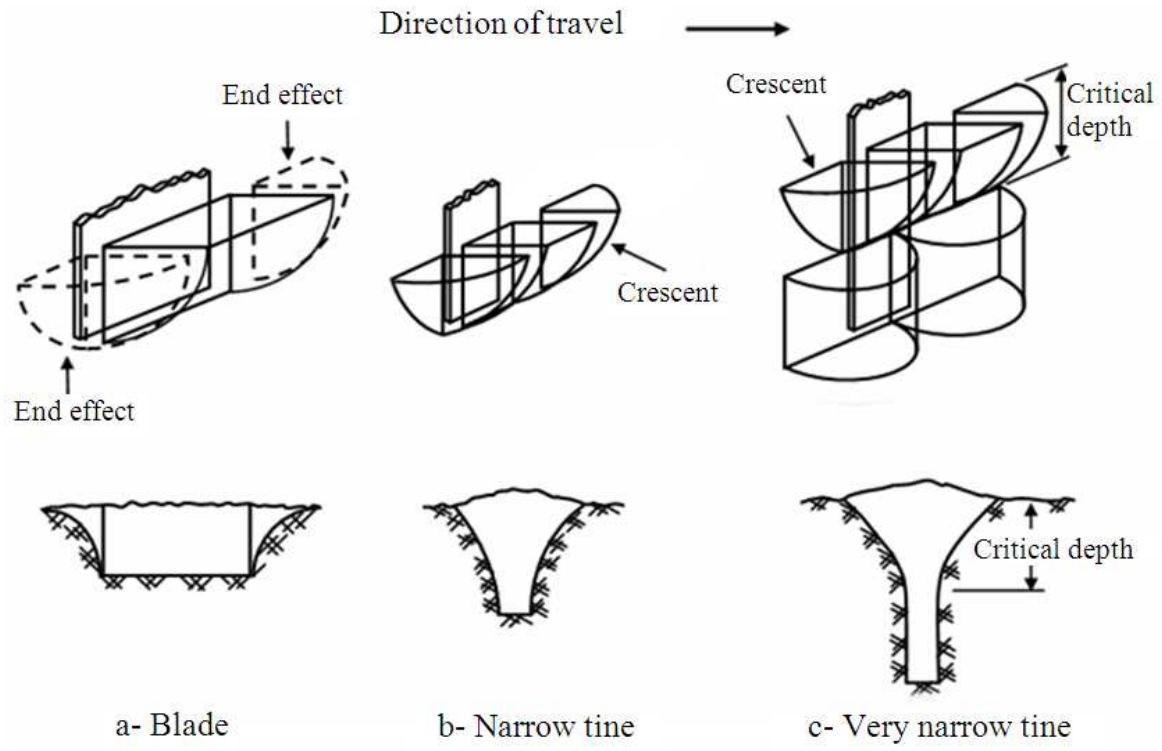

Figure 2-3 : Patterns of soil failure

2.2.3 Soil-tillage tool forces

A tillage implement moving with constant velocity is subjected to the following three main forces: 1) the weight of the implement, acting through the centre of gravity, 2) the forces acting upon the implement and 3) the forces acting between the implement and the prime mover [3]. For a simple tillage tool (Figure 2-1) two components are considered: 1) horizontal tool force, which is the amount of force required to pull or push the tool through the soil and 2) vertical tool force which is the tool force assisting or preventing penetration into the soil. Therefore, the soil reaction force on a tillage tool has two components, the horizontal tillage force P_H and the vertical tillage force P_V.

Ideally, the horizontal force P_H must be as small as possible and the vertical force P_V must be directed upward to assist penetration for major soil loosening operations

[8]. However, Godwin and Spoor [7] found that at a critical rack angle, the direction of vertical force changes from upward to downward, as shown in Figure 2-4. Godwin [8] expressed this critical angle for a simple plane steel tine as: $\alpha_c = \pi/2 - \delta$, where α_c is the critical rack angle and δ is the angle of soil-tool friction.

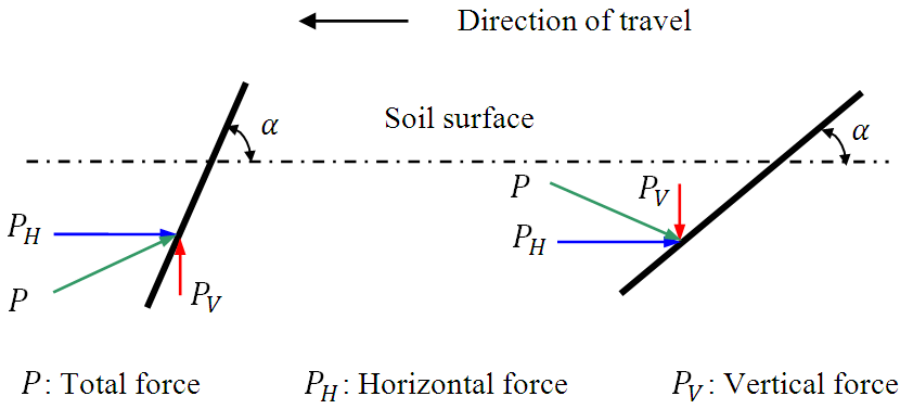

Figure 2-4 : Forces acting on the tool according to different tool orientations

Determining the amplitude and direction of tillage forces is of great value to both implement designers and farmers [9]. Three approaches have been developed for that purpose, namely analytical, numerical and empirical approaches. In the following a brief description of each approach is presented.

2.2.4 Analytical approach

The analytical approach is one of the first methods that has been used to predict the interaction between the soil and a tillage tool. This approach has been widely employed by many researchers in the field of soil tillage [10]. The first work for modeling the soil forces was the model of Reece [11], who recognized that the mechanics of earthmoving is similar in many respects to the bearing capacity of shallow foundations on soil as described by [12], Figure 2-5. The soil in front of a tool and above the failure surface is assumed to consist of two parts: 1) a Rankine passive zone and 2) a complex shear zone bounded by a part of a logarithmic spiral curve.

By using the force equilibrium equations over the entire system (soil, tool), Reece [11] proposed the universal earthmoving equation, presented in Equation 2.1, for describing the force required to cut the soil by a tool.

$$P = \left(\gamma d^2 N_\gamma + cdN_c + qdN_q\right)w \tag{2.1}$$

where P is the total force acting on the tool, γ is the soil density, d is the tool working depth, N_γ is the gravity coefficient, c is the soil cohesion factor, N_c is the cohesion coefficient, q is the surface surcharge pressure, N_q is the surcharge pressure coefficient and w is the tool width. The N-factors (N_γ, N_c , N_{ca}, N_q) are functions of the geometry of soil-tool interfaces, the internal friction angle of the soil and the soil-metal frictional angle.

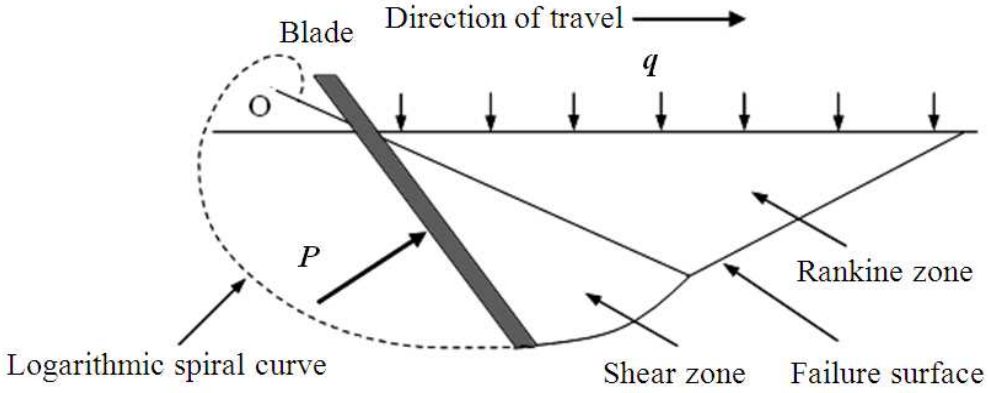

Figure 2-5 : Logarithmic spiral failure zone

Reece model formed a basis in the analytical approach, which is approximately valid for soil cutting tools with a width/depth ratio greater than one. With narrow tillage tools, the soil in front of a tool moves not only horizontally and vertically, but also sideways in the direction of the tool width (Figure 2-3). In this situation the soil failure configuration becomes more complicated and the Reece model is no longer sufficient in describing the three-dimensional failure surface [13]. Therefore, several semi-empirical models have been proposed to describe the three-dimensional failure surface, based upon the experimental observations and simplifications [7] [14] [15] [16] [17]. The principal differences between these models are the shape of soil failure surface and the form of equilibrium equations. The results of this approach are valid to some extent and its governing rules are sometimes used in other approaches such as numerical and empirical approaches.

2.2.5 Numerical approach

Two numerical methods can be recognized in tillage science: 1) finite element method (FEM) and 2) discrete element method (DEM). Overall, these methods are complicated and difficult to implement as they need good knowledge of mathematics and computer science. Among the numerical approaches, FEM has received more attention and was implemented in many works to describe the soil-tillage tool interaction [13] [18] [19] [20]. The principal differences between these models are the assumption of soil material

behavior, soil-metal interaction and soil failure criteria. Literature shows acceptable results obtained from this method. The main limitations of this method are individual creativity and patience when setting up boundary conditions, and the amount of computational time available [21].

The DEM method is an explicit numerical technique that treats soil as a collection of individual unconnected but interacting particles. Particles interact through a series of contact laws and the motion of the particles is controlled by Newton's laws of motion [20]. It is noted that the application of this method in the field of soil tillage is still limited.

2.2.6 Empirical approach

These methods typically correlate the implement draught with relevant parameters such as working depth, velocity, soil moisture content and density. They are very costly due to the instrumentations which are required to record data, precisely. Furthermore, they cannot be implemented at any desired time and place since providing required instrumentation may not be possible. In most cases, empirical methods represent only regional conditions. However, they could give an indication of the average force requirements, and their variability, for specific soil-implement combinations [9].

Artificial neural networks (ANN), which can be considered as the most common method in this approach, consists of essentially parallel computational models comprised of densely interconnected adaptive processing units with the simulation of knowledge acquisition and organization skills of the human brain [22]. The literature does not show many applications of this method in the field of soil-tillage tool interaction.

2.3 Probabilistic approach for modeling the variability of tillage forces

As mentioned before, there are several available models that can be used to predict the forces acting on a tillage tool at soil failure. Analytical and numerical modeling methods are usually used to achieve this goal. In the analytical methods, soil-tool forces are considered as functions of three categories of variables, namely soil engineering properties, tool design parameters and operational conditions. Soil engineering properties are conventionally considered to be constant, reflecting a homogeneous soil profile, and tillage forces are calculated for assigned tool design parameters and operational conditions [6] [8] [17]. When numerical methods, e.g. the finite element method (FEM), are adopted to model the soil-tillage tool interaction, two different theoretical approaches are introduced, namely the curve-fitting technique and the elastic-perfectly plastic assumption [21]. The elastic-perfectly plastic method considers Young's modulus of elasticity and Poisson's ratio as constants, while the curve-fitting method only accounts for a variable Young's modulus as a function of load history [18]. For both of these FEM methods, the soil is treated as a homogeneous structure with very few exceptions. Mouazen and Neményi [20] developed a three-dimensional FEM model for cutting non-homogeneous (vertically) sandy loam soil by a subsoiler with a chisel and shank. The non-homogeneity in the soil was proposed to simulate the differences in soil strength among different soil layers. However, they considered Young's modulus of elasticity and Poisson's ratio as constant in the FEM analysis. Moreover, Fielke [19] studied the effect of a variable Poisson's ratio on tillage forces and soil movement around the cutting edge.

In reality, soil is neither a continuous nor a homogeneous structure, but a three-phase medium composed of solid, liquid and gaseous particles [2]. Consequently, soil engineering properties vary in both vertical and horizontal directions [23]. Estimating tillage forces using analytical or numerical methods with the assumption that soil engineering properties are uniform does not reflect the nature of soil. Therefore, we intend to propose a probabilistic approach for modeling the variability of tillage forces due to the variability of tillage system parameters (soil engineering properties, tool design parameters and operational conditions). The variability of soil engineering properties reflects the heterogeneous nature of agricultural soils. The variability of tool design parameters is due to the tolerances of manufacturing processes. The variability of operational conditions is due to the fact that these parameters are partially controlled during a tillage operation.

The proposed approach consists of four steps and an overview of the different steps is shown in Figure 2-6. The first step attempts to estimate the tillage forces of narrow tines and to determine the main tillage system parameters (soil engineering properties, tool design parameters and operational conditions) affecting the tillage forces. The second step aims to model the variability of soil engineering properties and propose some assumptions about the variability of tool design parameters and operational conditions. The third step presents the method used to determine the dispersion effects of the tillage system parameters on the tillage forces. At this stage, we intend to neglect the variability of those tillage system parameters that has no significant effect on the tillage forces in order to simplify the quantification of the variability of tillage forces and to reduce the computational time. The last step is to estimate the variability of tillage forces based on the variability of the tillage system parameters. This methodology is based on the MCS technique. In addition, the correlation coefficient between the horizontal and vertical forces, required in the calculation of failure probability, is calculated in order to determine its effect on the failure probability.

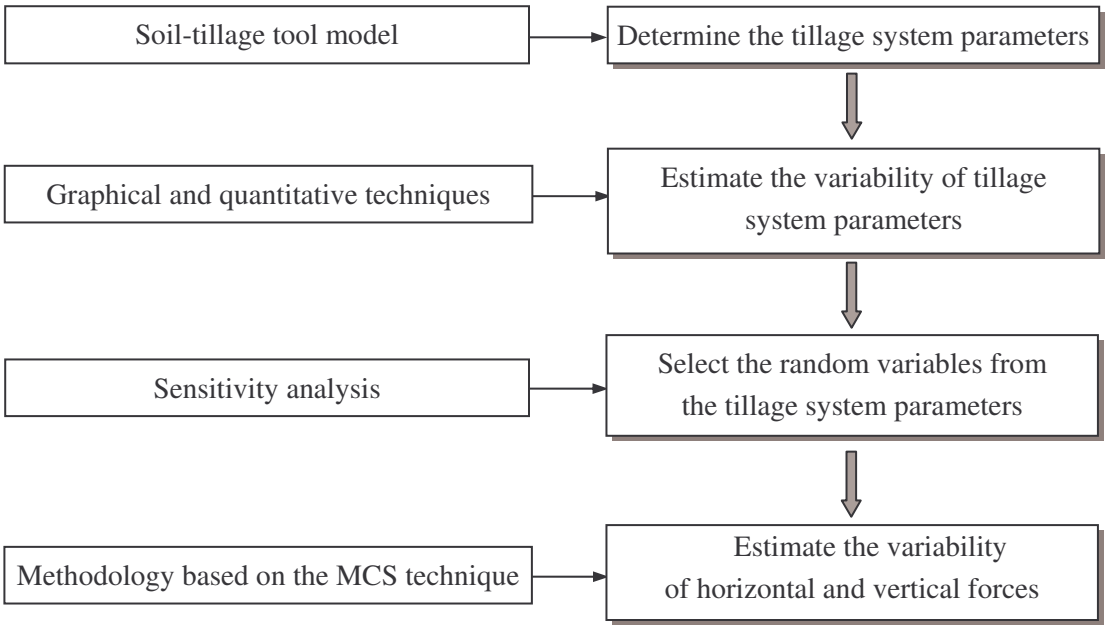

Figure 2-6 : Flowchart of the probabilistic approach steps

2.3.1 Determining tillage system parameters

The model of McKyes and Ali [14] is used to estimate the forces acting on a tillage tool and determine the tillage system parameters. This model was selected because it is simple and accurate [24], and has shown good agreement with experimental results, especially at low velocity [25].

McKyes and Ali [14] proposed a three-dimensional soil failure pattern ahead of a narrow tine as shown in Figure 2-7. They assumed that the soil failure surface from the tool tip to the soil surface was linear, and it created an unknown angle β_r with respect to the soil surface. The surface side failure crescents (AB and CD) were circular and situated at the edges of a straight front (BC) which has the same width as the narrow tine. The forward distance of the failure crescent from the blade on the surface was assumed to be equal to the radius r of the crescent.

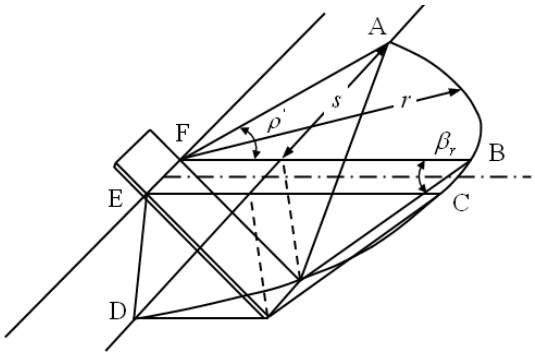

Figure 2-7 : Soil failure model for narrow blades

The forces acting on the soil segment are shown in Figure 2-8, including the effects of the density of soil, the internal friction angle, the soil cohesion, and the surface surcharge pressure.

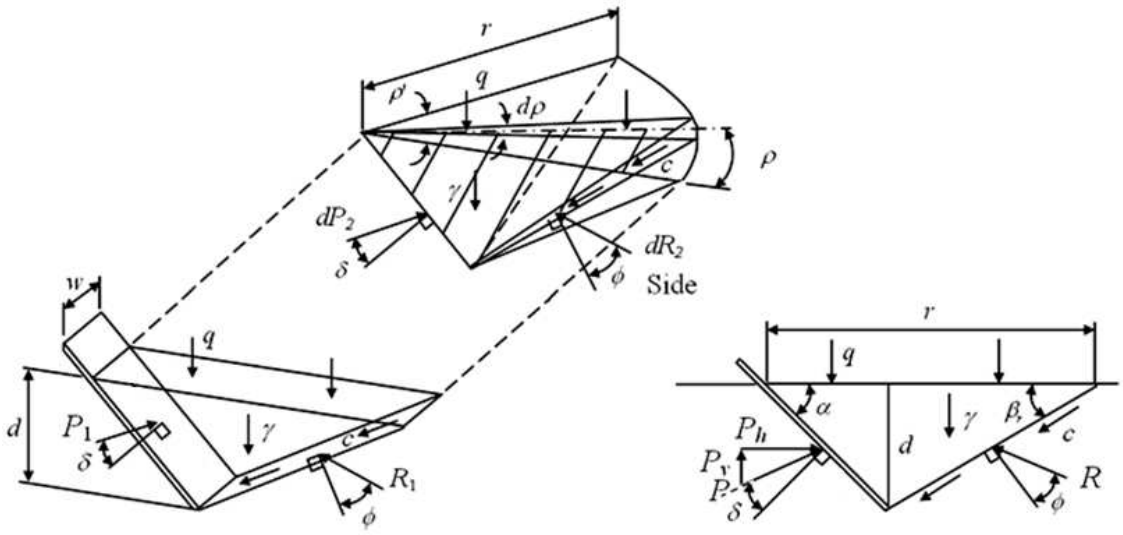

Figure 2-8 : Forces acting on soil segment

The total soil cutting force is the summation of three forces; the force caused by soil gravity, by cohesion and by surcharge pressure at the soil surface as expressed in Equation 2.1. McKyes and Ali [14] obtained the rupture angle β_r by minimizing the coefficient of

gravity N_γ, and they computed the side crescent s and the distance from the blade to the forward failure plan r from geometrical considerations as follows:

$$s = d\sqrt{cot^2(\beta_r) + 2\cot(\alpha)\cot(\beta_r)} \tag{2.2}$$

$$r = d[\cot(\alpha) + \cot(\beta_r)] \tag{2.3}$$

where, r is the distance from the blade to the forward failure plan, β_r is the rupture angle, α is the rake angle of the tool from the horizontal and s is the side crescent.

By taking into account the effects of soil-tool adhesion and tool speed, the total soil cutting force (Equation 2.1) can be rewritten as:

$$P = P_\gamma + P_c + P_{ca} + P_q + P_a \tag{2.4}$$

where, P_γ is the force caused by the soil density, P_c is the force caused by the soil cohesion, P_{ca} is the force caused by soil-tool adhesion, P_q is the force caused by the surface surcharge pressure and P_a is the force caused by tool speed. The total force can be rewritten again as the general earth pressure model as:

$$P = \left(\gamma d^2 N_\gamma + cdN_c + c_a dN_{ca} + qdN_q + \gamma v^2 dN_a\right)w \tag{2.5}$$

where, c_a is the soil-tool adhesion, N_{ca} is the adhesion coefficient, v is the tool speed and N_a is the inertial coefficient.

A simplified form of soil resistance is given by the Equation 2.6.

$$P = \left[\frac{1}{2}\gamma r\left(1 + \frac{2s}{3w}\right) + c\left(1 + \frac{s}{w}\right)\frac{\cos(\phi)}{\sin(\beta_r)\sin(\beta_r + \phi)} - c_a\frac{\cos(\alpha + \beta_r + \phi)}{\sin(\alpha)\sin(\beta_r + \phi)} + q\left(1 + \frac{s}{w}\right)\frac{r}{d}\right.$$
$$\left. + \gamma v^2\left(1 + \frac{s}{w}\right)\left(\tan(\alpha) + \frac{\cot(\beta_r + \phi)}{\tan(\beta_r)\cot(\alpha)}\right)\right]\frac{dw}{\cos(\alpha + \delta) + \sin(\alpha + \delta)\cot(\beta_r + \phi)} \tag{2.6}$$

Equation 2.6 falls into the general earth pressure model (Equation 2.5), when the *N*-factors are defined as:

$$N_\gamma = \frac{(r/2d)[1 + 2s/3w]}{\cos(\alpha + \delta) + \sin(\alpha + \delta)\cot(\beta_r + \phi)} \tag{2.7.a}$$

$$N_c = \frac{[\cos(\phi)/(\sin(\beta_r)\sin(\beta_r + \phi))](1 + s/w)}{\cos(\alpha + \delta) + \sin(\alpha + \delta)\cot(\beta_r + \phi)} \tag{2.7.b}$$

$$N_{ca} = \frac{-\cos(\alpha + \beta_r + \phi)/(\sin(\alpha)\sin(\beta_r + \phi))}{\cos(\alpha + \delta) + \sin(\alpha + \delta)\cot(\beta_r + \phi)} \tag{2.7.c}$$

$$N_q = \frac{(r/d)\left[1 + \frac{s}{w}\right]}{\cos(\alpha + \delta) + \sin(\alpha + \delta)\cot(\beta_r + \phi)} \tag{2.7.d}$$

$$N_a = \frac{[\tan(\alpha) + \cot(\beta_r + \phi)/(\tan(\beta_r)\cot(\alpha))](1 + s/w)}{\cos(\alpha + \delta) + \sin(\alpha + \delta)\cot(\beta_r + \phi)} \tag{2.7.e}$$

McKyes and Ali [14] calculated the width of the side crescent from geometrical considerations (Equation 2.2), whereas Kuczewski and Piotrowska [16] recommended a regression equation for a rake angle $\alpha \in [\pi/6, \pi/3,]$ as in Equation 2.8, where they calculated regression coefficients from experimental results.

$$s = (0.1045 + 0.4412\alpha) \tag{2.8}$$

The calculated force (Equation 2.6) is a function of the unknown angle β_r. McKyes and Ali [14] obtained this angle by minimizing the dimensionless term of gravity N_γ. Zhang and Kushwaha [24] found that angle β_r must be determined not only by the rake angle of the tool from the horizontal α, the angle of internal soil friction ϕ, the angle of soil-metal friction δ, the ratio of tool working depth to tool width d/w, but also by soil internal cohesion c, soil-metal adhesion c_a and the surcharge pressure at the soil q. So the rupture angle that governs the soil failure should be obtained by minimizing the soil cutting resistance in the passive movement condition according to the passive earth pressure theory.

Grisso et al. [15] also recommended the determination of the rupture angle by minimizing the total force P with respect to β_r. This can be accomplished by taking the derivative of P with respect to β_r and equating it to zero:

$$\frac{dP}{d\beta_r} = 0 \tag{2.9}$$

As the resulting differential equation (Equation 2.9) is quite complex, a MATLAB code is implemented to determine the failure angle which corresponds to the minimum total force. The horizontal and vertical forces are obtained by combining the total force P with the force of adhesion [4]:

$$P_H = P\sin(\alpha + \delta) + c_a dw\cot(\alpha) \tag{2.10}$$

$$P_V = P\cos(\alpha + \delta) - c_a dw \tag{2.11}$$

where, P_H is the horizontal force and P_V is the vertical force.

To validate the modifications which were performed on the McKyes and Ali model, we compared the predicted results of this model before and after modifications to experimental results reported by Onwuala and Watts [26]. Some physical properties of the soil, which was used in the experiments, are shown in Table 2-1.

Table 2-1 : Soil description

Soil type	Stewiacke soil (FAO/UNESCO)
Soil texture	Silty sand
Dray density for tests	$14.9\ kg/m^3$
Cohesion	$2\ kPa$
Angle of internal friction	$30°$
Angle of soil-metal friction	$15.22°$
Adhesion	$6.77\ kPa$

Predicted horizontal forces by the two models are compared to experimental data for the narrow tine with $w = 5.1\ mm$ and $\alpha = 45°$ and a tillage depth of $d = 22.9\ mm$, are shown in Figure 2-9. Whereas, the comparison between the predicted vertical forces and experimental results, at the same operating conditions, are shown in Figure 2-10. The error bars in the figures refer to 95% of confidence intervals for the mean of three replications.

To evaluate the performance of the models in predicting the experimental results, the deviation (%) of the theoretical results from the experimental ones is calculated as

$$\text{Deviation (\%)} = \left[\frac{\text{Experimental force} - \text{Theoretical force}}{\text{Experimental force}}\right] \times 100 \qquad (2.12)$$

The average percent deviations of the predicted forces from experimental results are shown in Table 2-2. The average deviation is calculated over the eight speed ranges used in the study.

Table 2-2 : Average percent deviation of predicted forces from experimental observation

Force type	Average % deviation from experiment	
	Before modifications	After modifications
Horizontal force	20	7
Vertical force	27	19

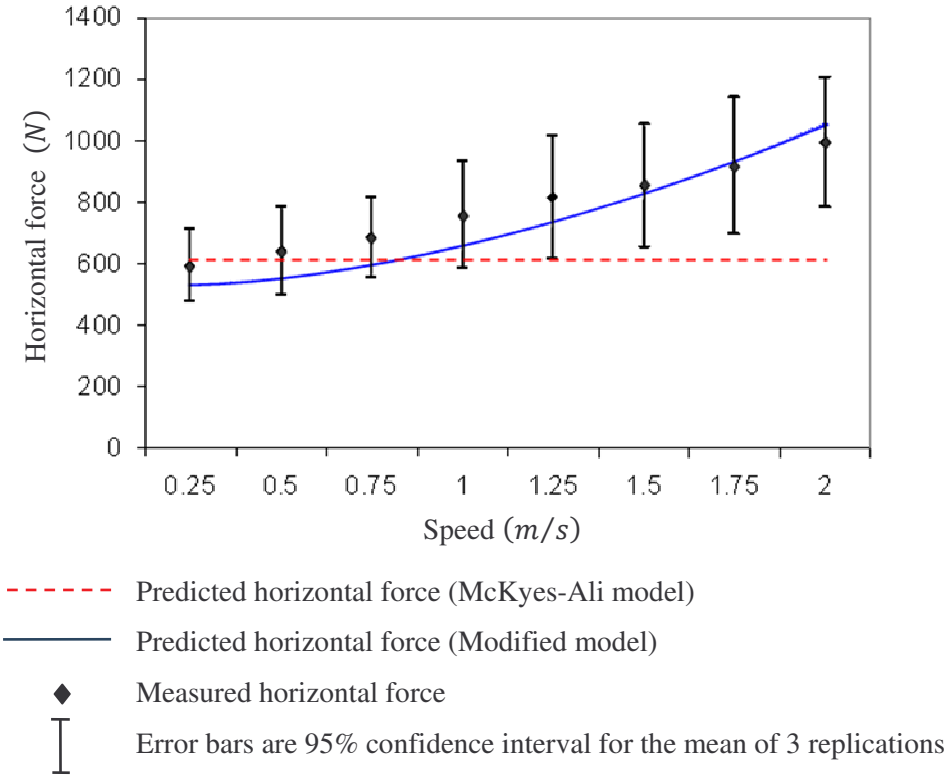

Figure 2-9 : Comparison between theoretical and experimental results for horizontal force

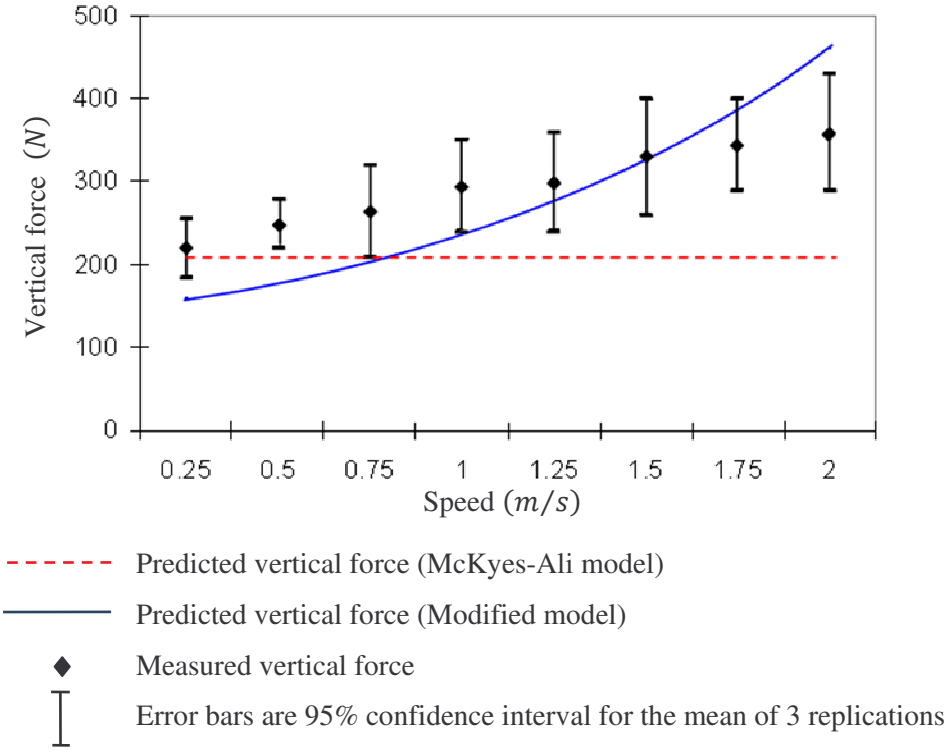

Figure 2-10 : Comparison between theoretical and experimental results for vertical force

The modified model is more accurate in predicting both vertical and horizontal forces than the McKyes-Ali model. The differences between the average percent deviations between the two models for the horizontal and vertical forces are 13% and 8%, respectively. The modified model has good agreement with the experimental observation for vertical force. While, this model tends to over-predict horizontal force at high speeds and to be under-predict at low speeds. The average percent deviations for the horizontal and vertical forces at field speeds $(4-6\,km/h)$ are 5.3% and 10.7%, respectively that means the modified model is more accurate at operating conditions.

According to Equations (2.6), (2.10) and (2.11), the tillage system parameters considered for the calculation of the horizontal and vertical forces can be grouped into three main categories: 1) soil engineering properties (soil density, soil cohesion, internal friction angle, soil-tool friction angle and soil-tool adhesion), 2) tool design parameters (tool width and rake angle) and 3) operational conditions (tool working depth, surcharge pressure at the soil surface and tool speed).

2.3.2 Modeling the variability of tillage system parameters

Over the years, many methods and techniques have been developed for modeling the variability of a random variable depending on the number of data points and assumptions about the shape of the underlying distribution [27] [28]. Parametric and non-parametric methods are usually used to achieve this purpose. Typically, the non-parametric methods are much easier to apply than the parametric methods and they require only few or no assumptions about the shape of the underling distribution. However, the latter methods are more powerful and more flexible than the former ones [27]. Parametric methods use both quantitative and graphical techniques to select the underling distribution of a random variable [29]. Preliminary estimation of the statistical information of the variability of a random variable can be extracted from the graphical techniques. A more complete description can be obtained by using the quantitative techniques [30].

In this dissertation, a combination of graphical and quantitative techniques for modeling the variability of soil engineering properties was used. This methodology, shown in Figure 2-11, can be summarized in the following steps:

Step 1: Calculating the mean and variance values for each parameter. The mean measures the central tendency in the data, while the variance measures the dispersion in the data

about the mean. Mean and variance values allow getting a preliminary description of the variability of a random variable.

Step 2: Establishing the histogram for each parameter for getting more complete description about the data. Three steps are needed to develop a histogram:

1) Arranging the data in increasing order.

2) Subdividing the data into several equal intervals and count the number of observations in each interval. The following empirical relationship was used to determine the number of interval [30]:

$$n_{int} = 1 + 3.3\log(n_s) \tag{2.13}$$

where n_{int} is the number of intervals and n_s is the number of samples.

3) Plotting the number of observations in each interval versus the random variables.

Step 3: Selecting the appropriate probability distribution by comparing the histogram shape with common probability density distributions, presented in Appendix I, and then choosing those which are more approximating to the shape of the histogram.

Step 4: Calculating the parameters of the probability distribution using the method of moments. The basic concept behind the method of moments is that all the parameters of a given distribution can be calculated using the information resulted from its moments. The relationships between the parameters of a distribution and the mean and the variance for the most common distributions are presented in Appendix I.

Step 5: Applying the goodness-of-fit tests that measure the compatibility of a random sample with a theoretical probability distribution function. Two commonly statistical tests were used for this purpose, namely Chi-square test and Kolmogorov-Smirnov (K-S) test [29]. The Chi-Square test is based on the error between the observed and the measured probability density function (PDF) of the distribution, while the K-S test is based on the error between the observed and assumed cumulative density function (CDF) of the distribution. The advantage of the K-S test over the Chi-square test is that it is not necessary to divide the data into intervals, thus the errors or the subjective judgment associated with the number or size of the interval is avoided. However, using both tests is important to get an adequate estimation. The appropriate probability distributions for the soil engineering properties were selected according to the results of the goodness-of-fit tests. More details about Chi-square and Kolmogorov-Smirnov tests are given in Appendix II.

This methodology provides an accurate estimation for the variability of soil engineering properties and allows one to select the best probability distributions that can simulate the variability of these properties. Since, preliminary statistical information of the variability of soil engineering properties can be extracted from graphical techniques, and a more complete description can be obtained using quantitative techniques.

The variability of tool design parameters and operational conditions were modeled after proposing the following two assumptions: 1) the tool width w and the rake angle α have uniform distributions with lower and upper bounds, based on the manufacturing accuracy, of $\pm 0.1\text{mm}$ for the width and $\pm 1^{\circ}$ for the rake angle, 2) the tool working depth d, the surcharge pressure q and the tool speed v have normal distributions with standard deviations equal to 5% of their mean values. Usually, a uniform distribution is used to model the uncertainties associated with manufacturing processes, and a normal distribution is used to model the uncertainty of a random variable when few data are available [28] [30].

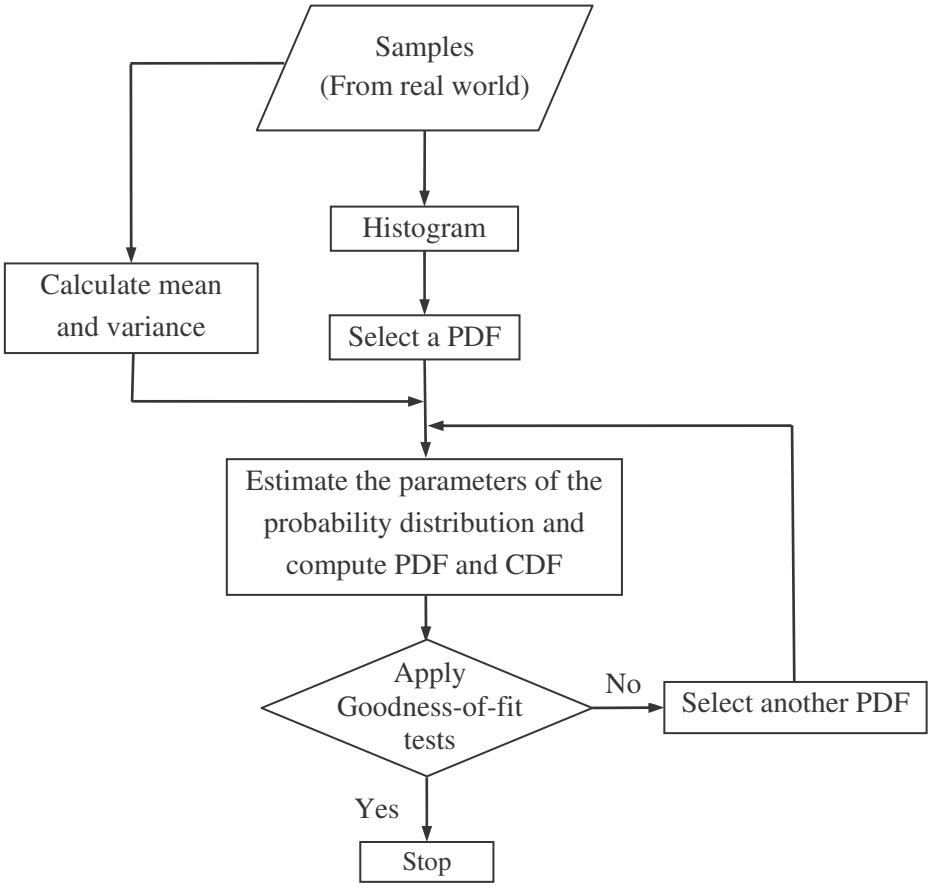

Figure 2-11 : Proposed methodology for modeling the variability in soil engineering properties

2.3.3 Sensitivity analysis

Sensitivity analysis aims at studying the relationships between the output and input variables. Differential sensitivity analysis is considered to be the most commonly employed method in sensitivity analysis [31]. This method deals with local sensitivity analysis by focusing on the evaluation of the partial derivatives $\partial f/\partial y$ of the function f. Many approximation methods are used to calculate the partial derivatives of f. Forward, backward and central differences are the most common forms. The central difference method requires more computing time, but it yields a more accurate approximation. Therefore, this method is used in this work to calculate the partial derivatives of the horizontal and vertical forces for the mean values of the tillage system parameters, and for a constant change equal to $\Delta y_i = 0.001 y_i$ where y_i is a tillage system parameter.

However, differential sensitivity analysis leads to a local sensitivity analysis at mean values of the input random variables and does not take into account the dispersion of the variables. Therefore, a new sensitivity method is proposed to overcome this limitation and to estimate the dispersion effects of tillage system parameters. The main advantage of the proposed method is its simplicity, compared to other available methods, such as the variance-based sensitivity [32], that are too complex to implement. Its main drawback is that it cannot take into account correlations between random variables (random variables should be independent). However, the proposed method provides more accurate estimations for the dispersion effects of tillage system parameters than the classical differential sensitivity methods.

This method is shown in Figure 2-12 and consists of two main steps. In the first step, the confidence interval bounds (y_{max}, y_{min}) were computed for each tillage system parameter according to Equation (2.14) and (2.15). The values of the confidence interval bounds depend on the probabilistic characteristics (distribution type and distribution parameters) of each parameter. The higher the dispersion of a parameter, the greater the difference between the confidence interval bounds.

$$\mathrm{P_r}[y \leq y_{min}] = \alpha/2 \tag{2.14}$$

$$\mathrm{P_r}[y \geq y_{max}] = 1 - \alpha/2 \tag{2.15}$$

where $\mathrm{P_r}[\cdot]$ is the probability operator, y_{max} is the upper confidence interval bound, y_{min} is the lower confidence interval bound, α is a constant and $100(1-\alpha)\%$ represents the confidence interval. The confidence interval was selected to be 95%. For the bounded

probability distributions (uniform distribution …), y_{max} and y_{min} represented the two limits of the random variable**.**

In the second step, the differences between the maximum and minimum values of the tillage forces were calculated in the confidence interval of each tillage system parameter when the values of other parameters were equal to their mean values. These differences indicate the dispersion effects of the tillage system parameters on the tillage forces. The greater the difference between the maximum and minimum values of the tillage forces, the greater the influence of the variability of the tillage system parameters on the tillage forces.

The relationships between the tillage forces and the tillage system parameters show that $P_H(\mathrm{y}_i)$ and $P_V(\mathrm{y}_i)$ are either increasing or decreasing functions (Appendix III). Therefore, the dispersion effects of the tillage system parameters were estimated by computing the differences between the tillage forces at the maximum and minimum value for each tillage system parameter (y_{max}, y_{min}).

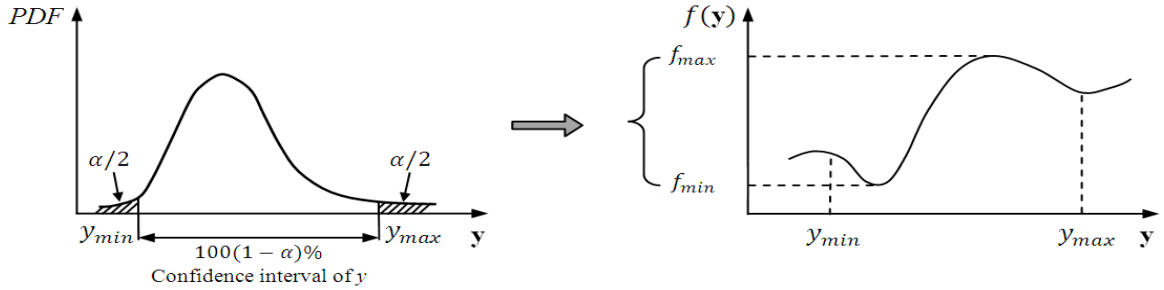

Figure 2-12 : The concept of estimating the effects of random variable dispersion

2.3.4 Determining the variability of tillage forces

A methodology based on the Monte Carlo simulation (MCS) technique was proposed for determining the variability of tillage forces, as shown in Figure 2-13. The number of generated values (n=50.000) was chosen to obtain an accurate correlation coefficient between the horizontal and vertical forces. The relationship between the number of generated values and the correlation coefficient show that the values of correlation coefficient converge when the number of generated values is more than 10.000 as illustrated in the example of Appendix IV. Therefore, the use of n=50.000 allows us to get an accurate estimation of the correlation coefficient between the horizontal and vertical forces. The proposed methodology consists of the following steps:

1- Generate n values for each tillage system parameter according to its probabilistic characteristics.

2- Compute the total force P according to Equation (2.6) for different values of $\beta_r (\beta_r \in [0 - 90^{\circ}])$, for the set of tillage system parameters obtained in step 1. This is followed by the selection of the minimum value of P to respect the passive earth pressure theory and the corresponding value of β_r.

3- Calculate the horizontal and vertical forces according to Equations (2.10) and (2.11), respectively.

4- Repeat Steps 1, 2 and 3 for each set of tillage system parameters.

5- Calculate the mean and variance values for the horizontal and vertical forces, and then apply the goodness-of-fit tests to select the distribution that can best model the randomness of these forces.

6- Compute the correlation coefficient between the horizontal and vertical forces according to Equation (2.16).

$$\mathrm{Corr}(P_H, P_V) = \rho(P_H, P_V) = \frac{\mathrm{Cov}(P_H, P_V)}{\sqrt{\mathrm{Var}(P_V)\mathrm{Var}(P_V)}} \tag{2.16}$$

where $\mathrm{Corr}(P_H, P_V)$ is the correlation coefficient between the horizontal and vertical forces, $\mathrm{Cov}(P_H, P_V)$is the covariance between the two forces and $\mathrm{Var}(\cdot)$ is the variance.

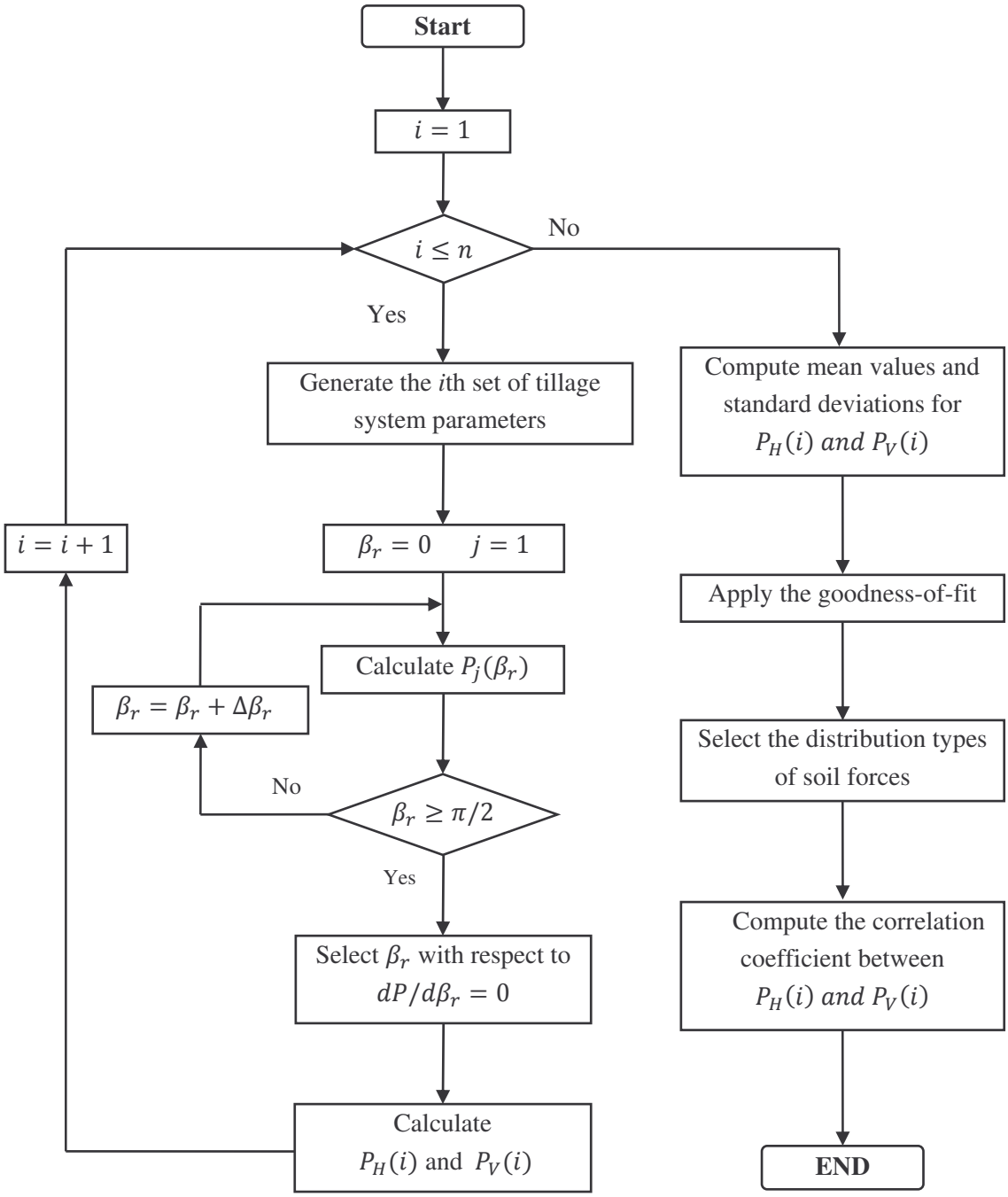

Figure 2-13 : Flowchart of the methodology for determining the variability of tillage forces

2.4 Determining the variability of tillage forces for the shank of a chisel plough

2.4.1 Modeling the variability of soil engineering properties

A total of 57 samples of soil engineering properties, collected from the literature (Appendix V), were considered for implementing the proposed methodology presented in Section 2.3.2. These data represent different soil texture types, namely sandy loam, clay loam, sandy clay loam, clay, and sand. This is based upon the fact that the chisel plough can be used for mechanical weed control, seedbed preparation, and other secondary tillage operations [2] in different sites.

Histograms and probability density functions (PDFs) of soil engineering properties are shown in Figure 2-14, and their probabilistic characteristics are given in Table 2-3. More details about the results of goodness-of-fit tests can be found in Appendix VI.

It is worth noting that the soil engineering properties do not have the same probability distributions and that only the internal friction angle has a normal distribution. In addition, it is noted that the histogram shapes are non-homogeneous, particularly the histograms of the external friction angle and soil-tool adhesion. This is most likely due to the following: 1) an insufficient sample size is considered in this work, 2) the samples are not representatives of real soil textures and 3) there are inter-correlations between the soil engineering properties (Appendix IV). However, from a statistical point of view, 57 samples are sufficient to model the variability of a random variable. As mentioned in the report of Fox [28], a set of 25 samples or more is sufficient to obtain an accurate estimation of the variability of a random variable. In order to improve the estimation of the variability of soil engineering properties, a larger number of samples should be employed and the inter-correlations between these properties should be investigated.

Table 2-3 : Probabilistic characteristics of soil engineering properties

Soil engineering properties	Type of distribution	Distribution parameters
Soil density, kN. m^{-3}	Lognormal	$\xi = 0.13, \mu = 2.7$
Soil cohesion, kPa	Weibull (2P)	$k = 15.51, \lambda = 1.66$
Internal friction angle, deg	Normal	$m = 32, \sigma = 3.96$
Soil-tool friction angle, deg	Weibull (3P)	$k = 87.14, \lambda = 31.52, \varepsilon = -64.08$
Soil-tool adhesion, kPa	Exponential	$\eta = 0.76$

ξ and μ are the shape and scale parameters of a lognormal distribution; ε, k and λ are, respectively, the location, scale and shape parameters of a Weibull distribution; m, σ are, respectively, the location and scale parameters of a normal distribution; η is the scale parameter of a exponential distribution.

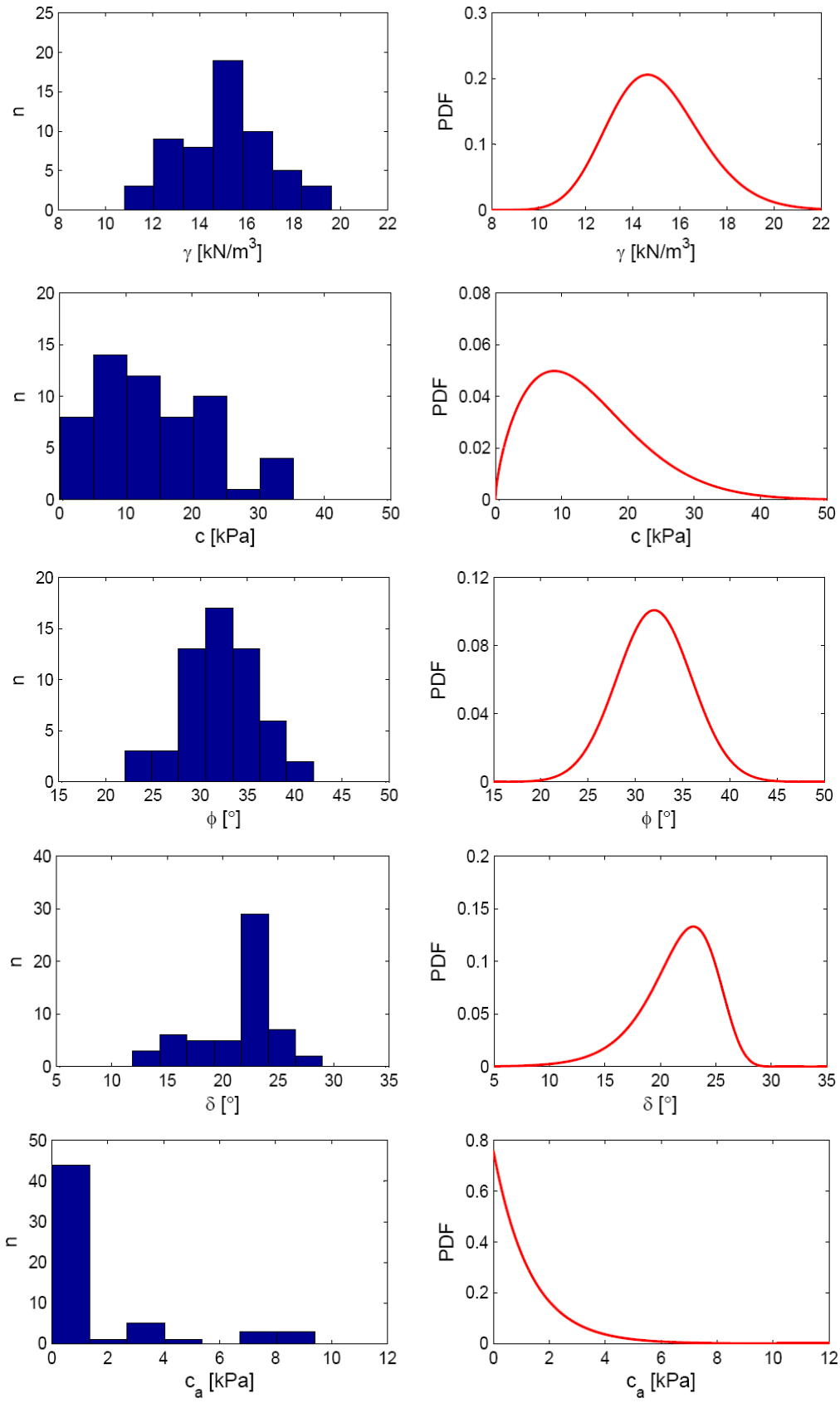

Figure 2-14 : Histograms and probability density functions for soil engineering properties

2.4.2 Effects of the variability of tillage system parameters on tillage forces

The effects of the variability of soil engineering properties, tool design parameters and operational conditions on tillage forces, using differential sensitivity analysis and the proposed method (presented in Section 2.3.3), are shown in Table 2-4. According to the results of differential sensitivity analysis, we observe that the influence of the variability of the rake angle on the horizontal force is larger than the influence of the variability of the other variables, whereas the vertical force is most influenced by the variability of the internal friction angle. The influences of the variability of soil-tool adhesion and surcharge pressure are very small compared to the influences of the variability of the other variables. These results are in agreement with many works reported in the literature [6] [14].

In contrast, the proposed method shows that the effect of the variability of soil cohesion on both the vertical and horizontal forces is the largest as compared with the effects of the variability of the other variables. This is caused by the high dispersion of the soil cohesion values around the mean value. Furthermore, only the variability of the surcharge pressure has no significant effect on either the horizontal or vertical forces. We conclude that only the surcharge pressure can be considered as a deterministic variable and the variability of the soil-tool adhesion and the other variables must be integrated into the probabilistic analysis of tillage forces.

Table 2-4 : Results of the differential sensitivity method and the proposed method

Soil tillage parameters	Differential sensitivity method		Proposed method	
	$\frac{\partial P_H}{\partial y_i} \times 10^{-6}$	$\frac{\partial P_V}{\partial y_i} \times 10^{-6}$	ΔP_H, kN	ΔP_V, kN
Soil density, kN. m^{-3}	13.224	5.7921	0.414	0.181
Soil cohesion, kPa	24.114	10.563	4.020	1.763
Soil-tool adhesion, kPa	0.0517	-0.0082	0.145	-0.023
Internal friction angle, deg	47.852	20.984	0.741	0.325
Soil-tool friction angle, deg	40.789	-6.4631	1.164	-0.171
Rake angle, deg	200.76	-19.923	0.199	-0.019
Tillage depth, m	1.2217	0.5334	0.963	0.418
Tool width, m	1.5080	0.5965	0.011	0.004
Surcharge pressure, kPa	0.0005	0.0002	0.002	0.001
Forward speed, m. s^{-1}	1.7708	0.7766	0.208	0.091

2.4.3 Determining the variability of tillage forces for the shank of a chisel plough

The methodology presented in Section 2.3.4 was applied to determine the variability of tillage forces for the shank of a chisel plough shown in Figure 2-15. In fact, the relative positions of tines on a tool frame both laterally and in the direction of motion have a significant effect on tine forces [6]. For simplicity, the variability of tillage forces for only one shank was determined, without considering the effects of tine interactions.

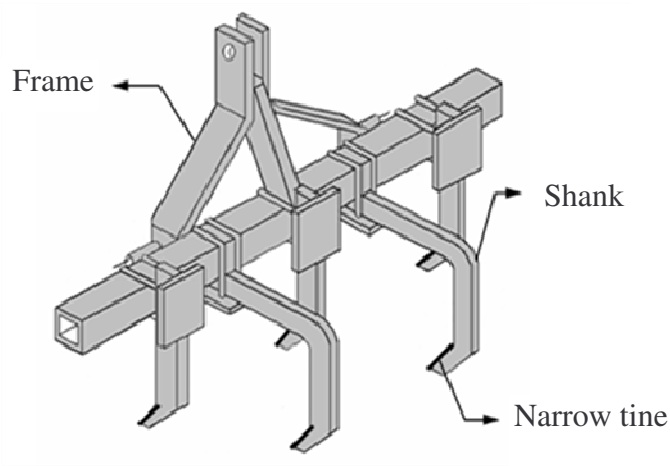

Figure 2-15 : Illustration of a five-shank chisel plough
(Tine width $w = 0.05$ m; rake angle $\alpha = 45°$;
tillage depth $d = 0.25$ m; tool speed $v = 1.67$ m. s^{-1})

Histograms and PDFs of the horizontal and vertical forces are shown in Figure 2-16. The probabilistic characteristics of these forces are presented in Table 2-5. From a statistical viewpoint, these results are in accord with the central limit theorem [29]. The majority of the horizontal and vertical force values are found to range between 0.5 and 6 kN and between 0.2 and 3 kN , respectively. The shape parameters of the horizontal and vertical forces are $\xi = 0.449, \xi = 0.447$, respectively. This means that the dispersions of these forces are very important and should be taken into consideration in the reliability analysis. Furthermore, the horizontal and vertical force values were positive for each set of tillage system parameters. In fact, the vertical force value depends on the rake angle. The positive vertical forces can be attributed to the rake angle of $45°$ considered in this study. Godwin [8] and Zhang and Kushwaha [24] reported that the vertical force becomes negative when the rake angle is larger than $60°$.

The correlation coefficient between the horizontal and vertical forces is found to be $\rho(P_H, P_V) = 0.93$. This means that the relationship between the two forces is quasi-linear and that an increase in horizontal force will cause an increase in vertical force [29]. In reality, the horizontal force P_H and vertical force P_V are calculated by combining the total force with the force of adhesion [4]. The effect of the total force on the horizontal and vertical forces is greater than the effect of the adhesion force such that the value of correlation coefficient is close to one.

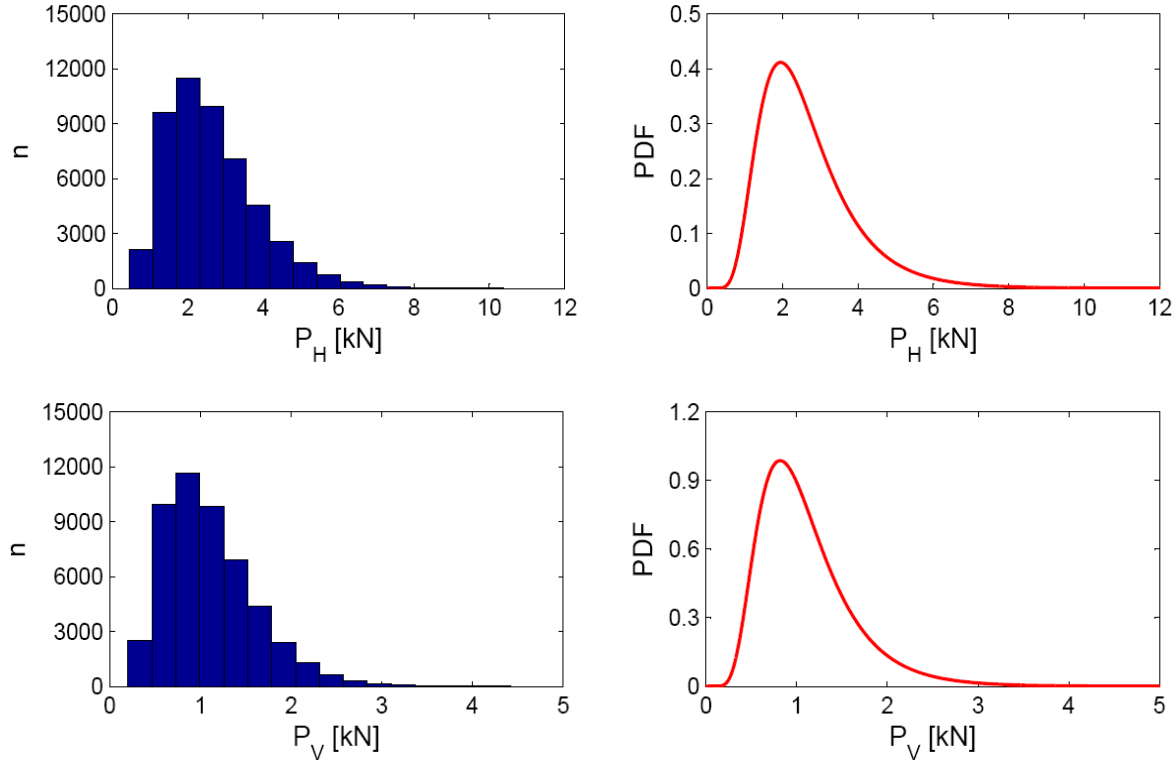

Figure 2-16 : Histograms and probability density functions for horizontal and vertical forces

Table 2-5 : Probabilistic characteristics of tillage forces

Force type	Distribution type	Distribution parameters
P_H, kN	Lognormal	$\mu = 0.872, \xi = 0.449$
P_V , kN	Lognormal	$\mu = 0.004, \xi = 0.447$

2.5 Conclusions

In this chapter, a probabilistic approach was proposed for modeling the variability in tillage forces. This approach accounts for: 1) the nature of agricultural soils that have heterogeneous and discontinuous structure 2) tolerances in tool design parameters due to manufacturing accuracies and 3) variations in operational conditions which are partially controlled. This approach was implemented for modeling the variability of tillage forces for the shank of a chisel plough.

The results allow us to draw the following conclusions: 1) both the horizontal and vertical forces have lognormal distributions with $\mu = 0.872, \xi = 0.449$ and $\mu = 0.004, \xi = 0.447$ for the horizontal and vertical forces, respectively and 2) the relationship between the horizontal and vertical forces is positive and quasi-linear with $\rho(P_H, P_V) = 0.93$. It is concluded that the dispersions of both forces are important and should be considered in the reliability analysis in the next chapter. Furthermore, the correlation coefficient has a high value and also it should be taken into account in the reliability analysis.

Chapter 3

Reliability-based design optimization

3.1 Introduction

This chapter is subdivided into seven sections. The first section presents the types of uncertainties in the design of structural systems and the developed approaches for dealing with the existence of these uncertainties in real engineering systems. A general formulation of the deterministic design optimization and its drawbacks are presented in the second section. The third section introduces the concept of failure probability and describes approximation methods and simulation techniques which are usually used to estimate the failure probability of a structure. A brief description of the reliability-based design optimization methods is then presented in the fourth section and more details are given for the reliability-index approach (RIA) and the sequential optimization and reliability assessment (SORA) used in this work. In the fifth section, the proposed reliability-based design optimization approach for tillage machines is presented. In the sixth section, a numerical application demonstrates the implementation of the proposed approach for the design of the shank of a chisel plough with considering the variability in tillage forces modeled in the previous chapter. Some conclusions end this chapter.

3.2 Design under uncertainty

A number of uncertainties are encountered during the design of structural systems. These uncertainties are resulting from the variability of applied loads and material properties, in addition to those resulting from the design modeling. They can be grouped in three main categories, namely inherent, model and statistical uncertainties [33]. Inherent uncertainty arises during the description of a physical process and still exists even if unlimited data is available. Model uncertainty results from the simplification of modeling a true physical process and can be minimized by using more sophisticated model. The third type of uncertainty is related to the fitting of a parametric distribution and this uncertainty can be decreased by increasing the number of fitting data points.

In the best case scenario in the design of structural systems, uncertainties can be reduced or minimized but they cannot be completely eliminated. Thus, all parameters of interest in an engineering design can be considered as random variables [30]. To overcome the presence of these uncertainties in the design analysis, two design approaches have been developed, namely deterministic and probabilistic designs. The deterministic design simplifies the problem by considering uncertain variables to be deterministic and accounts for uncertainties through the use of empirical safety factors. These factors that are based on the past experience, do not completely guarantee a safety or satisfactory performance [34].

The most important difference of the probabilistic design compared to the deterministic design is that in the probabilistic design uncertainties involved in the behavior of the structure under consideration are explicitly taken into account [33]. The probabilistic design performs calculations based on the probability distributions of design variables, instead of nominal or mean values only. This approach allows us to design for a specific reliability level.

3.3 Deterministic design optimization

The use of deterministic design optimization (DDO) approach in the design of structural systems is becoming more commonplace with the advent of computer technology and the development of finite element analysis (FEA) software. The name of this approach is derived from the use of safety factors in the constraint functions in the DDO problem to compensate the presence of uncertainties in the design variables. A general formulation of the DDO problem can be expressed by Equation (3.1).

$$\begin{aligned} &\text{Minimize } f(\{\mathbf{d}\}) \\ &\text{Subject to } g_j(\{\mathbf{d}\}) \geq 0 \qquad j = 1,2,\dots,N_{ineq} \\ &\qquad\qquad h_k(\{\mathbf{d}\}) = 0 \qquad k = 1,2,\dots,N_{eq} \\ &\qquad\qquad \mathbf{d}_i^l \leq \mathbf{d}_i \leq \mathbf{d}_i^u \qquad i = 1,2,\dots,N_{dv} \end{aligned} \tag{3.1}$$

where $f(\{\mathbf{d}\})$ is the objective function, $g_j(\{\mathbf{d}\})$ is an inequality constraint, $h_j(\{\mathbf{d}\})$ is an equality constraint, $\{\mathbf{d}\}$ is the vector of design variables subjected to upper and lower bounds and N_{ineq}, N_{eq} and N_{dv} are the number of inequality constraints, equality constraints and design variables respectively. Objective function, inequality constraints and equality constraints can be linear or non-linear. Therefore, several methods and algorithms have been developed to solve the DDO problem [35] [36] [37] [38].

Although the DDO approach provides an optimum design, it cannot guarantee the reliability level because the safety factors do not indicate the true safety of a design. Therefore, this approach can be unnecessarily restrictive on potential designs, in addition to providing no indication on the true design safety. For these reasons, design optimization based on reliability is needed to get optimum and reliable designs.

3.4 Structural reliability analysis

The reliability of a structure is defined as the probability that the structure is able to perform satisfactorily its functions for at least a given period of time, when used under stated conditions. Reversibly, the failure probability can be defined as the probability that the structure dose not perform satisfactorily its functions within a given period of time [33]. The reliability and the failure probability are always associated with a particular performance criterion that defines a certain limit state function $G(\{\mathbf{x}\},\{\mathbf{y}\}) = 0$ in physical space, where $\{\mathbf{x}\}$ is a vector of deterministic variables and $\{\mathbf{y}\}$ is a vector of random variables. The limit state represents the surface between the safe region $G(\{\mathbf{x}\},\{\mathbf{y}\}) > 0$ and the failure region $G(\{\mathbf{x}\},\{\mathbf{y}\}) < 0$ as illustrated in Figure 3-1.

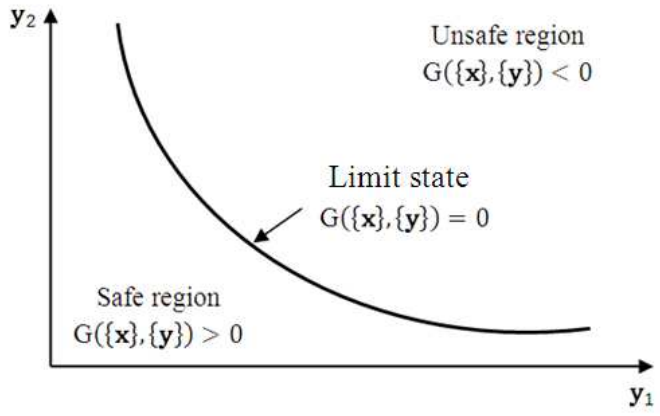

Figure 3-1 : Limit state concept

The limit state function can be linear or nonlinear, explicit or implicit function of the random variables. Therefore, it plays an important role in the development of structural reliability analysis methods [34].

Conventionally, the failure probability can be calculated by using the full distributional approach represented by the following integral:

$$P_f = \mathbf{P_r}[G(\{\mathbf{x}\},\{\mathbf{y}\}) < 0] = \int \cdots \int_{G(\{\mathbf{x}\},\{\mathbf{y}\})<0} f_{\{\mathbf{y}\}}(\mathbf{y}_1,\cdots,\mathbf{y}_n)\mathrm{d}\mathbf{y}_1\cdots\mathrm{d}\mathbf{y}_n \tag{3.2}$$

where P_f is the failure probability, $f_{\{\mathbf{y}\}}(\mathbf{y}_1,\cdots,\mathbf{y}_n)$ is the joint probability density function for the random variables $\{\mathbf{y}\}$ and $\mathbf{P_r}[.]$ is the probability operator when the integral is performed over the failure region $G(\{\mathbf{x}\},\{\mathbf{y}\}) < 0$.

Generally, evaluating the integral in Equation (3.2) is not simple because it represents a very small quantity and all of the necessary information for the joint density function is not available. Even if this information is available, evaluating the multiple integral is extremely complicated [34]. Therefore, several approximations of this integral are used to evaluate failure probability, namely the first-order reliability method (FORM) and the second-order reliability method (SORM), which are considered to be reliable computational methods [39]. These methods are described below. However, these methods require a background in probability and statistics. Other simulation techniques can be used to evaluate failure probability with only a minimal background in probability and statistics, but these methods require more computational time as compared to approximation ones. The method commonly used for this purpose is the Monte Carlo simulation technique [40].

3.4.1 Approximation methods

Approximation methods are based on the Taylor series approximations of the limit state function at the design point in normalized space. The most used approximations are the FORM and SORM methods [41]. The FORM method ignores the terms beyond the first-order term in the Taylor series, while the SORM method ignores the terms beyond the second-order term as illustrated in Figure 3-2.

The transformation of the limit state function from physical space to normalized space requires the transformation of random variables $\{\mathbf{y}\}$ to normalized independent variables $\{\mathbf{u}\}$, which can be given by:

$$\{\mathbf{u}\} = T(\{\mathbf{y}\}) \quad \Rightarrow \quad \{\mathbf{y}\} = T^{-1}(\{\mathbf{u}\}) \tag{3.3}$$

where $T(.)$ is the probabilistic transformation.

Different transformation methods have been developed to perform the probabilistic transformation depending on the information about the joint probability density function and the correlations between the design variables. Rosenblatt's transformation, Nataf's transformation, the equivalent normal distribution approximation and Hermite's transformation are some examples of these methods [42].

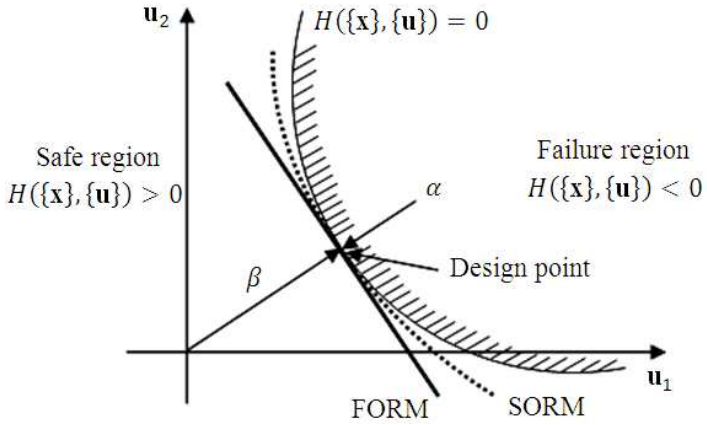

Figure 3-2 : Illustration of the FORM and SORM approximations

The search of the design point, also called the most probable failure point (MPFP), in the normalized space is a constrained optimization problem as expressed in Equation (3.4).

$$\begin{aligned} &\min \quad \mathrm{d} = \sqrt{\{\mathbf{u}\}^t\{\mathbf{u}\}} \\ &\text{s.t.} \quad \mathrm{H}(\{\mathbf{x}\},\{\mathbf{u}\}) = 0 \end{aligned} \tag{3.4}$$

where d is the distance from the origin of the axes to the limit state surface and $\{\mathbf{u}\}$ represents the coordinates of the checking point on the limit state function $\mathrm{H}(\{\mathbf{x}\},\{\mathbf{u}\})$ in normalized space.

Then, the failure probability can be calculated, according to the FORM method, by Equation (3.5).

$$P_{f\,\mathrm{FORM}} = \Phi(-\beta) \tag{3.5}$$

where $\Phi(\cdot)$ is the cumulative distribution function of a standard normal distribution and β is the reliability index which represents the minimum distance from the origin of the axes in normalized space to the limit state surface.

The accuracy of FORM method can be largely affected by the nonlinearity of the limit state function at the design point. However, for practical engineering problems, the FORM method gives sufficiently accurate estimation of the failure probability even when the limit state function is not linear [34].

The SORM approach was first explored by Fiessler et al. [43] using various quadratic approximations. A simple closed-form solution for the probability computation was proposed by Breitung [44] using the theory of asymptotic approximations as:

$$P_{f\,\mathrm{SORM}} = \Phi(-\beta)\prod_{i=1}^{n-1}(1+\beta\kappa_i)^{-1/2} \tag{3.6}$$

where κ_i denotes the principal curvatures of the limit state at the design point, and β is the reliability index computed by the FORM method.

The Breitung's form, presented in Equation (3.6), was improved by Hohenbichler [45] using various asymptotically exact formulae. Other complex asymptotic forms with three terms have proposed to calculate the probability of failure. Tvedt [46] proposed a three-term approximation in which the last two terms can be interpreted as correctors to Breitung's form. More accurate closed form formulas were derived using Maclaurin series expansion and Taylor series expansion [47] [48]. These formulas generally work well in the case of a large curvature radius and a small number of random variables.

3.4.2 Simulation techniques

Simulation techniques allow one to calculate the failure probability for both explicit and implicit limit state functions. Among the simulation techniques, the Monte Carlo simulation (MCS) is widely used for this purpose because of its simplicity and capability of handling problems with a large number of random variables [40]. The principal idea behind the MCS technique is to generate *N* values for each basic random variable, according to its probabilistic characteristics and then to evaluate the limit state function, deterministically, for each set of realizations of random variables, as shown in Figure 3-3. The failure probability can be calculated quite simply by Equation (3.7).

$$P_{f\mathrm{MCS}} = N_f / N \tag{3.7}$$

where N_f is the number of simulation cycles when $\mathrm{G}(\{\mathbf{x}\},\{\mathbf{y}\})$ is less than zero and *N* is the total number of simulation cycles, which equals to the number of generating values.

When more than one limit state function are involved in the reliability analysis. The MCS can be used directly to estimate the system failure, where the number of samples N_f is computed when one or all of the limit state functions are less than zero, depending on the system type, i.e. series system or parallel system. The accuracy of simulation can be determined by calculating the coefficient of variation (COV) of failure probability from Equation (3.8).

$$\mathrm{COV}(P_f) = \frac{\sqrt{\frac{(1-P_f)P_f}{N}}}{P_f} \tag{3.8}$$

where $\mathrm{COV}(P_f)$ is the coefficient of variation of failure probability and N is number of simulation cycles.

The accuracy in calculating failure probability increases when the number of simulation cycles increases. However, this requires more computational time. Therefore, other techniques have been developed to reduce the required number of samples, e.g. importance sampling and Latin hypercube sampling [49].

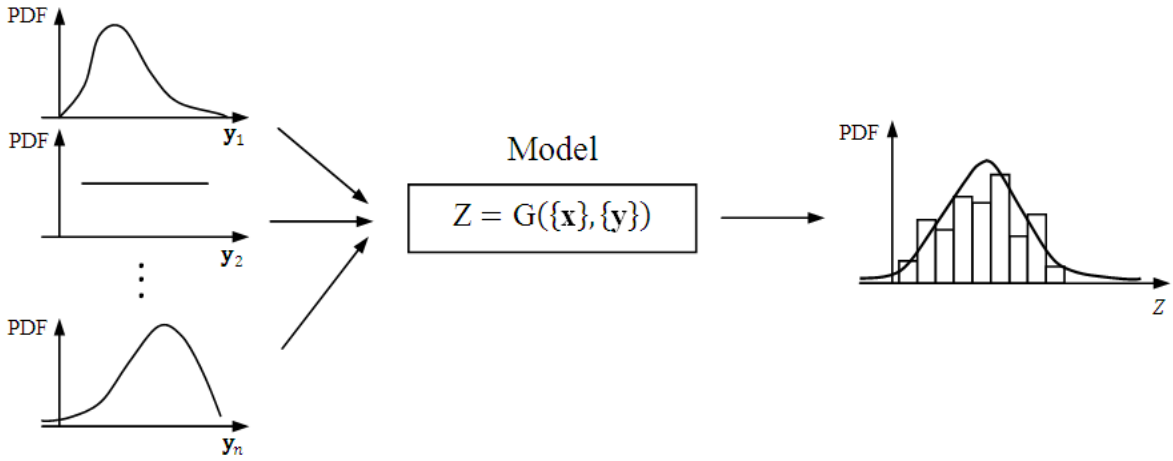

Figure 3-3 : Basic principle behind Monte Carlo simulation

3.5 Reliability-based design optimization

3.5.1 RBDO approaches

Reliability-based design optimization (RBDO) approaches have been developed to overcome the drawbacks of deterministic design optimization (DDO) methods, by quantifying the reliability of performance in probabilistic terms and include these terms directly in the design optimization as probabilistic constraints [50]. In the DDO approach, designer seeks the optimum values of design variables for which the objective function is the minimum and the deterministic constraints are satisfied. This approach does not take into consideration the uncertainties of design variables. In the RBDO approach, there is a trade-off between obtaining higher reliability and lowering cost.

During the last few years, a variety of different formulations have been developed for reliability based design optimization. A RBDO problem can be considered as an optimization problem subjected to both deterministic and probabilistic constraints that has a general form as expressed in Equation (3.9).

$$\begin{aligned} &\text{Minimize} && f(\{\mathbf{d}\}) \\ &\text{Subject to} && \begin{cases} \mathbf{P}_r[\mathrm{G}_i(\{\mathbf{d}\},\{\mathbf{y}\}) \le 0] \le P_{f_i}^T & i = 1,\dots,m \\ h_j(\{\mathbf{d}\}) \le 0 & j = m+1,\dots,M \end{cases} \end{aligned} \tag{3.9}$$

where $\{\mathbf{d}\}$ is the vector of design variables, $\{\mathbf{y}\}$ is the vector of random variables, f is the objective function, $\mathbf{P}_r[\cdot]$ is the probability operator, G_i is the ith performance function, $P_{f_i}^T$ is the target failure probability corresponding to ith performance function, h_j is the jth deterministic constraint, m is the number of performance functions and M is the total number of constraints.

The reliability constraints are the key constraints in the RBDO problem, as they require a considerable computation effort and this reveals the classical problems of efficiency, accuracy and stability. Several works have been developed to overcome the numerical difficulties and to improve both the efficiency and accuracy. Accordingly, one can distinguish between three different approaches [51], namely the two-level approach, the mono-level approach and the decoupled approach. The flowcharts of these approaches are illustrated in Figure 3-4.

The two-level approach consists of two nested optimization loops, where the inner loop deals with reliability assessment and the outer loop deals with cost optimization. Two approaches have been proposed to deal with the reliability constraints, namely the reliability index approach (RIA) and the performance measured approach (PMA). The reliability constraints are estimated, in the RIA method, by the reliability index approach by searching the most probable failure point (MPFP). While, the PMA method uses the minimum performance target point (MPTP) to satisfy the reliability constraints. The RIA and the PMA approaches are essentially inverses of one another and would provide the same solution if the constraints are active at the optimum. However, the PMA approach is superior to the RIA approach when many probabilistic constraints remain inactive throughout the optimization. A comparative study on the computational efficiency and the numerical stability of the RIA and RMA can be found in the report of Lee et al. [52].

The mono-level approach is proposed to avoid the use of two loops in RBDO problem. This approach replaces the reliability constraints by optimality conditions (e.g. the first order Karush-Kuhn-Tucker (KKT) optimality conditions of the first order reliability problem) or reformulates the RBDO problem in order to obtain a single loop optimization. Such methods can be found in the works of Ahn and Kwon [53], Kharmanda et al. [54] and Kuschel and Rackwitz [55].

The decoupled approach separates the reliability analysis from the optimization procedure so that the RBDO problem may be transformed to a sequence of deterministic optimization and reliability analysis. The methods proposed by Du and Chen [56] and Cheng et al. [57] are based on this concept.

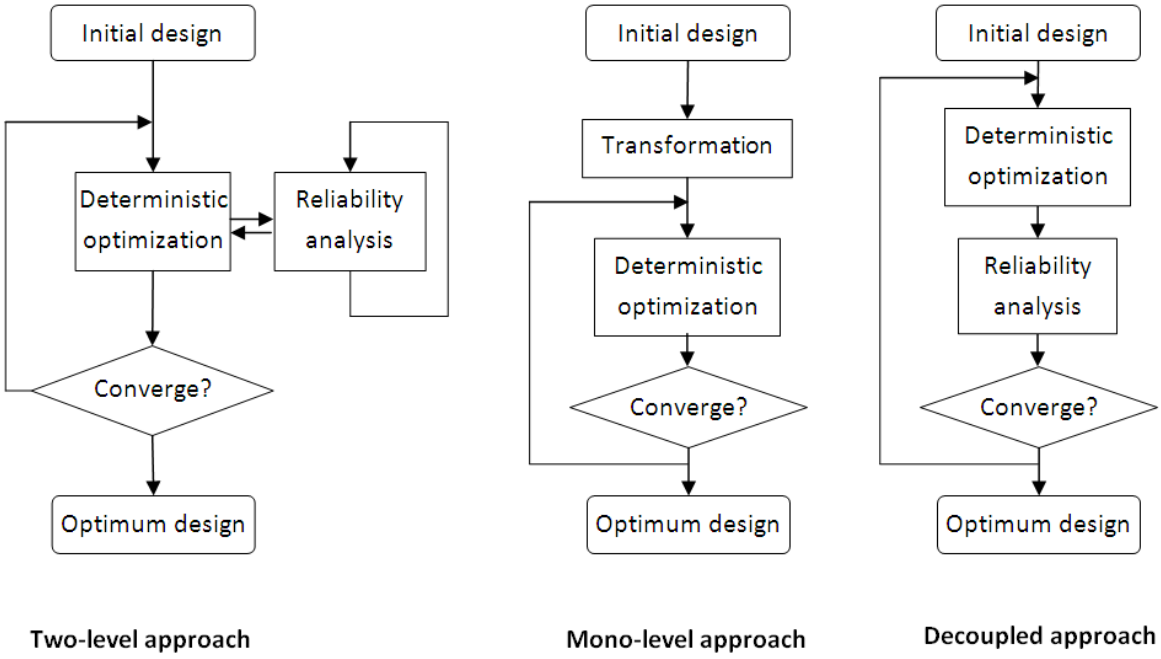

Figure 3-4 : Flowcharts of reliability-based design approaches

Yang and Gu [58] coded and tested four RBDO methods. They reported that the single-loop-single-vector (SLSV) approach converges nicely and requires few function evaluations. They also reported that the sequential optimization and reliability assessment method (SORA) shows promising results compared with those of two-level methods. The benchmark study of Aoues and Chateauneuf [51] compared the numerical performance of six RBDO methods through different numerical examples. They reported that the two-level approaches are simple to implement, but are usually inefficient for real structures. The mono-level approaches are based on some approximations, leading to some loss of precision. The decoupled approaches are generally efficient and accurate, but require specific implementation. Among the tested methods, they found that the single loop approach (SLA) is the most promising method for engineering structures, as it combines simplicity, efficiency and robustness. Despite the lower efficiency, the SORA method appears to be more robust and more accurate than the SLA method, and could thus be suitable for complex structural systems.

3.5.2 Reliability index approach (RIA)

The RIA method consists in using the FORM method to perform the reliability analysis, where the probabilistic constraints are replaced by the reliability index constraints, as presented in Equation (3.10). The main drawback of this method is due to the difficulties to compute the reliability constraints. However, it has the advantage of being simple to implement.

$$\begin{aligned} &\text{Minimize} && f(\{\mathbf{d}\}) \\ &\text{Subject to} && \begin{cases} \beta_i(\{\mathbf{u}\},) \geq \beta_i^T & i = 1, \dots, m \\ h_j(\{\mathbf{d}\}) \leq 0 & j = m+1, \dots, M \end{cases} \end{aligned} \tag{3.10}$$

where $\{\mathbf{u}\}$ is the vector of normalized variables, β is the reliability index and β^T is the target reliability index. The reliability index is computed by solving the constrained optimization problem of Equation (3.4).

3.5.3 Sequential optimization and reliability assessment (SORA)

The SORA method employs a decoupled strategy with a series of cycles of deterministic optimization and reliability assessment. In each cycle, optimization and reliability assessment are decoupled from each other; the reliability assessment is only conducted after the deterministic optimization to verify constraint feasibility. The key to this method is to shift the boundaries of violated constraints to the feasible direction based on the reliability information obtained in the previous cycle. The design is quickly improved from cycle to cycle and the computational efficiency is improved significantly [56]. The RBDO problem can be written, according to this method, as

$$\begin{aligned} &\text{Minimize} && f(\{\mathbf{d}\}^k) \\ &\text{Subject to} && \begin{cases} \mathrm{G}_i\left(\{\mathbf{d}\}^k - \delta_i^{k-1}, \{\check{\mathbf{y}}\}_i^{k-1}\right) \geq 0 & i = 1, \dots, m \\ h_j(\{\mathbf{d}\}^k) \leq 0 & j = m+1, \dots, M \end{cases} \end{aligned} \tag{3.11}$$

where k is the current cycle, $\{\check{\mathbf{y}}\}_i^{k-1}$ is the vector of minimum performance target point (MPTP) in physical space with respect to ith limit state, obtained in the previous cycle $k-1$ and δ_i^{k-1} is the shift parameter, given as

$$\begin{aligned} \{\check{\mathbf{y}}\}_i^{k-1} &= \mathrm{T}(\{\mathbf{u}^*\}^T) \\ \delta_i^{k-1} &= \{\mathbf{d}\}^{k-1} - \{\check{\mathbf{y}}\}_i^{k-1} \end{aligned} \tag{3.12}$$

where $\{\mathbf{d}\}^{k-1}$ is the vector of design variables, $\{\check{\mathbf{y}}\}_i^{k-1}$ is the MPTP in the physical space caculated by the probabilistic transformation T(·) of $\{\mathbf{u}^*\}^T$ which is obtained by solving the inverse reliability problem presented in Equation (3.13).

$$\begin{array}{ll} \text{Minimize} & \mathrm{G}_i(\{\mathbf{u}\}) \\ \text{Subject to} & \|\{\mathbf{u}\}\| = \beta_i^T \end{array} \tag{3.13}$$

where β_i^T is ith target reliability index corresponding to the ith limit state G_i. The use of the inverse reliability analysis instead of a full reliability analysis leads to time reduction and efficient strategy because the feasible region is identified with respect to the MPTP [51].

3.6 RBDO approach for tillage machines

The proposed RBDO approach for tillage machines is based on existing probabilistic design tools and RBDO methods. This approach consists of four main steps as illustrated in Figure 3-5.

The first step in the proposed approach is to decide on specific performance criteria and the functional relationships among the basic variables, corresponding to each failure scenario. For tillage machines, two different performance criteria can be considered. The first performance criterion is related to the mechanical resistance of tillage machines and the second one is related to the quality of tillage operation. Thus, the limit state functions that defined the safe region can be written as:

$$\mathrm{G}_1(\{\mathbf{x}\},\{\mathbf{y}\}) = \sigma_{ad} - \sigma_{max} \geq 0 \tag{3.14}$$

$$\mathrm{G}_2(\{\mathbf{x}\},\{\mathbf{y}\}) = \delta_{V_{ad}} - \delta_{V_{max}} \geq 0 \tag{3.15}$$

where σ_{ad} is the allowable stress, σ_{max} is the maximum stress, $\delta_{V_{ad}}$ is the allowable vertical displacement and $\delta_{V_{max}}$ is the maximum vertical displacement.

Limit state functions (Equations 3.14 and 3.15) are functions of basic random variables. These variables don't have the same variability and the same influence on the probability of failure. Therefore, the method proposed in Section 2.3.3 can be used to determine the vectors of deterministic $\{\mathbf{x}\}$ and random variables $\{\mathbf{y}\}$, in the second step. Integrating the results of sensitivity analysis into the reliability analysis reduces the computational time by omitting insignificant uncertainties of certain random variables.

In the third step, the MCS technique and FORM method are used to calculate the failure probability according to the limit state functions determined in the first step. The MCS technique is used directly to estimate the failure probability, when more than one

limit state function are involved in the reliability analysis. Then the number of samples N_f is computed when one of the limit state functions are less than zero. In the FORM method, the reliability index corresponding to each limit state function is calculated and then the bounding technique of Ditlevsen [59] is used to estimate the system failure when considering both limit state functions.

Based on the observation of Yang and Gu [58] and Aoues and Chateauneuf [51], the Sequential optimization and reliability assessment (SORA) method is selected to apply for the RBDO of tillage machines in the fourth step. In addition, Reliability index approach (RIA) method is applied to solve the same problem for the purpose of comparison the results of both methods.

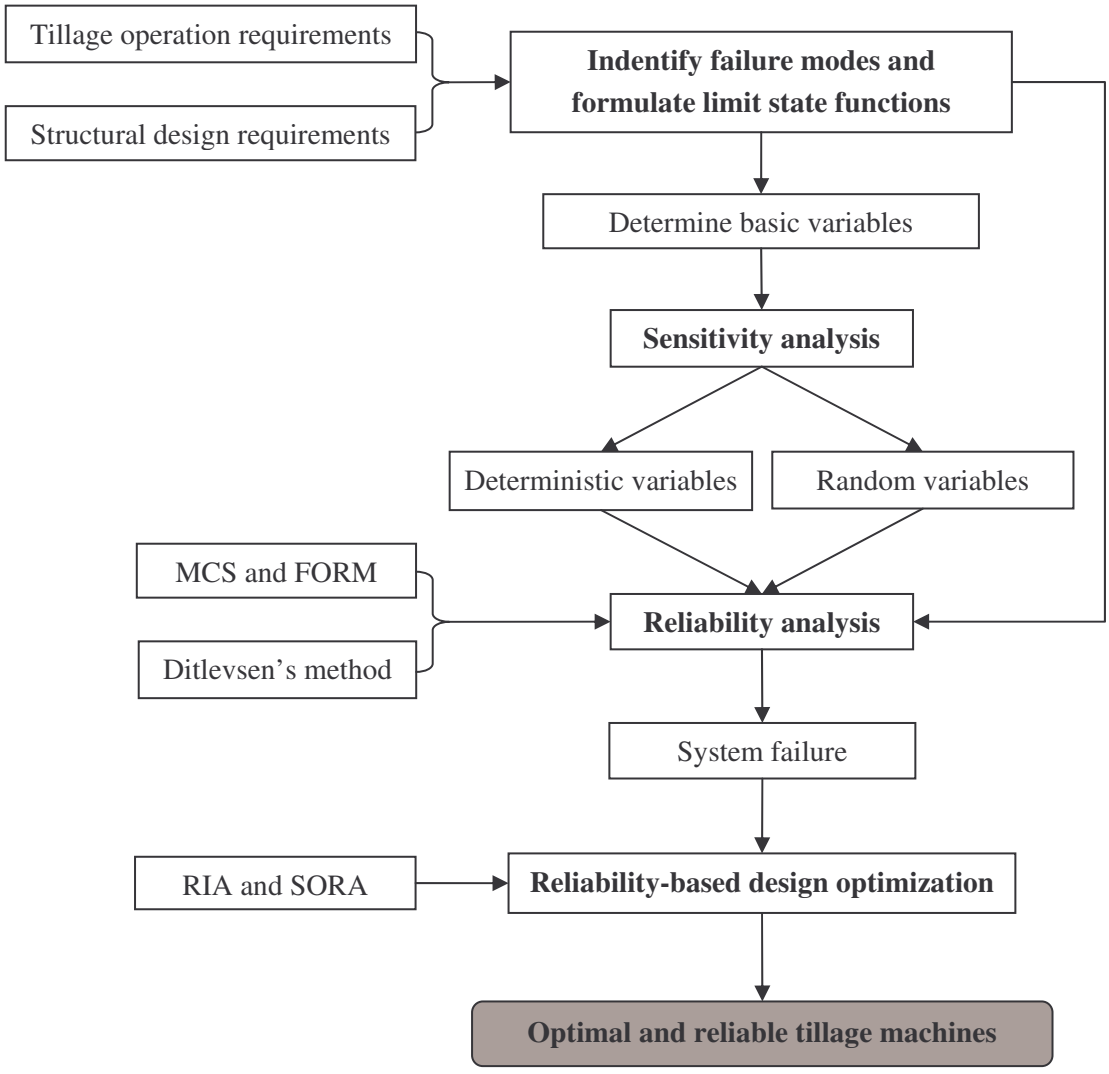

Figure 3-5 : Flowchart of the proposed RBDO approach for tillage machines

3.7 Numerical application

The proposed approach was implemented in MATLAB program (Mathworks INC. 2008) for finding the minimum volume of the shank chisel plough presented in Figure 3-6. The limit state functions of the studied shank were calculated using the finite element model CALFEM [60] and the optimization problem was solved by the optimization toolbox based on the SQP algorithm. The tolerance of convergence criteria was fixed to 10^{-3} for the absolute changes in design variables, the relative changes in the objective function and for the constraint verification. In addition, one million simulation cycles were used to evaluate failure probability according to the Monte Carlo simulation technique.

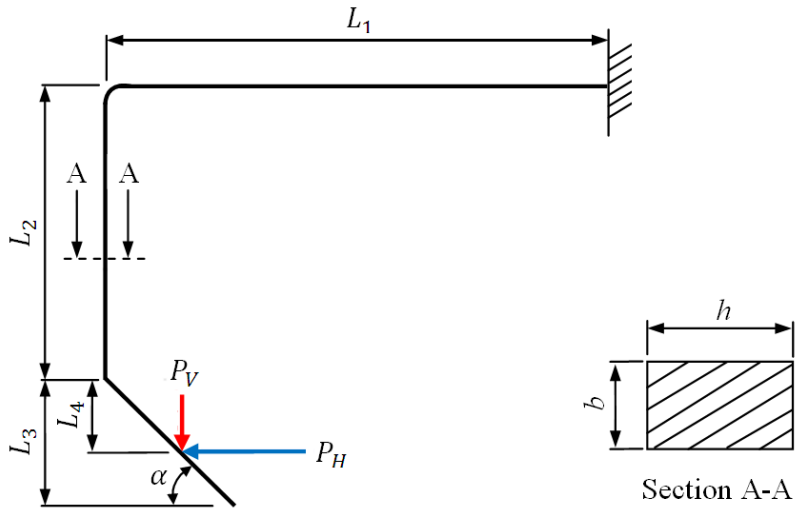

Figure 3-6 : A schematic drawing of the shank with acting forces

($L_1 = 60$ cm, $L_2 = 35$ cm, $L_3 = 15$ cm, $L_4 = 7.5$ cm, $\alpha = 45^{\circ}$, $h = 58$ mm, $b = 32$ mm, S 235)

3.7.1 Dispersion effects of random variables on limit state functions

The limit state functions (Equations 3.10 and 3.11) are functions of the following random variables, expressed by the following formula

$$G_i(\{\mathbf{x}\},\{\mathbf{y}\}) = f(P_H, P_V, \alpha, b, h, L_1, L_2, L_4) \tag{3.16}$$

The variability in the horizontal and vertical forces was determined using the methodology presented in Section 2.3.4. The variability in the rake angle α was considered during the determination of the variability in tillage forces so it is considered in this study as constant. The probability distributions of b, h, L_1 and L_2 were defined as uniform distributions with lower and upper bounds based on the manufacturing accuracy of $\pm 0.1mm$. Furthermore, we assumed that L_4, σ_{ad} and $\delta_{V_{ad}}$ have normal distributions with coefficient of variations

equal to 0.05. The statistical parameters for the random variables are presented in Table 3-1.

According to the sensitivity method, presented in Section 2.3.3, the dispersion effect of a random variable on limit state function can be estimated by computing the difference between the maximum and minimum values of limit state function for a confidence interval. The confidence interval was determined according to the probabilistic characteristics of the random variable. The results of sensitivity method are presented in Table 3-1.

Table 3-1 : Dispersion effects of basic random variables on limit state functions

Basic random variables	Statistical parameters of random variables		Results of sensitivity analysis	
	Distribution type	Distribution parameters	$\Delta G_1[kN]$	$\Delta G_2[mm] \times 10^{-3}$
$b[mm]$	Uniform	$L_b = 31.9, U_b = 32.1$	0.429	8.2
$h[mm]$	Uniform	$L_b = 57.9, U_b = 58.1$	0.468	13.7
$L_1[mm]$	Uniform	$L_b = 599.9, U_b = 600.1$	0	-0.6
$L_2[mm]$	Uniform	$L_b = 349.9, U_b = 350.1$	-0.029	-0.9
$L_4[mm]$	Normal	$m = 75, \sigma = 3.75$	3.070	95.3
$P_H[kN]$	Lognormal	$\mu = 0.872, \xi = 0.449$	-115.59	-3397.4
$P_V[kN]$	Lognormal	$\mu = 0.004, \xi = 0.447$	-8.365	1120.5
$\sigma_{ad}[MPa]$	Normal	$m = 235, \sigma = 11.75$	46.059	0
$\delta_{V_{ad}}[mm]$	Normal	$m = 6, \sigma = 0.3$	0	1176

(L_b and U_b are, respectively, lower and upper bounds of a uniform distribution; m and σ are, respectively, location and scale parameters of a normal distribution; ξ and μ are shape and scale parameters of a lognormal distribution)

We observe that the dispersion effects of the horizontal force on both limit state functions are larger than the dispersion effects of the other variables ($\Delta G_1 = -115.59[kN]$, $\Delta G_2 = -3397.4 \times 10^{-3}[mm]$) . In addition, the dispersion effects of the vertical force are significant comparing to the dispersion effects of the other variables. The dispersion effects of L_1 and L_2 are not important and they can be considered as deterministic variables in the reliability analysis. The vectors of deterministic and random variables are defined, according to the results of the sensitivity method, as

$$\{\mathbf{x}\} = (L_1, L_2)$$
$$\{\mathbf{y}\} = \left(b, h, L_4, P_H, P_V, \sigma_{ad}, \delta_{V_{ad}}\right) \quad (3.17)$$

Therefore, the uncertainties of L_1 and L_2 were omitted during the reliability analysis and the uncertainties of the other variables $\left(b, h, L_4, P_H, P_V, \sigma_{ad}, \delta_{V_{ad}}\right)$ were taken into consideration.

3.7.2 Reliability analysis

In order to determine the effect of limit state functions on the failure probability, the reliability analysis was applied three times; with two times considering one limit state function only (Equations 3.14 and 3.15) and in the third time, both limit state functions were taken into account. Furthermore, the reliability analysis was applied two times to determine the effect of the correlation coefficient between the tillage forces on the failure probability. At the first time, the correlation between the horizontal and vertical forces was ignored. Then, this correlation was taken into consideration in the second time. In the later case, two transformations were used [61] [62] to transform the correlated random variables $\{\tilde{\mathbf{y}}\}$ into uncorrelated or statistically independent random variables $\{\mathbf{u}\}$. The first one transforms the correlated random variables $\{\tilde{\mathbf{y}}\}$ to correlated reduced variables $\{\tilde{\mathbf{u}}\}$ and the second one transforms the correlated reduced variables $\{\tilde{\mathbf{u}}\}$ to uncorrelated reduced variables $\{\mathbf{u}\}$.

The coordinates of the design points according to the FORM method with considering both the presence and the absence of the correlation between the tillage forces are presented in Table 3-2.

Table 3-2 : Coordinates of the design points

	Non-correlated random variables		Correlated random variables	
	G_1	G_2	G_1	G_2
$b[mm]$	31.99	31.99	31.99	31.99
$h[mm]$	57.99	57.99	57.99	57.99
$L_4[mm]$	74.75	74.76	74.72	74.72
$P_H[kN]$	9.34	8.73	8.93	10.95
$P_V[kN]$	1.03	0.91	3.46	3.87
$\sigma_{ad}[MPa]$	230.87	235	231.08	235
$\delta_{V_{ad}}[mm]$	6	5.91	6	5.88

The failure probabilities obtained from the MCS technique and the FORM method, for both the absence and presence of the correlation between the horizontal and vertical tillage forces, are presented in Table 3-3.

Table 3-3 : Results of reliability analysis

		$P_{f1} \times 10^{-3}$	$P_{f2} \times 10^{-3}$	$P_{f-sys} \times 10^{-3}$
Non-correlated random variables	MCS	1.280	1.915	2.025
	FORM	1.118	1.819	1.819-2.329
Correlated random variables	MCS	1.635	0.340	1.640
	FORM	1.559	0.293	1.559-1.637

The following remarks can be extracted from the reliability analysis study:

- The obtained results from the MCS technique and the FORM method are quasi-identical when considering each one of the limit state functions for the two cases of non-correlated and correlated random variables, e.g. for the case of non-correlation between the random variables $P_{f1\,MCS} = 1.280 \times 10^{-3}$ and $P_{f1\,FORM} = 1.118 \times 10^{-3}$. This indicates that for this application there is no need to use higher-order approximations as the SORM method to improve the accuracy.
- The modification of the reliability level, resulted by the correlation between the horizontal and vertical forces, is significant especially, for the second limit state function.
- For the case of correlated random variables, the value of the failure probability for the second limit state function is not important and the difference between failure probability when considering the first limit state function P_{f1} and the system failure P_{f-sys} can be ignored.

From the above-mentioned points it can be concluded that the FORM method can be used to calculate the failure probability by considering the first limit state function only and with taking into account the presence of the correlation between the tillage forces. This makes the evaluation of the failure probability simpler and less time consuming, while at the same time provides results with sufficient accuracy.

3.7.3 RIA and SORA methods

The RIA and SORA methods were applied to find the minimum volume of the shank chisel plough. For both RBDO methods, b and h were considered as design variables and their initial values were $32\ mm$ and $58\ mm$, respectively. The deterministic constraints based on the design variables were assumed to be $b \geq 20$ and $b \geq 0.4h$. The reliability level was calculated by solving the inverse reliability problem for a target reliability index equals to $\beta^T = 3$ by considering only the first limit state function and the correlation between tillage forces.

The RIA method is converged to the minimum objective function of $f^* = 1.95 \times 10^6\ mm^3$ corresponding to the optimal point $\{\mathbf{d}\}^* = [25.96\ mm, 64.90\ mm]$, while the SORA method is converged to the minimum objective function of $f^* = 1.96 \times 10^6\ mm^3$ corresponding to the optimal point $\{\mathbf{d}\}^* = [26.02\ mm, 65.05\ mm]$, as illustrated in Figure 3-7.

The optimal solutions obtained by both methods are nearly identical. However, the RIA method requires 1100 evaluations for the finite element model, while the SORA method requires 397 evaluations. From a numerical viewpoint, the SORA method is more efficient than the RIA method. Therefore, the SORA method can be adopted for solving the RBDO problem for soil tillage machines.

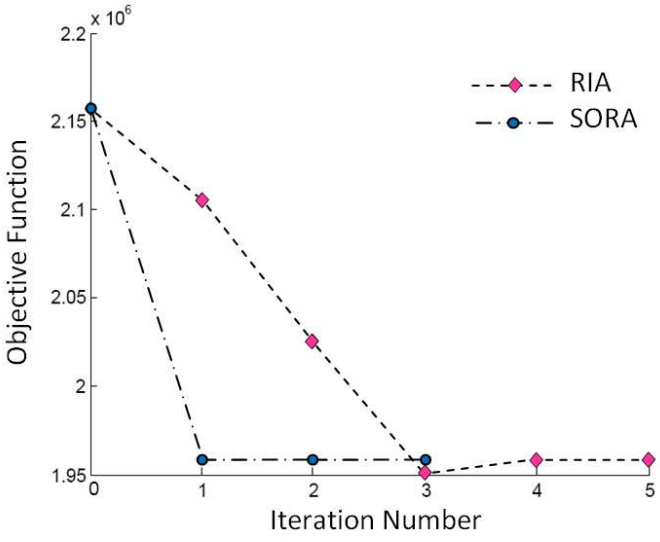

Figure 3-7 : Objective function history

By comparing the results of the SORA method by the initial design with $\beta^0 = 2.95$ and $f^0 = 2.15 \times 10^6$. We find that the SORA method improves slightly the

reliability index in order to respect the target reliability index and reduces the objective function by 9.25%. Furthermore, the percent change of the ratio β/f is increased by 11.2%.

3.7.4 Optimal reliability analysis

The SORA method was used in the optimal reliability analysis to find the optimal reliability that minimizes the expected total cost approximated by Equation (3.18).

$$\mathrm{C}_{Tot} = c_I f + c_f f P_f \tag{3.18}$$

where C_{Tot} is the total cost, c_I is a constant determines the impact of the objective function f on the total cost (in this example, f represents the shack volume) and c_f is a constant determines the impact of the failure probability P_f on the total cost. Figure 3-8 represents the relationships between the total cost and the failure probability for $c_I = 10$ [MU/kg] and $c_f = 1000$ [MU/kg].

The optimal reliability is found to be $P_{f\,Opt} = 0.95 \times 10^{-3}$ (i.e. $\beta_{Opt} = 3.105$) which is different from the target reliability used in this work $\beta^T = 3$. The total cost at the target reliability is larger than the total cost at the optimal reliability. Therefore, to find the best compromise between the objective function and the reliability level, the optimal reliability analysis should be integrated into the RBDO problem.

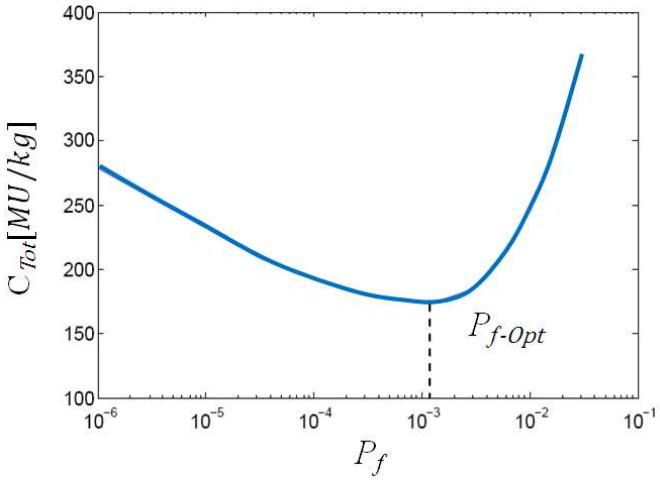

Figure 3-8 : Total cost-failure probability relationships

3.8 Conclusions

A reliability-based design optimization approach for tillage machines, based on existing probabilistic design tools and RBDO methods, was presented in this chapter. The four main steps of the proposed approach were explained and implemented for the design of the shank of a chisel plough. From the results of the reliability analysis study, it is shown that the FORM method can be used to calculate the failure probability of the studied shank by considering the first limit state function only and with taking into account the presence of the correlation between the tillage forces. These observations were taken into account when implementing the RIA and SORA methods. All the same, the results show that the SORA method is more efficient and reduces the computational time, comparing with the RIA method.

Overall, the proposed approach improves slightly the reliability index in order to respect the target reliability index $\beta^T = 3$ and reduces the objective function by 9.25%. On the contrary, the optimal reliability analysis provides different reliability index ($\beta_{Opt} = 3.105$) from that used in this work. Therefore, it is recommended to integrate the optimal reliability analysis into the RBDO approach to find the best compromise between the total cost and the reliability assurance.

Chapter 4

Modeling the spatial variability in tillage forces

4.1 Introduction

This chapter intends to propose a new model for modeling the spatial variability in tillage forces, by considering the variability in tillage forces derived from both the variability in tillage system parameters and soil failure patterns, for the purpose of fatigue analysis of tillage machines. This chapter consists of five sections. The first section shows the necessity to model the spatial variability in tillage forces for estimating the life time of tillage machines. The second section begins with the description of soil failure mechanism, followed by the types of soil failure and a discussion of the factors contributed to the changes of soil failure mechanism is given. In the third section, the proposed model is explained in detail. The basic assumptions for the proposed model are presented, followed by the methods used to model the global and local tillage forces and then the incorporation of these forces into the total tillage forces is described. The proposed model is implemented for modeling the spatial variability in tillage forces on the shank of a chisel plough in the fourth section. At the end of this chapter, some conclusions are presented.

4.2 Necessity of modeling the spatial variability in tillage forces

Mechanical loads on tillage machines show considerable variability due to the variability in tillage system parameters and the mechanical behavior of soil during failure. The variability in tillage system parameters reflects the variability in soil engineering properties and the variations in tool design parameters and operational conditions. Several analytical (e.g. McKyes and Ali [14]; Grisso et al. [15]) and numerical models (e.g. Mouazen and Neményi [20]; Shen and Kushwaha [63]) of soil-tool interaction have been developed to predict tillage forces for assigned tillage system parameters. Furthermore, the effects of tillage system parameters on tillage forces have been investigated [8] [17].

The soil failure involves the development of successive shear planes in front and at the side of tillage tools, which leads to distinct soil failure blocks as the tine moves forward through the soil. The repeated formation of soil crescents creates cyclic loading on the tillage tool. The variability in tillage forces due to the soil failure has been observed in many works in the literature. The current state of knowledge suggests that there are only experimental works available to estimate the within-field spatial variability in tillage forces [64] [65] [66]. These methods do not provide a tool for estimating the life time of tillage machines due to fatigue as it cannot account for all affecting parameters. Form a fatigue analysis viewpoint, it is essential to account for the effects of the variability in tillage forces on the resulted stress on tillage machines. Therefore, the main objective of this chapter is to propose a model for describing the spatial variability in tillage forces for the purpose of fatigue analysis of tillage machines.

4.3 Soil failure mechanisms

As mentioned before, the soil failure involves the development of successive shear planes that leads to distinct soil blocks as the tine moves forward through the soil. At the beginning of soil failure, the force required to cut the soil is quite high, because most of the soil is elastic and offers significant resistance [67]. As the tool moves, more and more soil begins to yield and fail, resulting in the propagation of failure planes or cracks from the tip of the tillage tool to the surface as illustrated in Figure 4-1. Once the soil begins to yield, the magnitude of the required force drops and reaches a residual level as the soil in front of the tool reaches a steady state in terms of crack propagation. As the tillage tool is dragged further, new failure planes are initiated in the soil in front of the tool and this cycle of peak and residual force repeats itself as shown in Figure 4-2.

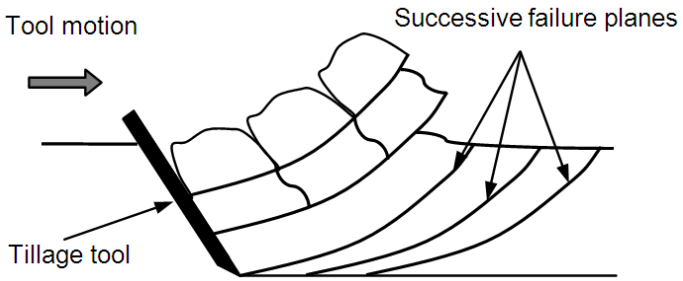

Figure 4-1 : Successive failure planes in front of the tool

Jayasuriya et al. [10] represented the relationships between the tine force and displacement in three soil types as shown in Figure 4-3. The tine force-displacement curve has high amplitude and low frequency in frictional-cohesive soils. It is observed the decrease of amplitude and the increase of the frequency in frictional soils. Both the amplitude and frequency decrease in cohesive soils.

Stafford [68] identified two types of soil failure, namely the brittle failure and the flow failure. Rajaram and Erbach [69] reported the following four soil failure mechanisms: 1) collapse failure, 2) fracture failure, 3) chip-forming failure and 4) plastic and frictional flow failures. They attributed the changes of soil failure mechanisms to two main factors: the soil type and the moisture content

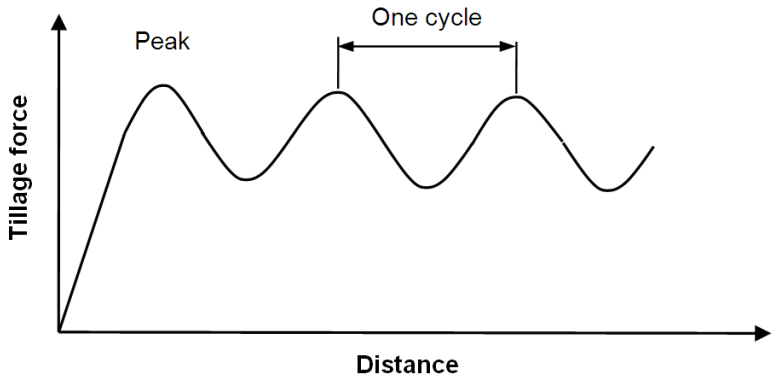

Figure 4-2 : Fluctuations in the tillage force due to formation of failure planes in the soil

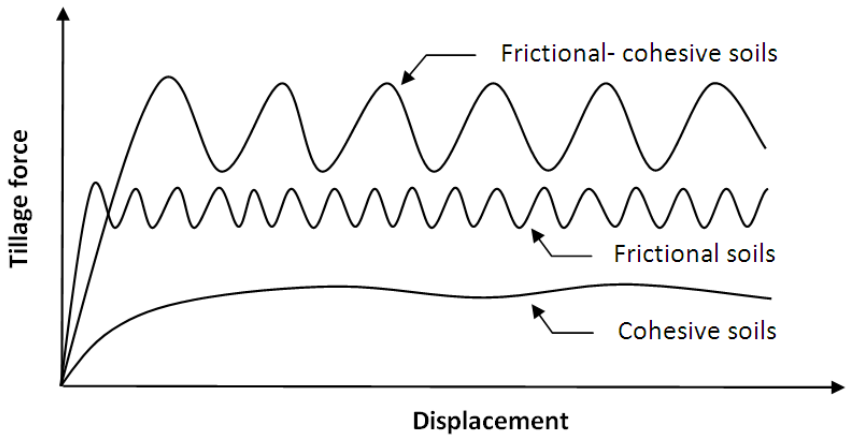

Figure 4-3 : Typical tine force-displacement curves

Makanga et al, [70] studied the effects of the tine rake angle and the aspect ratio (tillage depth/tool width) in a laboratory glass-sided soil bin with a dry compact loam soil with 5.2 % (d.b.) moisture content. They concluded that the horizontal and vertical soil

reactions under dry soil moisture conditions were cyclic. The cyclic variations in the soil reactions were due to the soil failure being repetitive and cyclic in nature throughout the tine travel. The maximum soil reactions were observed when the soil shearing began, while the minimum reactions corresponding to the stage when the shear surface was fully developed. In addition, they found that the wave length, the ratio of peak to trough value (the ratio of maximum tillage force to minimum tillage force) and the amplitude of variation in soil reactions were all affected by the tine design parameters.

4.4 Modeling the spatial variability of tillage forces

4.4.1 Basic assumptions for the proposed model

The basic assumptions behind the proposed model are that 1) the spatial variability of tillage forces derived from the variability in tillage system parameters is random, reflecting the heterogeneity in agricultural soils, the uncontrolled field operational conditions during tillage and the manufacturing tolerances of tool design parameters and 2) the spatial variability of tillage forces derived from the mechanical behavior of soil failure is cyclic, reflecting the repeated formation of soil crescents in front of the tool. In addition, we suppose that the total tillage force is the sum of two types of forces, namely the global tillage force and the local tillage force. The global tillage force is due to the tillage system parameters (soil engineering properties, tool design parameters and operational conditions) and the local tillage force is due to the soil failure of cyclic nature.

Conventionally, a tillage force P is determined by its horizontal P_H and vertical P_V components. Therefore, the horizontal and vertical forces can be calculated, according the earlier assumption, by Equations (4.1) and (4.2).

$$P_H = P_{HG} + P_{HL} \tag{4.1}$$

$$P_V = P_{VG} + P_{VL} \tag{4.2}$$

where P_{HG} is the global horizontal force in kN, P_{HL} is the local horizontal force in kN, P_{VG} is the global vertical force in kN and P_{VL} is the local vertical force in kN.

The variability in the global tillage forces (P_{HG}, P_{VG}) can be modelled using the methodology proposed in Chapter 2. This methodology is based on the estimation of tillage forces according to the McKyes-Ali model accounting for the variability in tillage system parameters. The local tillage forces (P_{HG}, P_{VG}) have been observed in many works in the literature but there are no available models can be used to estimate these forces. However,

the majority of reports are attributing these forces to nearly the same parameters contributing to the global tillage forces [71]. Therefore, we assume that the local tillage force components can be estimated as a percentage of the global tillage force components as shown in Equations (4.3) and (4.4).

$$P_{HL} = \tau . P_{HG} \tag{4.3}$$

$$P_{VL} = \tau . P_{VG} \tag{4.4}$$

where τ is the percentage of the local tillage force to the global tillage force. The high values of τ corresponding to a brittle soil failure and the little values of τ corresponding to a flow soil failure. In other words, the values of the local tillage forces (P_{HL}, P_{VL}) are important for the brittle soil failure since the force cyclic pattern is much more pronounced that with flow failure, while the values of these forces are nearly zero when the soil failure is of flow type [10].

The linear correlation between the global and local tillage forces may not be accurate for all soil texture types and all operational conditions. Thus, more work should be done to investigate the relationship between the global and local tillage forces.

Based on the earlier assumptions, the spatial variability in tillage forces can be represented by the spatial variability in the global and local tillage forces, as shown in Equations (4.5) and (4.6).

$$P_H(d) = P_{H1}(d) + P_{H2}(d) \tag{4.5}$$

$$P_V(d) = P_{V1}(d) + P_{V2}(d) \tag{4.6}$$

where P_{H1} represents the spatial variability in the global horizontal force in kN, P_{H2} represents the spatial variability in the local horizontal force in kN, P_{V1} represents the spatial variability in the global vertical force in kN, P_{V2} represents the spatial variability in the local vertical force in kN and d is the distance travelled in m.

4.4.2 Modeling the spatial variability in the global tillage forces

The spatial variability in the global tillage forces (P_{H1}, P_{V1}) is resulting from the within-field spatial variability of soil resistance and uncontrolled operational conditions. This spatial variability can be attributed to several factors, e.g. the characteristics of the field, the geography and topography of the field and the soil management system (no-till, reduced till or conventional tillage). Therefore, the spatial variability in the global tillage forces changes from one location to another within the same field and from field to field. To take these observations into account, we model the spatial variability in the global

tillage forces with the following assumptions: 1) the spatial variability in the global tillage forces is linear and 2) the distance S_1 between two successive changes of the values of global tillage forces is random.

The linearity of the spatial variability in the global tillage forces between the global tillage force samples may not be an accurate assumption. However, the increase of the global tillage force samples improves the accuracy of this model. Taking the distance S_1 as a random allows considering the variability in the field characteristics over the distance d. Based on these assumptions, the spatial variability in the global tillage forces can be expressed as in Equations (4.7) and (4.8). An illustration of the spatial variability in the global tillage forces over the distance d is shown in Figure 4-4.

$$P_{H1}(d) = P_{HG}(i) + \left(P_{HG}(i+1) - P_{HG}(i)\right)\frac{d - \sum_{k=1}^{i-1} S_1(k)}{S_1(i)} \qquad i = 1, \dots, n \qquad (4.7)$$

$$P_{V1}(d) = P_{VG}(i) + \left(P_{VG}(i+1) - P_{VG}(i)\right)\frac{d - \sum_{k=1}^{i-1} S_1(k)}{S_1(i)} \qquad i = 1, \dots, n \qquad (4.8)$$

where $P_{HG}(i)$ is the i*th* global horizontal force sample in kN, $P_{VG}(i)$ is the i*th* global vertical force sample in kN, S_1 is the distance between two successive changes of the global tillage force values in m, $\sum_{k=1}^{i-1} S_1(k)$ is the cumulative sum of $S_1(i)$ for $k =$ 1 to $i - 1$ and n is the number of the global tillage force samples.

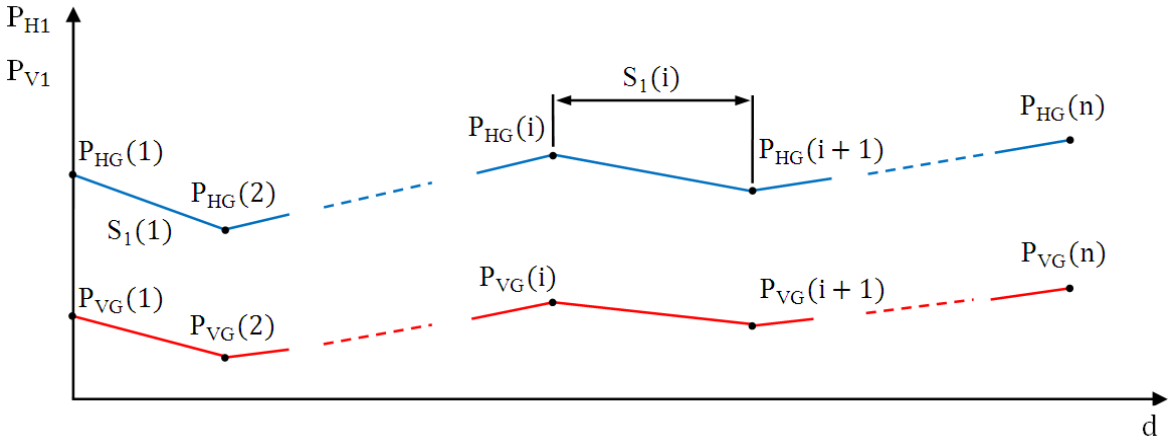

Figure 4-4 : Illustration of the spatial variability in the global tillage forces

4.4.3 Modeling the spatial variability in the local tillage forces

As mentioned before, the soil failure creates cyclic loading on tillage tools by the repeated formation of soil crescents. The global tillage forces are calculated at failure when the tillage forces achieve their maximum values. The total tillage forces reach their maximum values at failure (at this stage, the value of total tillage force is equal to the value of global tillage force) and then drop down after the first soil block has formed and these forces will increase to form the second soil block until achieve failure and so on. Therefore, we can suppose that the total tillage forces fluctuate below the global tillage forces.

Based on the fact that the effect of the soil failure in the tillage forces is cyclic, the sinusoid function is used to describe the spatial variability in the local tillage forces with the amplitude P_{HL} and cycle length S_2. Therefore, the spatial variability in the local tillage forces can be expressed as in Equations (4.9) and (4.10) and illustrated as in Figure 4-5. The terms $-P_{HL}(j)$ and $-P_{VL}(j)$ are added to these Equations to keep the values of local tillage forces fluctuate below the values of global tillage forces.

$$P_{H2}(d) = P_{HL}(j)\sin\left(2\pi\frac{d-\sum_{k=1}^{i-1}S_1(k)-\sum_{l=1}^{j-1}S_2(l)}{S_2(j)}\right)-P_{HL}(j)\quad j=1,\dots,m \tag{4.9}$$

$$P_{V2}(d) = P_{VL}(j)\sin\left(2\pi\frac{d-\sum_{k=1}^{i-1}S_1(k)-\sum_{l=1}^{j-1}S_2(l)}{S_2(j)}\right)-P_{VL}(j)\quad j=1,\dots,m \tag{4.10}$$

where $P_{HL}(j)$ is the j*th* local horizontal force in kN, $P_{VL}(j)$ is the j*th* local vertical force in kN, $S_2(j)$ is the cycle length of the j*th* cycle in m, l is the number of calculated values in a cycle and m is the number of cycles between two successive changes of the global tillage forces.

4.4.4 Modeling the spatial variability in the total tillage forces

By combining the spatial variability in the global and local tillage forces and taking into account the assumption that the local tillage force components can be estimated as a percentage of the global tillage force components, it concludes that the spatial variability in tillage forces can be represented by the following five parameters:

$$P_H(d) = f(P_{HG}, S_1, S_2, \tau) \tag{4.11}$$

$$P_V(d) = f(P_{VG}, S_1, S_2, \tau) \tag{4.12}$$

All of these parameters can be considered as variables to represent the variability in the forces on the tillage tool during the tillage operation, as shown in Figure 4-6.

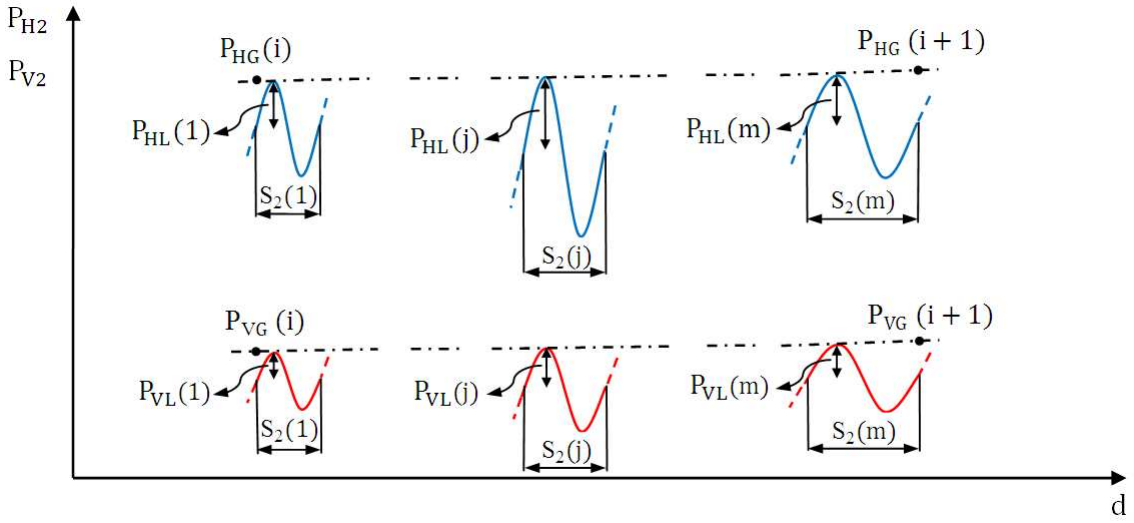

Figure 4-5 : Illustration of the spatial variability in the local tillage forces

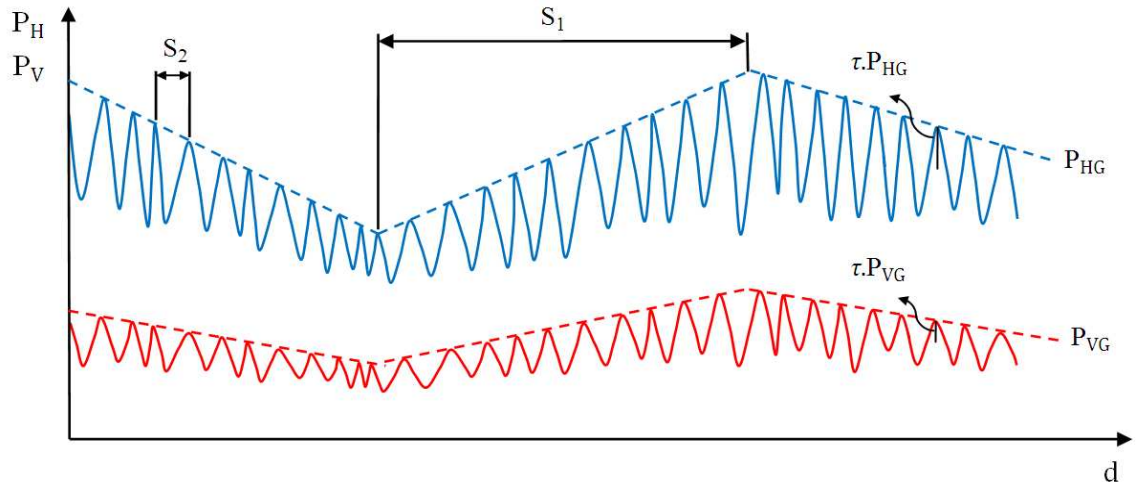

Figure 4-6 : Illustration of the spatial variability in the horizontal and vertical forces

4.4.5 Special cases

Two special cases of spatial variability in tillage forces, namely at constant global tillage forces and at insignificant local tillage forces are shown in Figure 4-7 and Figure 4-8, respectively. The first case supposes that all tillage system parameters do not vary during tillage. This assumption may be suitable for quasi-homogeneous soils and when the variations in the operational conditions are not important. The second case can be used to represent the spatial variability in tillage forces when the soil failure is of flow type. However, in most cases, both the global and local tillage forces should be taken into consideration in the description of the spatial variability in tillage forces.

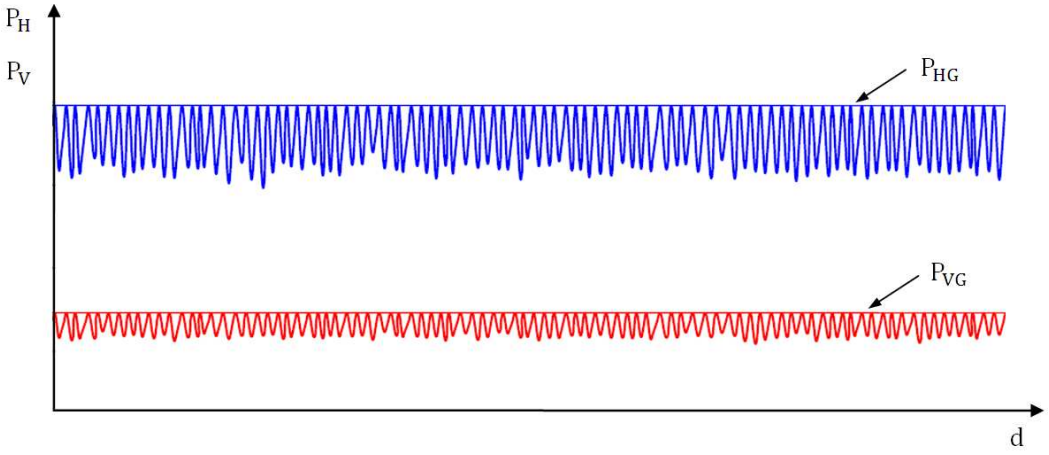

Figure 4-7 : Spatial variability in tillage forces for constant global tillage forces

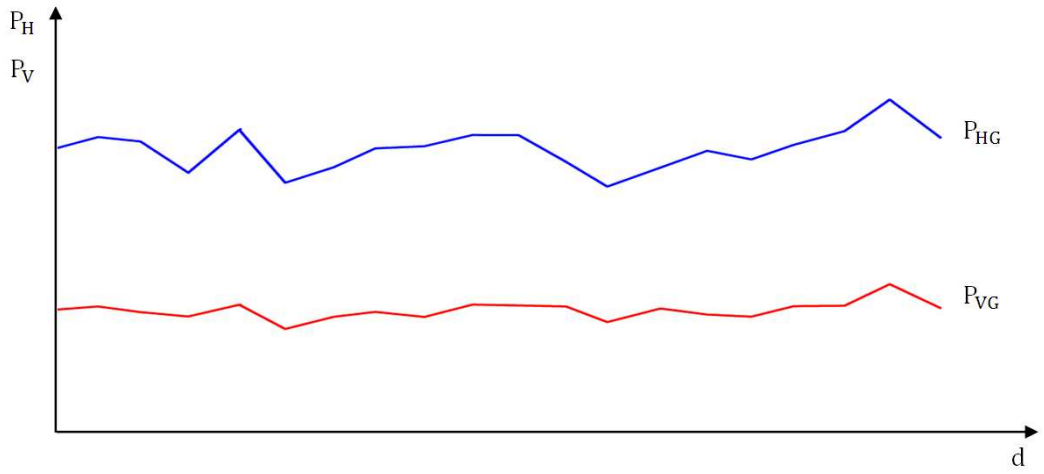

Figure 4-8 : Spatial variability in tillage forces when omitting local tillage forces

4.5 Modeling the spatial variability of tillage forces on the shank chisel plough

The proposed model, presented in Section 4.3, was implemented in MATLAB program (Mathworks INC. 2008) to model the spatial variability in tillage forces on the shank of a chisel plough shown in Figure 4-9. The shank section is rectangular with $h = 58\ mm$ and $b = 32\ mm$.

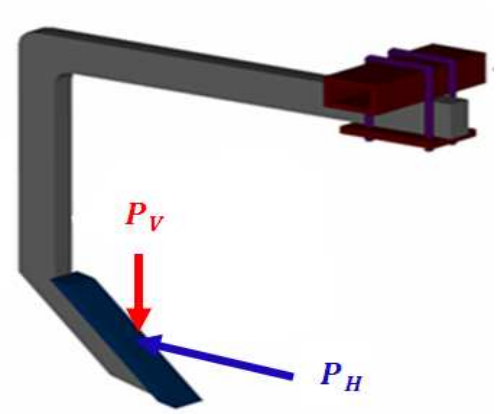

Figure 4-9 : Illustration of the shank of a chisel plough with tillage forces

We found in Section 2.4.3 that the variability in the global horizontal and vertical forces followed lognormal distributions. The distribution parameters of these forces were $\mu_{P_{HG}} = 0.872$, $\xi_{P_{HG}} = 0.449$, $\mu_{P_{VG}} = 0.004$ and $\xi_{P_{VG}} = 0.447$, where μ and ξ are the scale and shape parameters of a lognormal distribution, respectively. The correlation coefficient between P_{HG} and P_{VG} was found to be $\rho(P_{HG}, P_{VG}) = 0.93$. Therefore, the variability in the local horizontal and vertical forces should have lognormal distributions with the following distribution parameters $\mu_{P_{HL}} = \ln(\tau) + \mu_{P_{HG}}$, $\xi_{P_{HL}} = \xi_{P_{HG}}$, $\mu_{P_{VL}} = \ln(\tau) + \mu_{P_{VG}}$ and $\xi_{P_{VL}} = \xi_{P_{VG}}$.

In this work, τ was selected to be equal to 0.2 for brittle failure. Furthermore, we assumed that S_1 and S_2 have normal distributions. The distribution parameters of the model's parameters are listed in Table 4-1.

To generate correlated tillage forces P_{HG} and P_{VG}, two non-correlated normalized variables $\mathbf{u}_1$ and $\mathbf{u}_2$ were generated by the MATLAB function "normrnd" and then the random values of P_{HG} and P_{VG} were calculated using two transformations. The first one transforms non-correlated normalized variables $\mathbf{u}_1$ and $\mathbf{u}_2$ to correlated normalized variables $\tilde{\mathbf{u}}_1$ and $\tilde{\mathbf{u}}_2$ and the second one transforms correlated normalized variables to

correlated tillage forces P_{HG} and P_{VG}. The spatial variability of the horizontal and vertical forces can then be shown in Figure 4-10 for a distance of $1000\ m$.

Table 4-1 : Distribution parameters of the model's parameters

Model's parameters	Distribution type	Distribution parameters
$P_{HG}[kN]$	Lognormal	$\mu_{P_{HG}} = 0.872,\ \xi_{P_{HG}} = 0.449$
$P_{VG}[kN]$	Lognormal	$\mu_{P_{VG}} = 0.004,\ \xi_{P_{VG}} = 0.447$
$S_1[m]$	Normal	$m_{S_1} = 10,\ \sigma_{S_1} = 1$
$S_2[mm]$	Normal	$m_{S_2} = 50,\ \sigma_{S_2} = 5$
τ	Deterministic	$\tau = 0.2$

From Figure 4-10, it can be observed that a clear correlation exists in the spatial variability between the horizontal and vertical forces. This is resulted from the correlation between the global horizontal and vertical forces ($\rho(P_{HG}, P_{VG}) = 0.93$). Another observation is the proportionality between the global tillage forces (P_{HG}, P_{VG}) and the local tillage forces (P_{HL}, P_{VL}). The increase of global tillage forces increases the amplitudes of local tillage forces and vice-versa. These increases in force amplitudes are marked in cycles in Figure 4-10. This is caused by the calculation of the local tillage forces as a percentage of the global tillage forces.

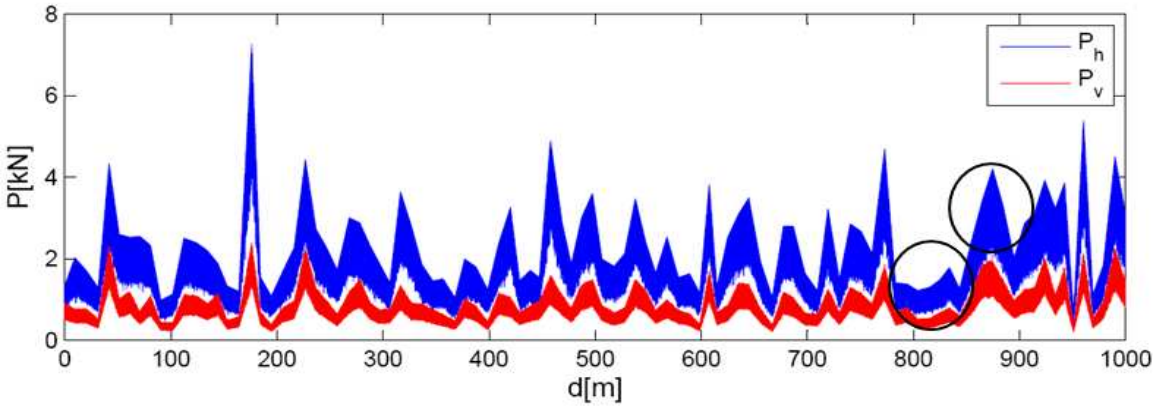

Figure 4-10 : The spatial variability of the horizontal and vertical forces across proposed 1000 m distance

4.6 Conclusions

This chapter aims at proposing a new model for modeling the spatial variability in tillage forces for the purpose of fatigue analysis of tillage machines. The proposed model uses the following five parameters (P_{HG}, P_{VG}, S_1, S_2, τ) to model the spatial variability in tillage forces. The main advantage of this model is its simplicity as illustrated in the numerical application. However, to improve its estimation, further research is needed to investigate the relationships between the global and local tillage forces (P_{HG}, P_{VG}) and the variability in the others parameters (S_1, S_2, τ).

Chapter 5

Fatigue analysis

5.1 Introduction

This chapter intends to estimate the life time of tillage machines, i.e. the expected travel distance to failure, with taking into consideration the spatial variability in tillage forces as modeled in the previous chapter. This chapter is subdivided into four sections. The first section starts by defining the fatigue and presenting different approaches developed to deal with this phenomenon. In the second section, special attention is given to the stress-base fatigue life analysis which is appropriate for estimating the life time of tillage machines. In this section, the effect of mean stress, modifying factors, random stress, multiaxial fatigue are discussed in the context of stress-based fatigue life. In the forth section, the proposed approach for estimating the expected travel distance to failure for tillage machines is presented and applied for the chisel plough shank. Some conclusions are presented at the end of this chapter.

5.2 Fatigue of materials and their approaches

Fatigue of materials is a well-known technical problem. Already in the 19th century several serious fatigue failures were reported and the first laboratory investigations were carried out. In that time, fatigue was thought to be a mysterious phenomenon because fatigue damage could not be seen. Failure apparently occurred without any previous warning. Noteworthy research on fatigue was done by August Wöhler, who is one of the most famous early fatigue researchers, and then significant efforts have done by many other researchers to well understand this phenomena. In the 20th century, we have learned that repeated load applications can start a fatigue mechanism in the material leading to nucleation of small cracks, followed by crack growth, and ultimately to complete structure rupture [72]. An historical overview of fatigue developments and contributions of fatigue searchers can be found in the work of Stephens et al. [73].

Fatigue can be defined as a process in which damage accumulates due to the repetitive application of loads that may be well below the yield stress of the material. This process is dangerous because a single application of the load would not produce any observable ill effect, and a conventional stress analysis might lead to an assumption of safety that does not exist. When the repeated loads are above a certain limit, microscopic cracks will begin to form at an internal or surface flaw where the stresses are concentrated. Over a number of cycles, a crack will reach a critical size and the structure will suddenly fracture. According to fatigue phases, fatigue analysis approaches can be subdivided into four main approaches [73] [74]. There are: stress-based fatigue life approach, strain-based fatigue life approach, crack growth approach and two-stage approach.

The stress-based fatigue life approach intends to estimate the fatigue life (number of loading cycles before failure) when stresses remain elastic even around stress concentrations. This approach is widely used in design applications where the applied stress is primarily within the elastic range of the material and the resulting fatigue life is long. If the stresses around the stress concentrations become plastic, the strain-based fatigue life is appropriate. Short fatigue lives generally occur under these conditions. The third approach can be used to determine how long it will take a crack to grow to a critical size. The two-stage approach consists of combining two approaches. Each approach has its own region of application with some degree of overlap between them. Selecting the appropriate approach depends on the given problem.

5.3 Stress-based fatigue life

The stress-based fatigue life was the first approach used in an attempt to understand and quantify metal fatigue. It was the standard design method for almost 100 years [74]. This approach is generally characterized by a high-cycle fatigue methodology. It is based on the S-N curve, also known as a Wöhler curve. The S-N curve is a graph of the amplitude of a cyclical stress against the logarithmic scale of cycles to failure. In some materials, particularly ferrous alloys, the S-N curve flattens out eventually, so that below a certain limit, called the fatigue limit or the endurance limit (typically $> 10^6$ cycles), the material may not fail and can be cycled infinitely [75], Curve “a” in Figure 5-1. For some other materials such as aluminum and copper alloys, no fatigue limit exists [76], Curve “b” in Figure 5-1. In such cases, the fatigue strength for a given number of cycles (e.g. 1×10^8 cycles) must be specified.

The S-N curve for a material, that has a limit fatigue, can be expressed as in Equation (5.1).

$$\sigma_a = \begin{cases} a.N^b & N < N_{FL} \\ \sigma_{FL} & N \geq N_{FL} \end{cases} \quad (5.1)$$

where σ_a is the stress amplitude, a is the regression intercept (also called the fatigue strength coefficient), b is the regression slope (also called the fatigue strength exponent), N is the number of cycles and N_{FL} is the number of cycles corresponding to the fatigue limit σ_{FL}.

The most basic S-N curves are generated using a fully-reversed stress, as presented in Figure 5-2, where the ratio (R) between the maximum and minimum stress is equal to -1. When the stress applied on a structure is constant over the structure life and the ration (R) is equal to -1, the Equation (5.1) can be used directly to determine the number of cycles to failure, i.e. the fatigue life. If the number of cycles to failure N is greater than the number of cycles corresponding to the fatigue limit N_{FL}, it can be accepted that the structure has an infinite life.

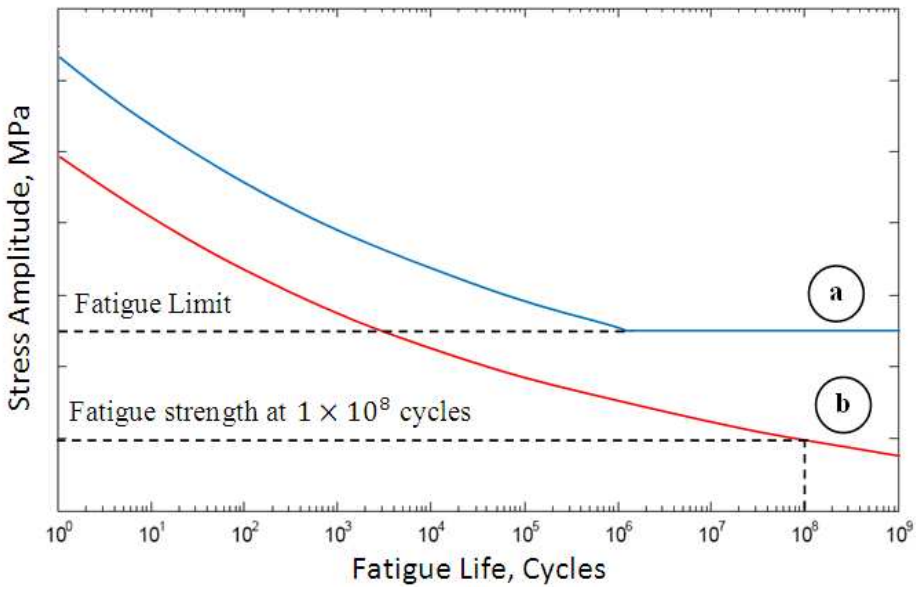

Figure 5-1 : Typical S-N curves

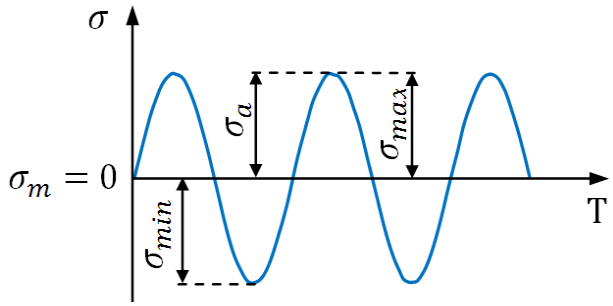

Figure 5-2 : Fully-reversed stress

(σ_{max} is the maximum stress, σ_{min} is the minimum stress, σ_m is the mean stress, $\sigma_a$is the stress amplitude)

5.3.1 Effect of mean stress

When the ratio R is not equal to -1, a Haigh diagram is usually used to estimate the fatigue life. This diagram plots the mean stress along the x-axis and the stress amplitude along the y-axis and the lines of constant life are drawn through the data points. A very substantial amount of testing is required to generate a Haigh diagram, and it is usually impractical to develop curves for all combinations of mean and amplitude stresses. Therefore, several empirical criteria that relate the stress amplitude to the mean stress have been developed to address this difficulty. These criteria define various curves to connect the fatigue limit on the stress amplitude axis to either the yield strength or the ultimate strength on the mean stress axis [77]. The zone under the curves defined the safe zone against fatigue while the zone above the curves represents the failure zone. Figure 5-3 illustrates three of these criteria, namely the criterion of Goodman, Gerber and Soderberg. Bannantine et al. [74] reported that the Soderberg criterion is very conservative and test data tend to fall between the Goodman and Gerber curves.

Kwofie [78] proposed a function, presented in Equation (5.2), to take into account the effect of mean stress. This function allows determining the stress amplitude according to the material constant, material properties, number of cycles to failure and to different fatigue criteria.

$$\sigma_a = a\left[1 - \beta_m \frac{\sigma_m}{\sigma_u}\right] N^b \tag{5.2}$$

where β_m is a numerical constant, representing the mean stress sensitivity of the material, σ_m is the mean stress and σ_u is the ultimate strength. The value of the numerical constant β_m depends on the fatigue criterion (Goodman, Gerber, Soderberg …).

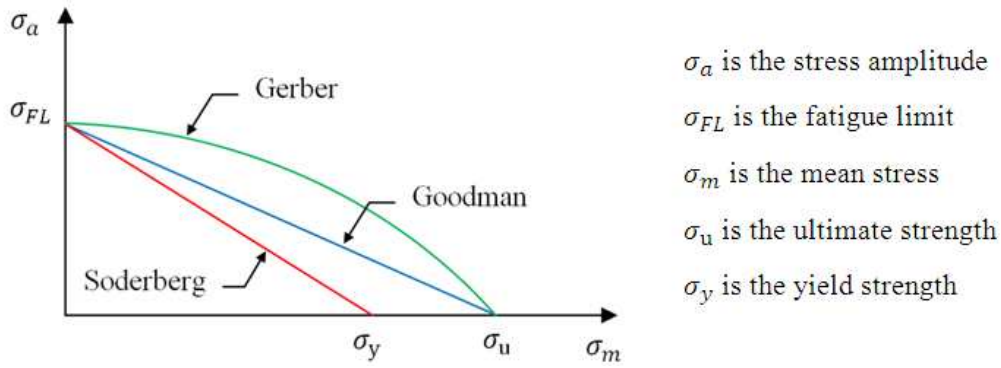

Figure 5-3 : Comparison of mean stress - stress amplitude relationships

5.3.2 Modifying factors

Materials, as they are tested, are always in a different condition from the materials as they are actually used. Various factors change the fatigue limit of a material obtained from the typical S-N curves. They are: size of component, type of loading, surface finish, surface treatment, temperature and environment. The corrected fatigue limit can be calculated by taking the effects of these factors as in Equation (5.3).

$$\sigma_{FL\,\text{corrected}} = \sigma_{FL} k_{\text{size}} k_{\text{loading}}\, k_{\text{surface finish}} k_{\text{surface treatment}} k_{\text{temperature}}\, k_{\text{environment}} \qquad (5.3)$$

Overall, these factors tend to decrease the fatigue limit. Extensive studies about the effects of these factors on the fatigue limit can be found in [72] [73] [74].

5.3.3 Fatigue analysis for random stress

In practice, a structure is exposed to a random stress. In such cases, the random stress should be reduced to a series of simple cycle stresses using counting methods, e.g. range pair method and rainflow method. More details about these methods can be found in [73] [74] [79]. These methods allow one to determine the amplitude and mean value $(\sigma_{a_i}, \sigma_{m_i})$ for each stress cycle at a fixed time interval T_o. The damage fraction caused by the i*th* cycle of stress can be computed by Equation (5.4).

$$D_i = 1/N_{f_i}(\sigma_{a_i}, \sigma_{m_i}) \qquad (5.4)$$

where $N_{f_i}(\sigma_{a_i}, \sigma_{m_i})$ is the number of cycles to failure according to the amplitude σ_{a_i} and the mean value σ_{m_i}.

The total damage, caused by all cycles, can be computed by a cumulative damage model. More than sixty fatigue damage models have been proposed for this purpose. However, the linear damage rule (called Miner's rule or the Palmgren-Miner linear damage

hypothesis) is still dominantly used because of its simplicity [80]. Miner's law assumes that the total damage can be expressed as the sum of damage fractions. The linear damage rule has two main shortcomings [74]. First, it predicts that the damage caused by a stress cycle is independent of where it occurs in the load history. Second, it predicts that the rate of damage accumulation is independent of stress level. Many nonlinear damage models have been proposed to overcome the shortcomings of Miner's law [73]. These models have a general form such as presented in Equation (5.5).

$$D = \sum_{i=1}^{k} \left(1/N_{f_i}\right)^{\vartheta_i} \tag{5.5}$$

where the exponent ϑ_i depends on the stress level.

There are some practical problems involved when using these models. They required material and shaping constants which must be determined from a series of step tests. In some cases this requires a considerable amount of testing [74]. The expected life time of a structure can be calculated by dividing the time interval T_o on the total damage D. When the random stress is multiaxial, an equivalent uniaxial random stress is needed to determine by a suitable multiaxial fatigue criterion [81].

5.3.4 Multiaxial fatigue

Engineering components are generally subjected to complex stress states in which the three principal stresses are non-proportional or their directions change during a loading cycle. In the past, a majority of fatigue research has been conducted under uniaxial loading conditions. Early development of multiaxial fatigue theories were based on the extensions of static yield theories to fatigue under combined stresses. Despite some of the fundamental weaknesses, these methods are often used. They are easy to implement and may be useful in obtaining a first approximation [74]. In 1955, Sines developed a multiaxial theory that is very similar to the distortion energy theory (Von Mises criteria) but includes a hydrostatic term. Several theories were developed based on the Sines's approach. In the early 1970s, critical plane multiaxial fatigue theories were developed. There are theories based on the premise that failure occurs due to damage developed on a critical plane, and are based on cracking observations. Reviews of multiaxial fatigue criteria can be found in [81] [82].

5.4 Fatigue analysis of tillage machines

5.4.1 Proposed approach

Tillage machines are subjected to random stress caused by the variability of tillage forces during tillage operation. As mentioned in Chapter 4, the soil failure creates a cycling loading in tillage machines that may be affects the life time of these machine. For that reason, we propose to study the effects of the variability of tillage forces on the tillage machines. The main steps of this analysis in presented in Figure 5-4.

The multiaxial stress state caused by the variability of tillage forces is determined by the Finite Element method. The equivalent stress, resulted from the multiaxial stress, is calculated by the Von Mises criterion. The rainflow algorithm is used to extract the stress cycles and determine their means and amplitudes. The damage fraction is calculated by Equation (5.4) and we propose to use the Kwofie's function and the Soderberg's criterion to determine N_{f_i}. This is based on the fact that the applied stress on tillage machines is primarily within the elastic range of the material. According to the Soderberg's criterion, the numerical constant β_m Kwofie's function equals to σ_u/σ_y and N_{f_i} can be calculated as in Equation (5.6).

$$N_{f_i} = \left[\frac{\sigma_{a_i}}{a\left(1 - \sigma_{m_i}/\sigma_y\right)}\right]^{1/b} \tag{5.6}$$

where $N_{f_i}$is the number of cycles to failure according to the amplitude σ_{a_i} and the mean value σ_{m_i} for the i*th* cycle, σ_y is the yield strength, a is the regression intercept and b is the regression slop. The total damage, caused by all cycles, is computed by the Miner's law presented in Equation (5.7).

$$D = \sum_{i=1}^{k} D_i \tag{5.7}$$

where k is the number of cycles determined by the rainflow algorithm for the distance interval d_o. The expected travel distance to failure is calculated by dividing the distance interval by the total damage, as expressed in Equation (5.8) to fulfill the assumption that the failure will occur when $D \geq 1$.

$$d_f = d_0/D \tag{5.8}$$

where d_f is the expected travel distance to failure, d_o is the distance interval and D is the total damage.

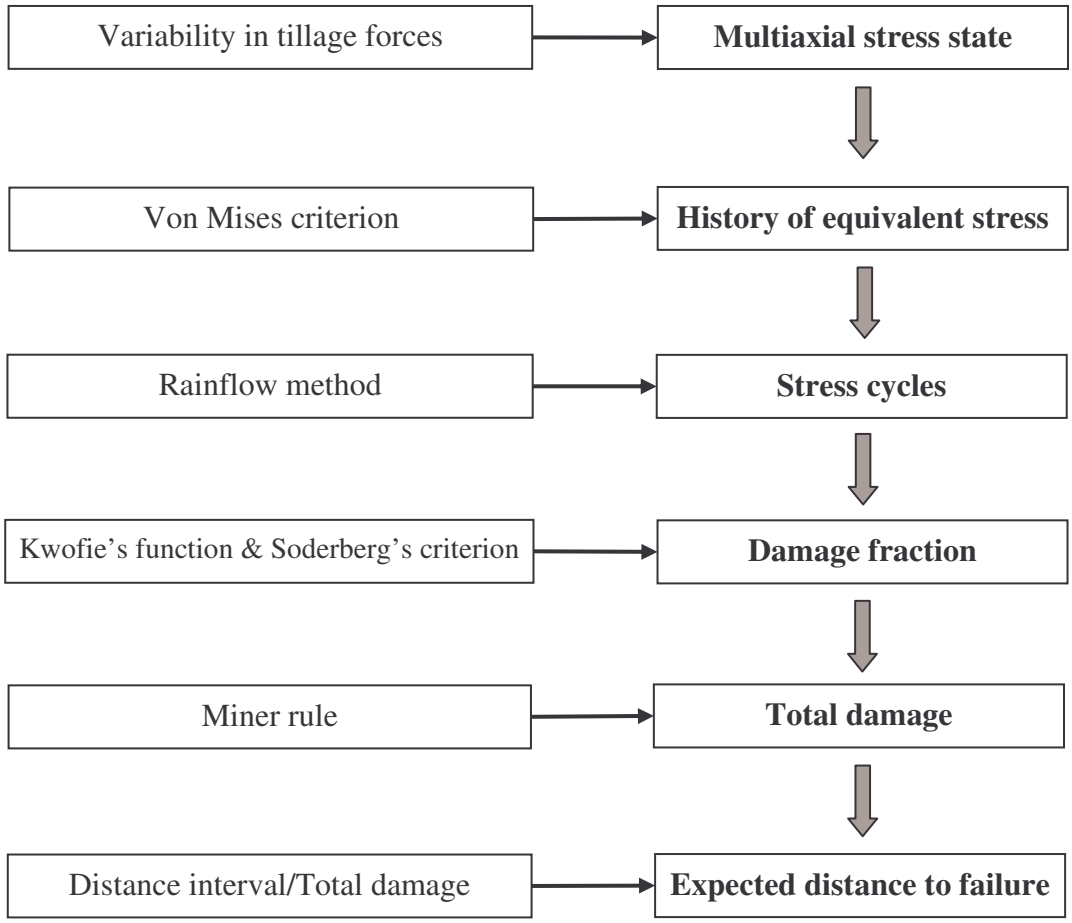

Figure 5-4 : Flowchart of fatigue analysis of tillage machines

5.4.2 Numerical application

The proposed approach was implanted in MATLAB program (Mathworks INC. 2008) to determine the effects of the variability of tillage forces on the life time of the shank of a chisel plough shown in Figure 4-9 by calculating the expected travel distance to failure. The material constants (the regression intercept and the regression slop) and the yield stress of the material of the studied shank are $a = 754$ MPa, $b = 0.121$ and $\sigma_y = 250$ MPa, respectively.

Firstly, the point of the maximum equivalent stress was determined by means of the finite element method and ANSYS program (ANSYS INC. V11). The use of ANSYS allowed us to see the point of maximum equivalent stress for different combinations of tillage forces (P_H, P_V). After several trials, we concluded that the position of the maximum equivalent stress is unchanged. Figure 5-5 shows the meshed model, boundary conditions

and the point of maximum equivalent stress (in MPa) determined for the mean values of tillage forces $P_H = 2.641\ kN$ and $P_V = 1.106\ kN$.

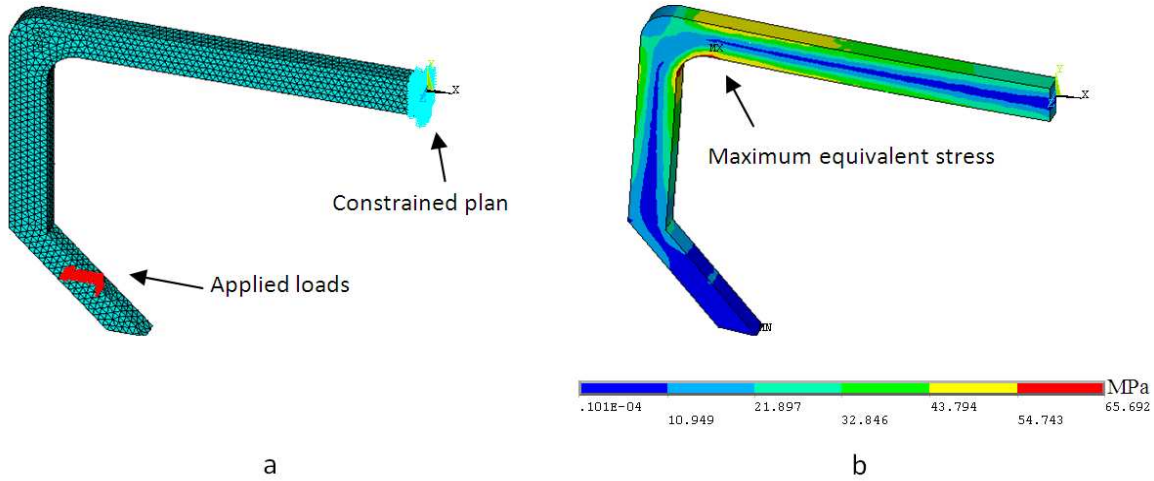

Figure 5-5 : a- Meshed model and boundary conditions; b- Maximum equivalent stress

The equivalent stress, presented in Figure 5-6, was calculated at the point of maximum equivalent stress using the finite element model, implemented in the CALFEM toolbox of MATLAB [60] as the proposed approach was implanted in MATLAB program. The equivalent stress was calculated according to the Von Mises criterion by means of the variability of tillage forces presented in Figure 4-10.

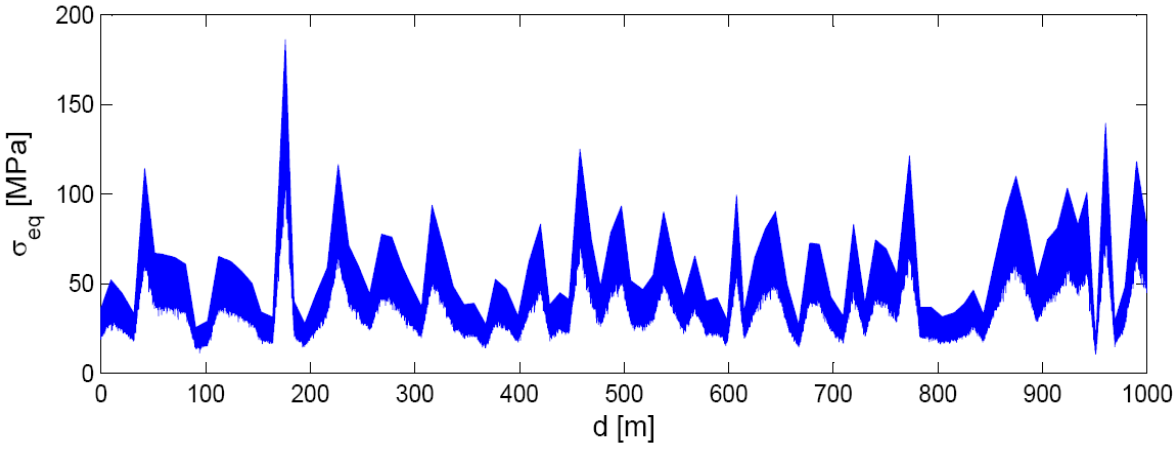

Figure 5-6 : Equivalent stress history across proposed 1000 m distance

The rainflow algorithm [83] was used to extract the stress cycles with their amplitude and mean values. The histograms of stress amplitude and mean stress are shown in Figure 5-7. Both the histograms indicate that the dispersions of mean stress and stress amplitude are significant. This reflects the high dispersions of the spatial variability in tillage forces.

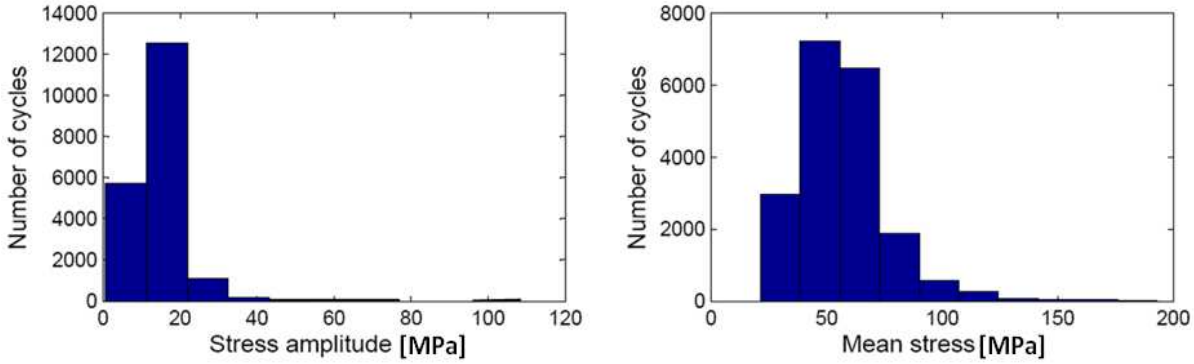

Figure 5-7 : Histograms of stress amplitude and mean stress

The total damage, calculated over the distance interval ($d_o = 1000m$), is equal to $D = 1.212 \times 10^{-6}$. By dividing the distance d_o by the total damage D, the expected distance to failure is found to be $d_f = 0.825 \times 10^6\ km$. Despite the fact that the equivalent stress is smaller than the yield stress (Figure 5-6), the failure will occur after a certain distance d_f. This example shows the significant effect of the spatial variability in tillage forces on the life time of tillage machines. Since agricultural soils are characterized to be high spatial variability [66], it is expected that this variability will reduce the life time of tillage tools.

The expected distance to failure is plotted as a function of the shank dimensions (b, h) in Figure 5-8. For all combinations of b and h, the equivalent stress is smaller than the yield stress. The minimum expected distance to failure $d_{f\,min} = 2.004 \times 10^4\ km$ occurs when $b = 25\ mm$ and $h = 55\ mm$, the maximum expected distance to failure $d_{f\,max} = 9.213 \times 10^8\ km$ occurs when $b = 35\ mm$ and $h = 70\ mm$. This Figure allows one determining the shank dimensions according to the required distance to failure, e.g. for $d_f = 10 \times 10^7\ km$ the shank dimensions are $b = 25\ mm$ and $h = 65\ mm$.

To investigate the effect of the percentage (τ) of the local tillage forces to the global tillage forces on the expected distance to failure (d_f), the percentage τ is plotted against the logarithmic scale of d_f in Figure 5-9. It is observed that with an increase of τ

from 0.1 to 0.4, a reduction of d_f of $1.2 \times 10^5\ km$ will take place, meaning that the reduction of d_f due to the augmentation of τ is very significant. Therefore, to reduce the τ values, (by consequence, the values of the local tillage forces) it is recommended to perform the tillage operation when the moisture content is closed to the liquid limits, where the soil conditions became most favorable for soil-working. This can improve significantly the expected distance to failure and by consequence the life time of tillage machines.

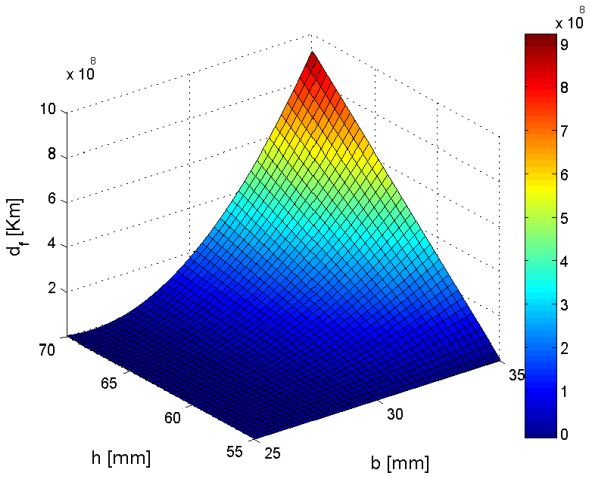

Figure 5-8 : Distance to failure-Shank dimensions plot

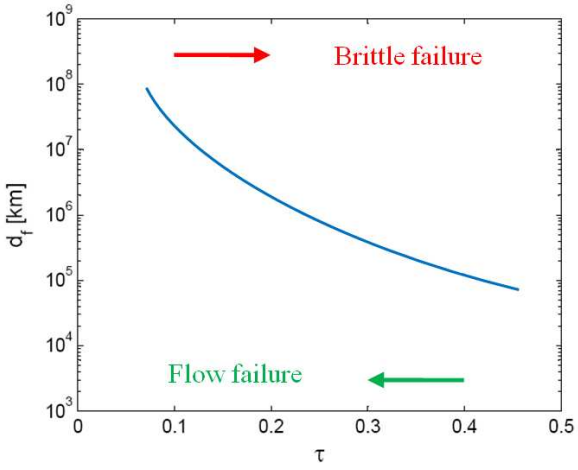

Figure 5-9 : $\tau - d_f$ relationship

5.5 Conclusions

In this chapter, an approach is proposed to estimate the life time of tillge machines based on available fatigue analysis methods. The proposed approach was applied to calculated the expected travel distance to failure for the shank of a chisel plough. The expected distance to failure d_f for the shank cross section of $h = 58\,mm$ and $b = 32\,mm$ was found to be $d_f = 0.825 \times 10^6$. In addition, different values of h and b were used to calculate the expected distance to failure. Based on this work the following conclusions can be drawn:

- The failure by fatigue will occure even the equivalent stress is smaller than the yield stress of the material.
- The changes of the expected distance to failure by the shank dimenssions are very important $(d_{f\,min} = 2.004 \times 10^4\ km, d_{f\,max} = 9.213 \times 10^8\ km)$.
- The effect of the percentage of the local tillage forces to the global tillage forces (τ) on the expected distance to failure (d_f) is very significant.

Chapter 6

Conclusions and future work

In this chapter we present a summary of this dissertation, conclusions concerning the results and recommendations for future work.

6.1 Summary and conclusions

In Chapter 2, a probabilistic approach is proposed for modeling the variability of the tillage forces. An existing three-dimensional analytical model of tool forces from McKyes was used to model the interaction between the tillage tools and the soil. The variability of tillage forces was modeled by taking into account the variability of soil engineering properties (soil density, soil cohesion, internal friction angle, soil-tool friction angle and soil-tool adhesion), the tool design parameters (tool width and rake angle) and the operational conditions (tool working depth, surcharge pressure at the soil surface and tool speed). The variability of the soil engineering properties was modeled by means of experimental observations. The dispersion effect of each tillage system parameter on the tillage forces was determined by a sensitivity analysis. The proposed approach was implemented for modeling the variability of tillage forces for the shank of a chisel plough. The results show that both the horizontal and the vertical forces have lognormal distributions with $\mu = 0.872, \xi = 0.449$ and $\mu = 0.004, \xi = 0.447$ for the horizontal and the vertical forces, respectively. The correlation between the horizontal and vertical forces is positive and quasi-linear with $\rho(P_H, P_V) = 0.93$.

In Chapter 3, a reliability-based design optimization approach was developed, for the first time, for integrating the variability of tillage forces into the design optimization of tillage machines. The failure probability was estimated according to two performance criteria related to the structural design requirement and the quality of tillage operation. Two reliability methods, namely the Monte Carlo simulation technique and the first-order reliability method were used for estimating the failure probability. Two reliability-based design optimization methods, namely the reliability index approach (RIA) and the

Sequential optimization and reliability assessment (SORA), were used to integrate the reliability constraints into the design optimization. This approach was implemented for the design of the shank of a chisel plough. The results show that the SORA method is more efficient and reduces the computational time, comparing with the RIA method. This approach improves slightly the reliability index in order to respect the target reliability index $\beta^T = 3$ and reduces the objective function by 9.25%. The optimal reliability analysis indicates that the optimal reliability index $\beta_{Opt} = 3.105$ is different from that used in the work. It is concluded that the optimal reliability analysis should be integrated into the RBDO problem to find the best compromise between the total cost and the reliability assurance.

Chapter 4 proposes a new model to describe the spatial variability of tillage forces for the purpose of fatigue analysis of tillage machines. The proposed model took into account both the variability in tillage system parameters (soil engineering properties, tool design parameters and operational conditions) and the cyclic effects due to the soil behaviour on the spatial variability in the tillage forces. The main advantage of this model is its simplicity as it needs only five parameters (P_{HG}, P_{VG}, S_1, S_2, τ) to model the spatial variability in tillage forces. The proposed model was implemented to describe the spatial variability in tillage forces for the shank of a chisel plough, used in Chapter 2, across a distance of 1000 m in order to calculate the expected travel distance to failure for this machine in the folowing chapter.

Chapter 5 presents the methods used to calculate the life time of tillage machines, i.e. expected travel distance to failure, taking into account the results obtained in Chapter 4. The stress-based fatigue life approach was used for this purpose, based on the fact that the applied stress on tillage machines is primarily within the elastic range of the material. Stress cycles with their mean values and amplitudes were determined by the rainflow algorithm. The damage friction caused by each cycle of stress was computed according to the Soderberg criterion and the total damage was calculated by Miner's law. The results show that failure by fatigue will occur even when the equivalent stress is smaller than the yield stress of the material. The range of the expected distance to failure by the shank dimenssions are very important ($d_{f\,min} = 2.004 \times 10^4\ km, d_{f\,max} = 9.213 \times 10^8\ km$). The effect of the percentage of the local tillage forces to the global tillage forces (τ) on the expected distance to failure (d_f) is very significant.

6.2 Recommendations for future work

In Chapter 2, a total of 57 samples, collected from the literature, were considered for modeling the variability in soil engineering properties. In addition, the inter-correlations between these properties were omitted. In order to improve the estimation of the variability of soil engineering properties, a larger number of samples should be employed and the inter-correlations between these properties should be investigated. Uniform and normal distributions were used to model the variability of tool design parameters and operational conditions. This is because no data are available on the variability of these parameters. Experimental observations can be employed in the future work to improve the accuracy of the estimation of these parameters. The proposed method to estimate the dispersion effects of tillage system parameters on tillage forces, presented in Section 2.3.3, does not take into account the inter-correlations between these parameters. Therefore, we recommend either to develop this method or to use other available methods such as the variance-based sensitivity methods.

The reliability-based design approach proposed in Chapter 3 was based on the variability in tillage forces resulted from the variability in tillage system parameters. The variability derived from the mechanical behaviour of the soil during failure was omitted for simplifying the calculation procedures. It is possible to take both of these sources of variability into account to get more accurate results. A further research is needed in order to consider the remaining parts of the chisel plough which should lead to optimizing the chisel plough design from a reliability point of view. It would also decrease the overall volume of the chisel plough and consequently, the associated manufacturing and operational costs.

The proposed model presented in Chapter 4 for modeling the spatial variability in tillage forces was based on the linearity of the spatial variability in the global tillage forces. This may not be an accurate assumption. Therefore, a non-linear relationship assumption should be investigated and the effects on the spatial variability of tillage forces should be compared with the former case. In addition, further research is needed to investigate the relathionships between global and local tillage forces (P_{HG}, P_{VG}) and also the variability in the other parameters of model (S_1, S_2, τ).

In Chapter 5, the Soderberg criterion was used to consider the effect of mean stress in the fatigue analysis. Experiments show that this criterion is very conservative and test

data tend to fall between the Goodman and Gerber curves. It is possible to perform the fatigue analysis using the former criteria. Miner's law was used to calculate the total damage caused by all stress cycles. It is noted that this law has two main shortcomings: 1) it predicts that the damage caused by a stress cycle is independent of where it occurs in the load history and 2) it predicts that the rate of damage accumulation is independent of stress level. However, when material and shaping constants are available, a nonlinear damage approach, e.g. damage curve approach (DCA), double damage curve approach (DDCA) and double linear damage rule (DLDR), can be used for this purpose. The equivalent stress was calculated by the Von misses criterion. This criterion was used in this work because it is easy to implement and it is useful in obtaining a first approximation. It is recommended to use more accurate approach such as Sines's approach in the future work. The expected travel distance to failure was calculated over 1000 m. The spatial variability in tillage forces within this distance may not represent the real variability in these forces, i.e. the considered history of tillage forces is not representative. Therefore, fatigue analysis should be performed over an extended spatial range in order to get a more accurate estimation for the expected travel distance to failure.

Bibliography

[1] Srivastava, A K, Goering, C E and Rohrbach, R P., *Engineering principles of agricultural machines.* s.l. : American Society of Agricultural Engineers, 1993. Vol. Revised Printing .

[2] Klenin, N I, Popov, I F and Sakun, V A., *Agricultural machines.* New Delhi : Amerind Publishing Company, 1985.

[3] Kepner, R A, Bainer, R and Barger, E L., *Principles of farm machinery.* 2nd Edition . Connecticut : AVI Publishing Company, Inc., 1972.

[4] McKyes, E., *Soil cutting and tillage.* Amsterdam : Elsevier, 1985.

[5] , *Terminology and definitions for agricultural tillage implements.* s.l. : ASAE , 2004. ASAE S414.1 FEB04.

[6] Godwin, R J and O'Dogherty, M J., "Integrated soil tillage force prediction models." Journal of Terramechanics, 2007, Issue 1, Vol. 44, pp. 3–14.

[7] Godwin, R J and Spoor, G., "Soil failure with narrow tines." Journal of Agricultural Engineering Research, 1977, Issue 3, Vol. 22, pp. 213-228 .

[8] Godwin, R J., "A review of the effect of implement geometry on soil failure and implement forces." Soil & Tillage Research, 2007, Issue 2, Vol. 97, pp. 331-340.

[9] Desbiolles, J M.A, et al., "A novel approach to the prediction of tillage tool draught using a standard tine." Journal of Agricultural Engineering Research, 1997, Vol. 66, pp. 295-309.

[10] Jayasuriya, H P W and Salokhe, V M., "A review of soil–tine models for a range of soil." Journal of Agricultural Engineering Research, 2001, Vol. 79, pp. 1-13.

[11] Reece, A R., "The fundamental equations of earth-moving mechanics." s.l. : Institute of Mechanical Engineering, 1965. Proceedings of the symposium on earth moving machinery. Vol. 179, pp. 8–14.

[12] Terzaghi, K., *Theoretical soil mechanics.* New York : John Wiley & Sons, 1943 .

[13] Shen, J and Kushwaha, R L., *Soil-machine interaction: a finite element perspective.* New York : Marcel Dekker, 1998.

[14] McKyes, E and Ali, O S., "The cutting of soil by narrow blades." Journal of Terramechanics, 1977, Vol. 14, pp. 43-58.

[15] Grisso, R D, Perumpral, J V and Desai, C S., "A soil-tool interaction model for narrow tillage tools." Transactions ASAE Paper 80-1518, 1980.

[16] Kuczewski, J and Piotrowska, E., "An improved model for forces on narrow soil cutting tines." Soil and Tillage Research, 1998, Vol. 46, pp. 231-239.

[17] Godwina, R J, et al., "A force prediction model for mouldboard ploughs incorporating the effects of soil characteristic properties, plough geometric factors and ploughing speed." Biosystems Engineering, 2007, Vol. 97, pp. 117-129.

[18] Chi, L and Kushwaha, R L., "Three-dimensionnal, finit element interaction between soil and tillage tool." Transactions ASAE, 1991, Vol. 34, pp. 361-366.

[19] Fielke, J M., "Finite element modelling of the interaction of the cutting edge of tillage implements with soil." Journal of Agricultural Engineering Research, 1999, Vol. 74, pp. 91-101.

[20] Mouazen, A M and Neményi, M., "Finite element analysis of subsoiler cutting in non-homogeneous sandy loam soil." Soil & Tillage Research, 1999, Vol. 51, pp. 1-15.

[21] Mouazen, A M and Neményi, M., "A review of the finite element modelling techniques of soil tillage." Mathematics and Computers in Simulation, 1998, Vol. 48, pp. 23-32.

[22] Kushwaha, R L and Zhang, Z X., "Evaluation of factors and current approaches related to computerized design of tillage tools: a review." Journal of Terramechanics, 1998, Vol. 35, pp. 69-86.

[23] Cui, K, Défossez, P and Richard, G., "A new approach for modelling vertical stress distribution at the soil/tyre interface to predict the compaction of cultivated soils by using the PLAXIS code." Soil & Tillage Research, 2007, Vol. 95, pp. 277-287.

[24] Zhang, J and Kushwaha, R L., "A modified model to predict soil cutting resistance." Soil & Tillage Research, 1995, Vol. 34, pp. 157-168.

[25] Grisso, R D and Perumpral, J V., "Review of models for predicting performance of narrow tillage tool." Transactions ASAE, 1985, Vol. 28, pp. 1062-1067.

[26] Onwualu, A P and Watts, K C., "Draught and vertical forces obtained from dynamic soil cutting by plane tillage tools." Soil & Tillage Research, 1998, Vol. 48, pp. 239-253.

[27] Siegel, S and Castellan, N J., *Nonparametric statistics for the behavioral sciences.* New York : McGraw-Hill, 1988.

[28] Fox, E P., "The role of statistical testing in NDA." [book auth.] E Nikolaidis, D M Ghiocel and S Singhal. *Engineering design reliability handbook.* New York : CRC Press, 2005.

[29] Ang, A H-S and Tang, W H., *Probability concepts in engineering planning and design.* New York : John Wiley & Sons, 1975. Vol. 1: Basic principles.

[30] Haldar, A and Mahadevan, S., *Probability, reliability, and statistical methods in engineering design.* New York : John Wiley & Sons, 2000.

[31] Irving, A D., "Stochastic sensitivity analysis." Applied Mathematical Modelling, 1992, Vol. 16, pp. 3-15.

[32] Chan, K, Saltelli, A and Tarantola, S., "Sensitivity analysis of model output: Variance-based methods make the difference ." 1997. Proceedings of the 1997 Winter Simulation Conference . pp. 261-286.

[33] Ditlevsen, O and Madsen, H O., *Structural reliability methods.* Internet edition 2.2.2. 2005.

[34] Haldar, A and Mahadevan, S., *Reliability assessment using stochastic finite element analysis.* New York : John Wiley & Sons, 2000.

[35] Bhatti, M A., *Practical optimization methods with mathematical applications.* New York : Springer-Verlag, 2000.

[36] Lange, K., *Optimization.* New York : Springer-Verlag, 2004.

[37] Pedregal, P., *Introduction to optimization.* New York : Springer-Verlag, 2004.

[38] Arora, J S., *Introduction to optimum design.* Second Edition. California : Elsevier, 2004.

[39] Zhao, Y-G and Ono, T., "A general procedure for first/second-order reliability method (FORM/SORM)." Structural Safety, 1999, Vol. 21, pp. 95-112.

[40] Fishman, G S., *Monte Carlo, concepts, algorithms, and applications.* New York : Springer, 1996.

[41] Der Kiureghian, A., "First- and second-order reliability methods." [book auth.] E Nikolaidis, D M Ghiocel and S Singhal. *Engineering design reliability handbook.* Boca Raton, FL : CRC Press, 2005, p. Chapter 14 .

[42] Lemaire, M., *Fiabilité des structures.* Paris : Lavoisier, 2005.

[43] Fiessler, B, Neumann, H J and Rackwitz, R., "Quadratic limit states in structural reliability." Journal of Engineering Mechanics, 1979, Vol. 105, pp. 661-676 .

[44] Breitung, K., "Asymptotic approximation for multinormal integrals." Journal of Engineering Mechanics, 1984, Issue 3, Vol. 110, pp. 357–366.

[45] Hohenbichler, M, et al., "New light on first- and second-order reliability methods." Structural Safety, 1987, Issue 4, Vol. 4, pp. 267-284 .

[46] Tvedt, L., "Second-order reliability by an exact integral." s.l. : Springer, 1988 . 2nd IFIP Working Conference on Reliability and Optimization on structural Systems. pp. 377–384.

[47] Koyluoglu, H U and Nielsen, S R K., "New approximations for SORM integrals." Structural Safety, 1994, Vol. 13, pp. 235–246.

[48] Cai, G Q and Elishakoff, I., "Refined second-order reliability analysis." Structural Safety, 1994, Vol. 14, pp. 267–276.

[49] Olsson, A, Sandberg, G and Dahlblom, O., "On Latin hypercube sampling for structural reliability analysis." Structural Safety, 2003, Issue 1, Vol. 25, pp. 47-68.

[50] Torng, T Y., "Practical reliability- based design optimization strategy for structural design." [book auth.] E Nikolaidis, D M Ghiocel and S Singhal. *Engineering design reliability handbook.* s.l. : CRC Press, 2005, 31.

[51] Aoues, Y and Chateauneuf, A., "Benchmark study of numerical methods for reliability-based design optimization." Structural and Multidisciplinary Optimization, 2010, Vol. 41, pp. 277-294.

[52] Lee, J-O, Yang, Y-S and Ruy, W-S., "A comparative study on reliability-index and target-performance-based probabilistic structural design optimization." Computers & Structures, 2002, Issue 3-4, Vol. 80, pp. 257-269.

[53] Ahn, J and Kwon, J H., "An efficient strategy for reliability-based multidisciplinary design optimization using BLISS." Structural and Multidisciplinary Optimization, 2006, Vol. 31, pp. 363-372.

[54] Kharmanda, M G, Mohamed, A and Lemaire, M., "Efficient reliability-based design optimization using a hybrid space with application to finite element analysis." Structural and Multidisciplinary Optimization, 2002, Issue 3, Vol. 24, pp. 233 – 245.

[55] Kuschel, N and Rackwitz, R., "Two basic problems in reliability-based structural optimization." Mathematical Methods of Operations Research, 1997, Vol. 46, pp. 309-333.

[56] Du, X and Chen, W., "Sequential optimization and reliability assessment method for efficient probabilistic design." Journal of Mechanical Design, 2004, Vol. 126, pp. 225-233.

[57] Cheng, G, Xu, L and Jiang, L., "A sequential approximate programming strategy for reliability-based structural optimization." Computers & Structures, 2006, Vol. 84, pp. 1353-1367.

[58] Yang, R J and Gu, L., "Experience with approximate reliability-based optimization methods." Structural and Multidisciplinary Optimization, 2004, Vol. 26, pp. 152–159.

[59] Ditlevsen, O., "Reliability bounds for structural systems." Journal of Structural Mechanics, 1979, Vol. 7, pp. 453-472.

[60] Austrell, P E, et al., *CALFEM; A finite element toolbox to MATLAB; Version 3.4.* Lund : Structural Mechanics, LTH, Sweden, 2004.

[61] Der Kiureghian, A and Liu, P-L., "Structural reliability under incomplete probability information." Journal of Engineering Mechanics, 1986, Vol. 112, pp. 85-104.

[62] Liu, P-L and Der Kiureghian, A., *Optimization algorithms for structural reliability analysis.* Department of Civil Engineering, University of California. 1986. Technical Report, No. UCB/SESM 86/09. UCB/SEMM-89/05.

[63] Shen, J and Kushwaha, R L., "Quick finite element analysis of soil tool interactions." Computers and Electronics in Agriculture, 1993, Issue 4, Vol. 9, pp. 289-299 .

[64] Sirjacobs, D, et al., "On-line soil mechanical resistance mapping and correlation with soil physical properties for precision agriculture." Soil and Tillage Research, 2002, Vol. 64, pp. 231-242.

[65] Hanquet, B, Sirjacobs, D and Destain, M F., "Analysis of soil variability measured with a soil strength sensor." Precision Agriculture, 2004, Vol. 5, pp. 227-246.

[66] Mouazen, A M and Ramon, H., "Development of on-line measurement system of bulk density based on on-line measured draught, depth and soil moisture content." Soil and Tillage Research, 2006, Issue 2, Vol. 86, pp. 218-229.

[67] Karmakar, S, Sharma, J and Kushwaha, R L., "Critical state elasto-plastic constitutive models for soil failure in tillage – A review." Canadian Biosystems Engineering, 2004, Vol. 46.

[68] Stafford, J V., "Force prediction models for brittle and flow failure of soil by draught tillage tools." Journal of Agricultural Engineering Research, 1984, Vol. 29, pp. 51-60.

[69] Rajaram, G and Erbach, D C., "Soil failure by shear versus modification by tillage: A review." Journal of Terramechanics : s.n., 1996, Vol. 33, pp. 265-272.

[70] Makanga, J T, Salokhe, V M and Gee-Clough, D., "Effects of tine rake angle and aspect ratio on soil reactions in dry loam soil ." Journal of Terramechanics, 1997, Vol. 34, pp. 235-250.

[71] Rajaram, G and Erbach, D C., "Drying stress effect on mechanical behaviour of a clay-loam soil." Soil & Tillage Research , 1998, Vol. 49, pp. 147-158.

[72] Schijve, J., *Fatigue of structures and materials.* Second Edition. s.l. : Springer Science+Business Media, B.V., 2009.

[73] Stephens, R I, et al., *Metal fatigue in engineering* . Second Edition. New York : John Wiley & Sons, 2001.

[74] Bannantine, J A, Comer, J J and Handrock, J L., *Fundamentals of metal fatigue analysis.* New Jersey : Prentice Hall, 1990.

[75] Schijve, J., "Fatigue of structures and materials in the 20th century and the state of the art." International Journal of Fatigue, 2003, Vol. 25, pp. 679-702.

[76] Marines, I, Bin, X and Bathias, C., "An understanding of very high cycle fatigue of metals." International Journal of Fatigue, 2003, Vol. 25, pp. 1101-1107.

[77] Sendeckyj, G P., "Constant life diagrams - a historical review." International Journal of Fatigue, 2001, Vol. 23, pp. 347-353.

[78] Kwofie, S., "An exponential stress function for predicting fatigue strength and life due to mean stresses." International Journal of Fatigue, 2001, Vol. 23, pp. 829–836.

[79] Collins, J A., *Failure of materials in mechanical design : analysis, prediction, prevention.* Second Edition . New York : John Wiley & Sons, 1993.

[80] Fatemi, A and Yang, L., "Cumulative fatigue damage and life prediction theories: a survey of the state of the art for homogeneous materials." International Journal of Fatigue, 1998 , Issue 1, Vol. 20, pp. 9-34.

[81] Wang, Y-Y and Yao, W-X., "Evaluation and comparison of several multiaxial fatigue criteria." International Journal of Fatigue, 2004, Issue 1, Vol. 26, pp. 17-25 .

[82] Karolczuk, A and Macha, E., "A review of critical plane orientations in multiaxial fatigue failure criteria of metallic materials." International Journal of Fracture, 2005, Issue 3-4, Vol. 134.

[83] Nieslony, A., "Determination off ragments of multiaxial service loading strongly influencing the fatigue of machine components." Mechanical Systems and Signal Processing, 2009, Vol. 23, pp. 2712–2721.

[84] Sharifat, K., *Soil translocation with tillage tools.* Department of Agricultural and Bioresource Engineering, University of Saskatchewan. 2006. PhD Thesis.

[85] Ayers, P D., "Moisture and density effects on soil shear strength parameters for coarse grained soils." Transactions of the American Society of Agricultural Engineers, 1987, Issue 5, Vol. 30, pp. 1282-1287.

[86] Fielke, J M., "Interactions of the cutting edge of tillage implements with soil." Journal of Agricultural Engineering Research, 1996, Issue 1, Vol. 63, pp. 61-71.

[87] Rahman, S., *Studies on different liquid manure injection tools under laboratory (soil bin) and grassland conditions.* Department of Biosystems Engineering , University of Manitoba. 2000. PhD Thesis.

[88] Manuwa, S I and Ademosun, O C., "Draught and soil disturbance of model tillage tines under varying soil parameters." Agricultural Engineering International: CIGR EJournal, 2007, Vol. 9, pp. 1-18.

[89] Rosa, U A., *Performance of narrow tillage tools with inertial and strain rate effects.* Department of Agricultural and Bioresource Engineering, University of Saskatchewan. 1997. p. PhD Thesis.

[90] Hettiaratchi, D R.P and Alam, M M., "Calculation, validation and simulation of soil reactions on concave agricultural discs." Journal of Agricultural Engineering Research, 1997, Issue 1, Vol. 68, pp. 63-75 .

[91] Mouazen, A M and Ramon, H., "A numerical–statistical hybrid modelling scheme for evaluation of draught requirements of a subsoiler cutting a sandy loam soil, as affected by moisture content, bulk density and depth." Soil and Tillage Research, 2002, Vol. 63, pp. 155-165.

Appendix I: Commonly used probability distributions

1- Normal distribution:

One of the most commonly used distributions in engineering problems is the normal or Gaussian distribution. The general formula for the probability density function (PDF) of the normal distribution is expressed in the following equation**:**

$$f(\mathbf{y}) = \frac{1}{\sigma\sqrt{2\pi}} \exp\left[-\frac{1}{2}\left(\frac{\mathbf{y}-m}{\sigma}\right)^2\right] \qquad -\infty < \mathbf{y} < +\infty \tag{I.1}$$

where m is the location parameter (mean value) and σ is the scale parameter (standard deviation). They can be calculated for n samples by the following equations:

$$m = \frac{1}{n}\sum_{i=1}^{n} \mathbf{y}_i \tag{I.2}$$

$$\sigma = \sqrt{\frac{1}{n}\sum_{i=1}^{n} (\mathbf{y}_i - m)^2} \tag{I.3}$$

Probability density function of the standard Normal distribution, where $m = 0, \sigma = 1$, is expressed in the following equation:

$$f(\mathbf{y}) = \frac{1}{\sqrt{2\pi}} \exp\left[-\frac{\mathbf{y}^2}{2}\right] \qquad -\infty < \mathbf{y} < +\infty \tag{I.4}$$

Probability density functions for different values of m and σ are shown in Figure I-1.

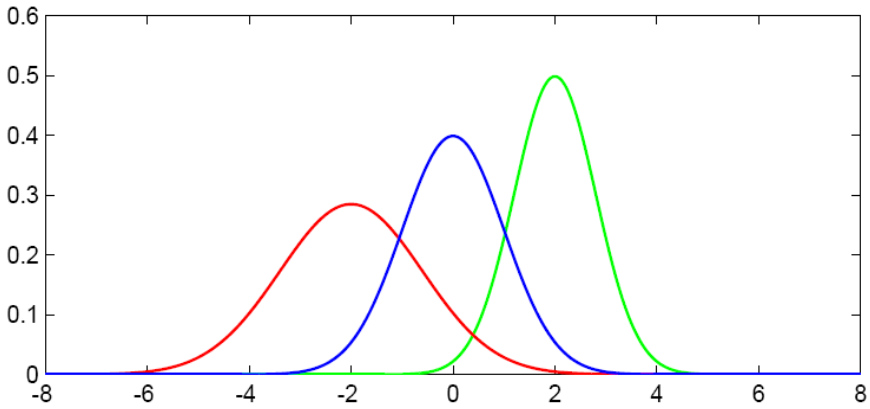

Figure I-1 : $m = -2, \sigma = 1.4$; $m = 0, \sigma = 1$; $m = 2, \sigma = 0.8$

The corresponding cumulative distribution function (CDF) can be expressed by

$$F(\mathbf{y}) = \int_{-\infty}^{y} \frac{1}{\sigma\sqrt{2\pi}} \exp\left[-\frac{1}{2}\left(\frac{\mathbf{y}-m}{\sigma}\right)^2\right] dy \tag{I.5}$$

It is not simple to calculate the CDF by the Equation (I.5). However, it can be calculated by the following equation:

$$F(\mathbf{y}) = \Phi\left(\frac{\mathbf{y}-m}{\sigma}\right) \tag{I.6}$$

And the probability between a and b by the equation:

$$\mathbf{P}(a < y \leq b) = \Phi\left(\frac{\mathrm{b}-m}{\sigma}\right) - \Phi\left(\frac{\mathrm{a}-m}{\sigma}\right) \tag{I.7}$$

where Φ is the cumulative distribution function of the standard normal distribution. Cumulative distribution functions for different values of m and σ are shown in Figure I-2.

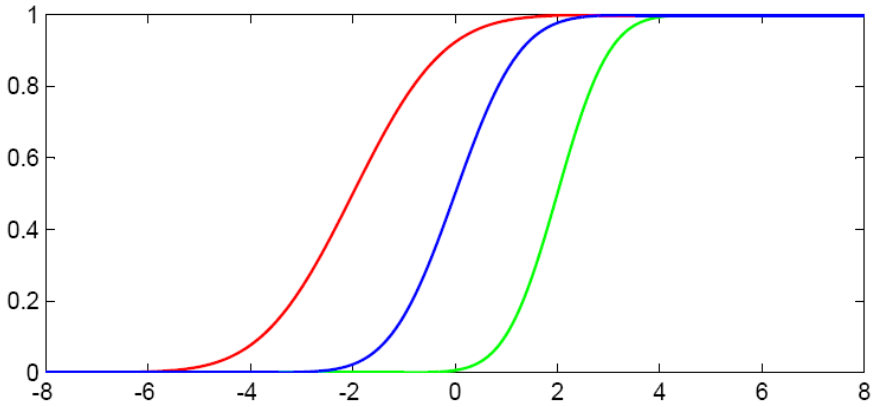

Figure I-2 : $m = -2, \sigma = 1.4$; $m = 0, \sigma = 1$; $m = 2, \sigma = 0.8$

2- Lognormal distribution:

The general formula for the probability density function of the lognormal distribution is expressed by the following equation:

$$f(\mathbf{y}) = \frac{1}{\sqrt{2\pi}\,.\,\xi\,.\,\mathbf{y}} \exp\left[-\frac{1}{2}\left(\frac{\ln(\mathbf{y})-\mu}{\xi}\right)^2\right] \qquad 0 < \mathbf{y} < +\infty \tag{I.8}$$

where ξ is the shape parameter and μ is the scale parameter. They are defined as:

$$\mu = \ln(m) - \frac{1}{2}\ln\left(1 + (\sigma/m)^2\right) \tag{I.9}$$

$$\xi = \sqrt{\ln(1 + (\sigma/m)^2)} \tag{I.10}$$

The formula of the standard lognormal distribution, where $\mu = 0$, is presented in the following equation:

$$f(\mathbf{y}) = \frac{1}{\sqrt{2\pi}\,.\xi.\mathbf{y}} \exp\left[-\frac{1}{2}\left(\frac{\ln(\mathbf{y})}{\xi}\right)^2\right] \qquad 0 < \mathbf{y} < +\infty \tag{I.11}$$

The following is the plot of the lognormal probability density function for different values of μ and ξ.

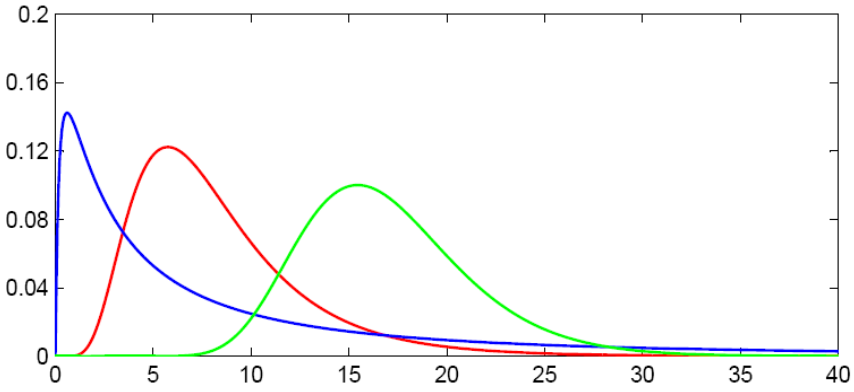

Figure I-3 : $\mu = 1.75, \xi = 1.5$; $\mu = 2, \xi = 0.5$; $\mu = 2.8, \xi = 0.25$

The cumulative distribution function of the lognormal distribution as like the normal distribution does not exist in a simple closed formula. However, it can obtain by the following equation:

$$F(\mathbf{y}) = \Phi\left(\frac{\ln(\mathbf{y}) - \mu}{\xi}\right) \tag{I.12}$$

And the probability between a and b by the relation:

$$\mathbf{P}(a < y \leq b) = \Phi\left(\frac{\ln(b) - \mu}{\xi}\right) - \Phi\left(\frac{\ln(a) - \mu}{\xi}\right) \tag{I.13}$$

The following is the plot of the lognormal cumulative distribution functions for different values of μ and ξ.

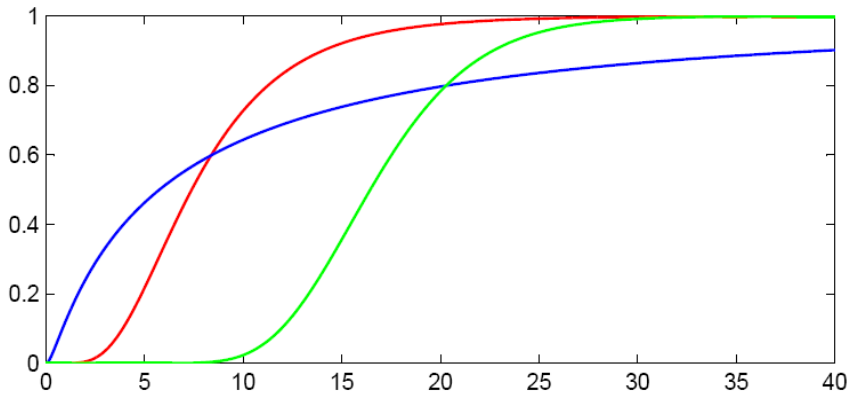

Figure I-4 : $\mu = 1.75, \xi = 1.5$; $\mu = 2, \xi = 0.5$; $\mu = 2.8, \xi = 0.25$

3- Uniform distribution:

The general formula for the probability density function of the uniform distribution is presented in the following equation**:**

$$f(\mathbf{y}) = \begin{cases} 0 & \mathbf{y} < a \\ 1/(b-a) & a \leq \mathbf{y} \leq b \\ 0 & \mathbf{y} > b \end{cases} \qquad \text{(I.14)}$$

where a is the location parameter and (b-a) is the scale parameter. The following is the plot of the uniform probability density function.

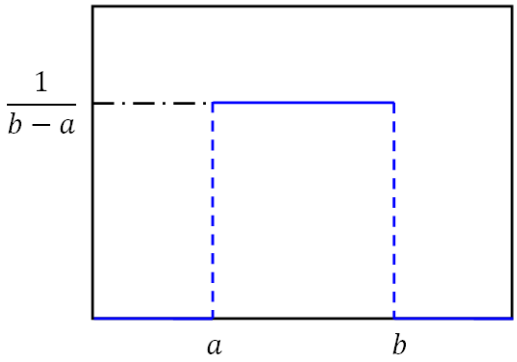

Figure I-5 : Probability density function for uniform distribution

The standard uniform distribution, where $a = 0$ and $b = 1$, is expressed by the following equation:

$$F(\mathbf{y}) = 1 \qquad 0 \leq \mathbf{y} \leq \mathbf{1} \qquad \text{(I.15)}$$

The formula of the cumulative distribution function for the uniform distribution is expressed by the following equation**:**

$$F(\mathbf{y}) = \begin{cases} 0 & \mathbf{y} < a \\ (\mathbf{y} - a)/(b - a) & a \leq \mathbf{y} \leq b \\ 0 & \mathbf{y} > b \end{cases} \tag{I.16}$$

The following is the plot of the uniform cumulative distribution function.

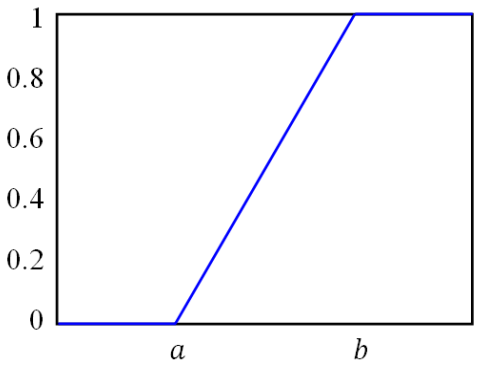

Figure I-6 : Cumulative distribution function for uniform distribution

4- Exponential distribution:

The probability density function (PDF) of an exponential distribution has the form:

$$f(\mathbf{y}) = \eta . \exp(-\eta . \mathbf{y}) \qquad \mathbf{y} \geq 0 \tag{I.17}$$

where $\eta > 0$ is a parameter of the distribution, often called the rate parameter. The relationships between the rate parameter and the mean and variance are: $m = 1/\eta$ and $\sigma^2 = 1/\eta^2$, respectively. Figure I.7 presents the exponential probability density function for three values of η.

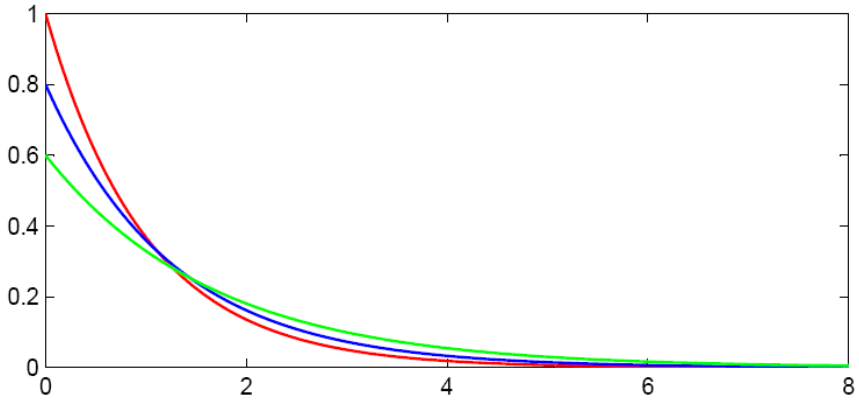

Figure I-7 : $\eta = 1$; $\eta = 0.8$; $\eta = 0.6$

The standard exponential distribution, where $\eta = 1$, is given by $f(\mathbf{y}) = \exp(-\mathbf{y})$.

The formula for the cumulative distribution function of the exponential distribution has the following form:

$$F(\mathbf{y}) = 1 - \exp(-\eta.\mathbf{y}) \qquad \mathbf{y} \geq 0 \tag{I.18}$$

The following is the plot of the exponential cumulative distribution function for three values of η.

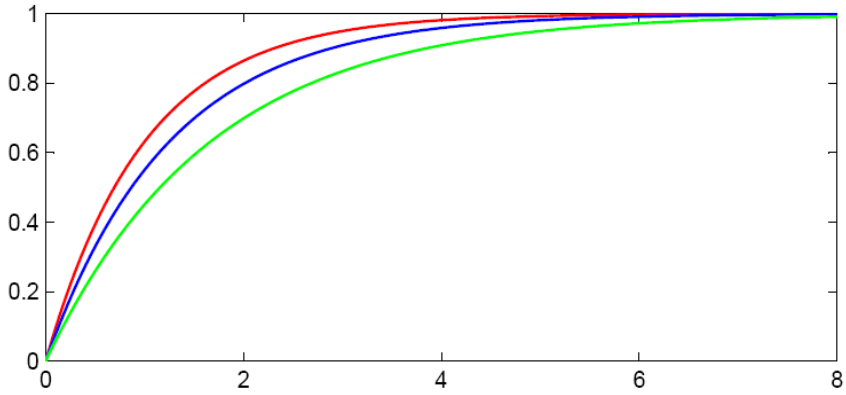

Figure I-8 : $\eta = 1$; $\eta = 0.8$; $\eta = 0.6$

5- Weibull distribution:

5-1 2-parametre Weibull distribution:

The formula for the probability density function of the general 2-parametre Weibull distribution is expressed by the following equation:

$$f(\mathbf{y}) = \frac{k}{\lambda}\left(\frac{\mathbf{y}}{\lambda}\right)^{k-1}.\exp\left[-\left(\frac{\mathbf{y}}{\lambda}\right)^{k}\right] \qquad \mathbf{y} \geq 0 \tag{I.19}$$

where $k > 0$ is the shape parameter and $\lambda > 0$is the scale parameter. The relationships between the shape and scale parameters from the first hand and the mean and variance from the second hand are given by:

$$m = \lambda.\Gamma(1 + 1/k) \tag{I.20}$$

$$\sigma^2 = \lambda^2[\Gamma(1 + 2/k) - \Gamma^2(1 + 1/k)] \tag{I.21}$$

where Γ is the gamma function and it can be calculated as: $\Gamma(\mathbf{z}) = (\mathbf{z} - 1)!$.

The Weibull probability density functions for different values of λ and k are presented in Figure I-9.

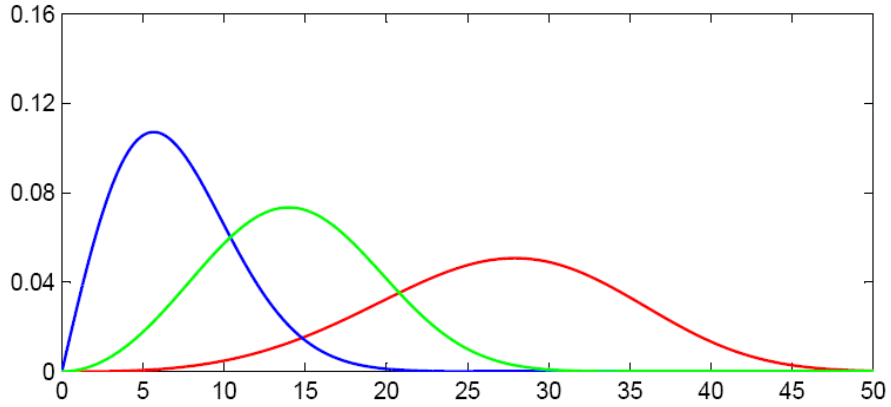

Figure I-9 : $\lambda = 2, k = 8$; $\lambda = 3, k = 16$; $\lambda = 4, k = 30$

The case where $\lambda = 1$ is called the standard Weibull distribution. The equation for the standard Weibull distribution reduces to**:**

$$f(\mathbf{y}) = k(\mathbf{y})^{k-1}.\exp[-(\mathbf{y})^{k}] \qquad \mathbf{y} \geq 0 \tag{I.22}$$

The formula for the cumulative distribution function of the 2-parameter Weibull distribution is**:**

$$F(\mathbf{y}) = 1 - \exp\left[-\left(\frac{\mathbf{y}}{\lambda}\right)^{k}\right] \qquad \mathbf{y} \geq 0 \tag{I.23}$$

The following is the plot of the 2-parametre Weibull cumulative distribution function with different values of λ and *k*.

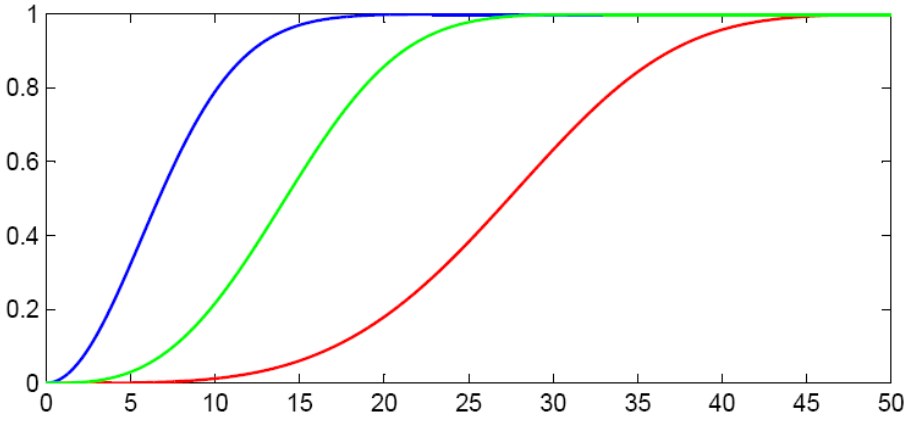

Figure I-10 : $\lambda = 2, k = 8$; $\lambda = 3, k = 16$; $\lambda = 4, k = 30$

5-2 3-parametre Weibull distribution:

The probability density function of the general 3-parametre Weibull distribution can de expressed as:

$$f(\mathbf{y}) = \frac{k}{\lambda}\left(\frac{\mathbf{y}-\varepsilon}{\lambda}\right)^{k-1}.\exp\left[-\left(\frac{\mathbf{y}-\varepsilon}{\lambda}\right)^{k}\right] \qquad \mathbf{y} \geq 0 \tag{I.24}$$

where $k > 0$ is the shape parameter, $\lambda > 0$ is the scale parameter and ε the location parameter. The formula for the cumulative distribution function of the 3-parameter Weibull distribution is**:**

$$F(\mathbf{y}) = 1 - \exp\left[-\left(\frac{\mathbf{y}-\varepsilon}{\lambda}\right)^{k}\right] \qquad \mathbf{y} \geq 0 \tag{I.25}$$

6- Extreme Value Type 1 Distribution (Gumbel distribution):

6-1 Minimum case:

The general formula for the probability density function of the Gumbel (minimum) distribution is:

$$f(\mathbf{y}) = \frac{1}{B}\exp\left(\frac{\mathbf{y}-A}{B}\right).\exp\left[-\exp\left(\frac{\mathbf{y}-A}{B}\right)\right] \tag{I.26}$$

where A is the location parameter and B is the scale parameter of a Gumbel distribution. The probability density function of the standard Gumbel distribution, where: $A = 0, B = 1$, can be written as

$$f(\mathbf{y}) = \exp(\mathbf{y}).\exp[-\exp(\mathbf{y})] \tag{I.27}$$

The following is the plot of the standard Gumbel probability density function for the minimum case.

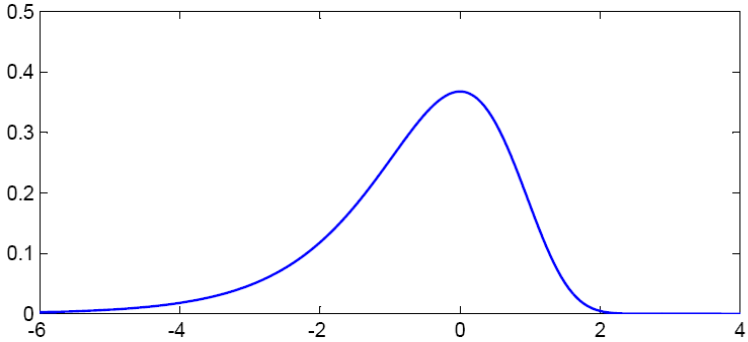

Figure II-11 : Standard Gumbel probability density function

The the cumulative distribution function of the standard Gumbel distribution (minimum) is expressed in the following equation:

$$F(\mathbf{y}) = 1 - \exp[-\exp(\mathbf{y})] \tag{I.28}$$

The following is the plot of the standard Gumbel cumulative distribution function for the minimum case:

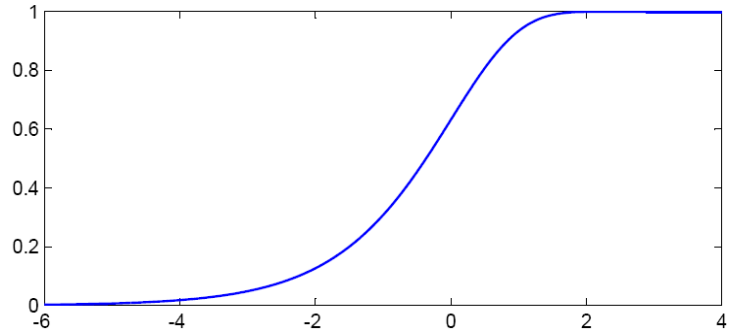

Figure I-12 : Standard Gumbel cumulative distribution function

6-2 Maximum case:

The general formula for the probability density function of the Gumbel (maximum) distribution is:

$$f(\mathbf{y}) = \frac{1}{B}\exp\left(-\frac{\mathbf{y}-A}{B}\right).\exp\left[-\exp\left(-\frac{\mathbf{y}-A}{B}\right)\right] \tag{I.29}$$

The Probability density function of the standard Gumbel distribution (maximum), where: $A = 0, B = 1$ is given by the following equation

$$f(\mathbf{y}) = \exp(-\mathbf{y}).\exp[-\exp(-\mathbf{y})] \tag{I.30}$$

The following is the plot of the standard Gumbel probability density function for the maximum case.

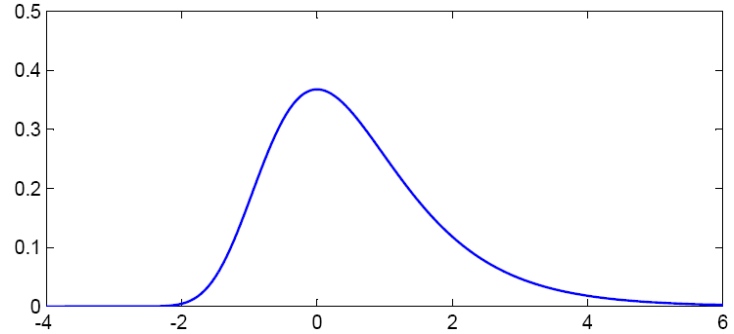

Figure I-13 : Standard Gumbel probability density function

The formula for the cumulative distribution function of the Standard Gumbel distribution (maximum) is:

$$F(\mathbf{y}) = \exp[-\exp(-\mathbf{y})] \tag{I.31}$$

The following is the plot of the Standard Gumbel cumulative distribution function for the maximum case:

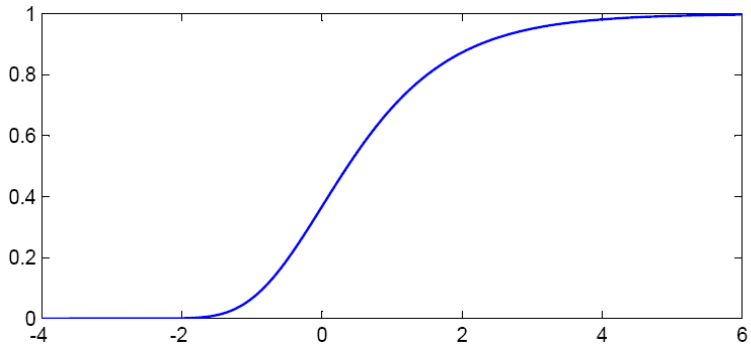

Figure I-14 : Standard Gumbel cumulative distribution function

7- Beta distribution:

The beta distribution is a very flexible and useful distribution, and can be used when a random variable is known to be bounded by two limits, a and b. Probability density function of a beta distribution is given by the following equation

$$f(\mathbf{y}) = \frac{1}{\mathrm{B}(\alpha,\beta)} \cdot \frac{(\mathbf{y}-\mathrm{a})^{\alpha-1}(\mathrm{b}-\mathbf{y})^{\beta-1}}{(\mathrm{b}-\mathrm{a})^{\alpha+\beta-1}} \qquad \mathrm{a} \le \mathbf{y} \le \mathrm{b} \tag{I.32}$$

where α and β are the parameters of the distribution and $\mathrm{B}(\alpha,\beta)$ is the beta function. The parameters of a beta distribution can be estimated from the mean and standard deviation of the available data using the following relationships

$$m = \mathrm{a} + \frac{\alpha}{\alpha+\beta}(\mathrm{b}-\mathrm{a}) \tag{I.33}$$

$$\sigma^2 = \frac{\alpha \cdot \beta}{(\alpha+\beta)^2 \cdot (\alpha+\beta+1)}(\mathrm{b}-\mathrm{a})^2 \tag{I.34}$$

The beta function can be calculated using gamma function as

$$\mathrm{B}(\alpha,\beta) = \frac{\Gamma(\alpha)\cdot\Gamma(\beta)}{\Gamma(\alpha+\beta)} \tag{I.35}$$

If the lower limit a is equal to zero and the upper limit b is equal to one, we get the standard beta distribution

$$f(\mathbf{y}) = \frac{1}{\mathrm{B}(\alpha,\beta)} \cdot (\mathbf{y})^{\alpha-1} \cdot (1-\mathbf{y})^{\beta-1} \qquad 0 \le \mathbf{y} \le 1 \tag{I.36}$$

The probability density function for different values of α and β are shown in Figure I-15. When α and β are both equal to one, the beta distribution becomes a uniform distribution.

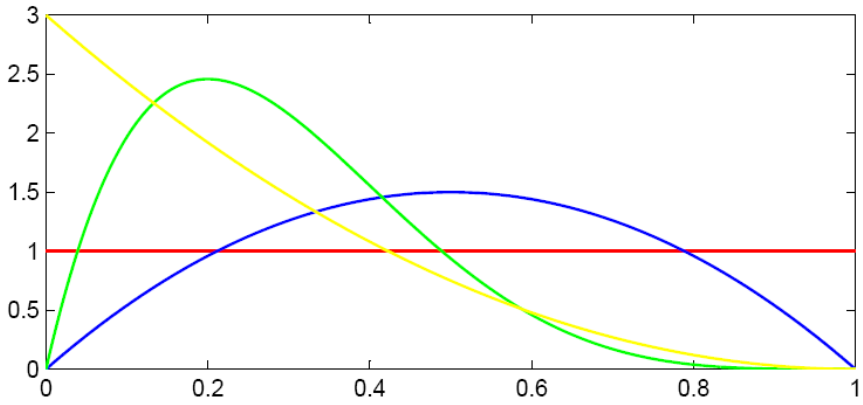

Figure I-15 : $\alpha = 1, \beta = 3$; $\alpha = 2, \beta = 5$; $\alpha = 2, \beta = 2$; $\alpha = 1, \beta = 1$

The cumulative distribution function of a standard beta distribution is

$$F(\mathbf{y}) = \frac{\mathrm{B}_{\mathrm{y}}(\alpha,\beta)}{\mathrm{B}(\alpha,\beta)} \tag{I.37}$$

where $\mathrm{B}_{\mathrm{y}}(\alpha,\beta)$ is the incomplete beta function. Cumulative distribution functions for different values of α and β are shown in Figure I-16.

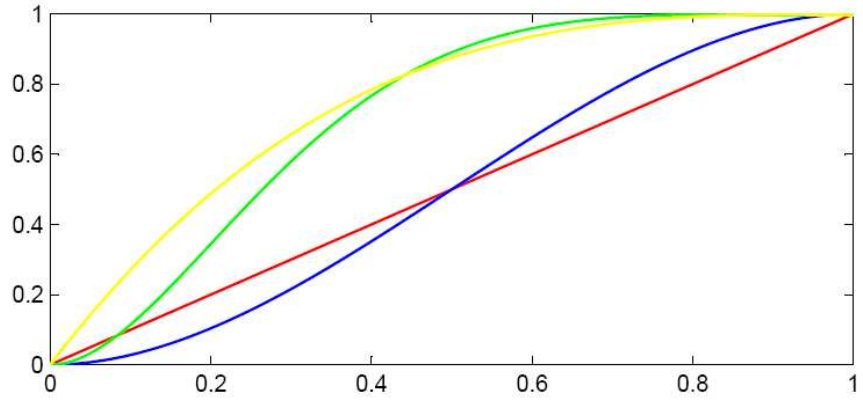

Figure I-16 : $\alpha = 1, \beta = 3$; $\alpha = 2, \beta = 5$; $\alpha = 2, \beta = 2$; $\alpha = 1, \beta = 1$

Appendix II: Chi-square and Kolmogorov-Smirnov tests

The Chi-Square test is based on the error between the observed and the measured PDF of the distribution. The assumed distribution will be acceptable at the significance level α if

$$\sum_{i=0}^{m} \frac{(n_i - e_i)^2}{e_i} < c_{1-\alpha,f} \tag{II.1}$$

where m is the number of intervals, $(n_1, n_2, \ldots n_m)$ are the observed frequencies of m interval of the random variables, $(e_1, e_2, \ldots e_m)$ are the corresponding theoretical frequencies of an assumed distribution, $f = m - 1 - k$ is the degree of freedom, k is the number of distribution parameters estimated from the data. Values of $c_{1-\alpha,f}$ for the Chi-Square test are given in Table II-1.

The Kolmogorov-Smirnoy (K-S) test is based on the error between the observed and assumed CDF of the distribution. The first step is to arrange the data in increasing order, and then the maximum difference between the two cumulative distribution functions of the ordered data can be estimated as

$$D_n = \max|F_Y(y_i) - S_n(y_i)| \tag{II.2}$$

where $F_Y(y_i)$ is the theoretical CDF of the assumed distribution at the *i*th observation of the ordered samples y_i and $S_n(y_i)$ is the corresponding stepwise CDF of the observed ordered samples. $S_n(y_i)$ can be estimated as

$$S_n(y_i) = \begin{cases} 0 & y < y_1 \\ \dfrac{m}{n} & y_m < y < y_{m+1} \\ 1 & y \geq y_m \end{cases} \tag{II.3}$$

If the maximum difference D_n is less than or equal to the value D_n^{α}, the assumed distribution is acceptable at the significance level α. Values of D_n^{α} at various significance levels α are giving in Table II-2.

A significance level of 5% implies that for 5 out of a total of 100 different samples, the assumed theoretical distribution cannot be an acceptable model. However, significance levels between 1% and 10% are common.

Table II-1 : CDF of the Chi-Square distribution with *f* degrees of freedom

$$P(C \le c_{\alpha,f}) = \int_0^{c_{\alpha,f}} \frac{1}{2^{f/2}\Gamma(f/2)} s^{(f/2)-1} e^{-s/2} ds$$

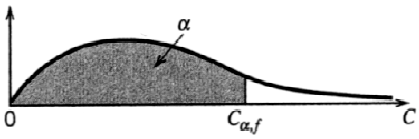

f \ α	0.001	0.005	0.010	0.025	0.050	0.100	0.900	0.950	0.975	0.990	0.995	0.999
1	1.57e–06	3.93e–05	1.57e–04	9.82e–04	3.93e–03	1.58e–02	2.706	3.841	5.024	6.635	7.879	10.83
2	2.00e–03	1.00e–02	0.0201	0.0506	0.1026	0.2107	4.605	5.991	7.378	9.210	10.60	13.82
3	2.43e–02	7.17e–02	0.1148	0.2158	0.3518	0.5844	6.251	7.815	9.348	11.34	12.84	16.27
4	9.08e–02	0.2070	0.2971	0.4844	0.7107	1.064	7.779	9.488	11.14	13.28	14.86	18.47
5	0.2102	0.4118	0.5543	0.8312	1.145	1.610	9.236	11.07	12.83	15.09	16.75	20.51
6	0.3810	0.6757	0.8721	1.237	1.635	2.204	10.64	12.59	14.45	16.81	18.55	22.46
7	0.5985	0.9893	1.239	1.690	2.167	2.833	12.02	14.07	16.01	18.48	20.28	24.32
8	0.8571	1.344	1.647	2.180	2.733	3.490	13.36	15.51	17.53	20.09	21.95	26.12
9	1.152	1.735	2.088	2.700	3.325	4.168	14.68	16.92	19.02	21.67	23.59	27.88
10	1.479	2.156	2.558	3.247	3.940	4.865	15.99	18.31	20.48	23.21	25.19	29.59
11	1.834	2.603	3.053	3.816	4.575	5.578	17.28	19.68	21.92	24.73	26.76	31.26
12	2.214	3.074	3.571	4.404	5.226	6.304	18.55	21.03	23.34	26.22	28.30	32.91
13	2.617	3.565	4.107	5.009	5.892	7.041	19.81	22.36	24.74	27.69	29.82	34.53
14	3.041	4.075	4.660	5.629	6.571	7.790	21.06	23.68	26.12	29.14	31.32	36.12
15	3.483	4.601	5.229	6.262	7.261	8.547	22.31	25.00	27.49	30.58	32.80	37.70
16	3.942	5.142	5.812	6.908	7.962	9.312	23.54	26.30	28.85	32.00	34.27	39.25
17	4.416	5.697	6.408	7.564	8.672	10.09	24.77	27.59	30.19	33.41	35.72	40.79
18	4.905	6.265	7.015	8.231	9.390	10.86	25.99	28.87	31.53	34.81	37.16	42.31
19	5.407	6.844	7.633	8.907	10.12	11.65	27.20	30.14	32.85	36.19	38.58	43.82
20	5.921	7.434	8.260	9.591	10.85	12.44	28.41	31.41	34.17	37.57	40.00	45.31
21	6.447	8.034	8.897	10.28	11.59	13.24	29.62	32.67	35.48	38.93	41.40	46.80
22	6.983	8.643	9.542	10.98	12.34	14.04	30.81	33.92	36.78	40.29	42.80	48.27
23	7.529	9.260	10.20	11.69	13.09	14.85	32.01	35.17	38.08	41.64	44.18	49.73
24	8.085	9.886	10.86	12.40	13.85	15.66	33.20	36.42	39.36	42.98	45.56	51.18
25	8.649	10.52	11.52	13.12	14.61	16.47	34.38	37.65	40.65	44.31	46.93	52.62
26	9.222	11.16	12.20	13.84	15.38	17.29	35.56	38.89	41.92	45.64	48.29	54.05
27	9.803	11.81	12.88	14.57	16.15	18.11	36.74	40.11	43.19	46.96	49.65	55.48
28	10.39	12.46	13.56	15.31	16.93	18.94	37.92	41.34	44.46	48.28	50.99	56.89
29	10.99	13.12	14.26	16.05	17.71	19.77	39.09	42.56	45.72	49.59	52.34	58.30
30	11.59	13.79	14.95	16.79	18.49	20.60	40.26	43.77	46.98	50.89	53.67	59.70
40	17.92	20.71	22.16	24.43	26.51	29.05	51.81	55.76	59.34	63.69	66.77	73.40
45	21.25	24.31	25.90	28.37	30.61	33.35	57.51	61.66	65.41	69.96	73.17	80.08
50	24.67	27.99	29.71	32.36	34.76	37.69	63.17	67.50	71.42	76.15	79.49	86.66
55	28.17	31.73	33.57	36.40	38.96	42.06	68.80	73.31	77.38	82.29	85.75	93.17
60	31.74	35.53	37.48	40.48	43.19	46.46	74.40	79.08	83.30	88.38	91.95	99.61
70	39.04	43.28	45.44	48.76	51.74	55.33	85.53	90.53	95.02	100.43	104.21	112.32
80	46.52	51.17	53.54	57.15	60.39	64.28	96.58	101.88	106.63	112.33	116.32	124.84
90	54.16	59.20	61.75	65.65	69.13	73.29	107.57	113.15	118.14	124.12	128.30	137.21
100	61.92	67.33	70.06	74.22	77.93	82.36	118.50	124.34	129.56	135.81	140.17	149.45

Table II -2 : Values of D_n^{α} for the Kolmogorov-Smirnov test

n	$D_n^{0.2}$	$D_n^{0.15}$	$D_n^{0.1}$	$D_n^{0.05}$	$\boldsymbol{D_n^{0.01}}$
5	0.446	0.474	0.510	0.563	0.669
6	0.410	0.436	0.470	0.521	0.618
7	0.381	0.405	0.438	0.486	0.577
8	0.358	0.381	0.411	0.457	0.543
9	0.339	0.360	0.388	0.432	0.514
10	0.322	0.342	0.368	0.409	0.486
11	0.307	0.326	0.352	0.391	0.468
12	0.295	0.313	0.338	0.375	0.450
13	0.284	0.302	0.325	0.361	0.433
14	0.274	0.292	0.314	0.349	0.418
15	0.266	0.283	0.304	0.338	0.404
20	0.231	0.246	0.264	0.294	0.352
25	0.210	0.220	0.240	0.264	0.320
30	0.190	0.200	0.220	0.242	0.290
35	0.180	0.190	0.210	0.230	0.270
40	0.170	0.180	0.190	0.210	0.250
45	0.160	0.170	0.180	0.200	0.240
50	0.150	0.160	0.170	0.190	0.230
>50	$\frac{1.07}{\sqrt{n}}$	$\frac{1.14}{\sqrt{n}}$	$\frac{1.22}{\sqrt{n}}$	$\frac{1.36}{\sqrt{n}}$	$\frac{1.63}{\sqrt{n}}$

Appendix III: Tillage forces-tillage system parameters relationships

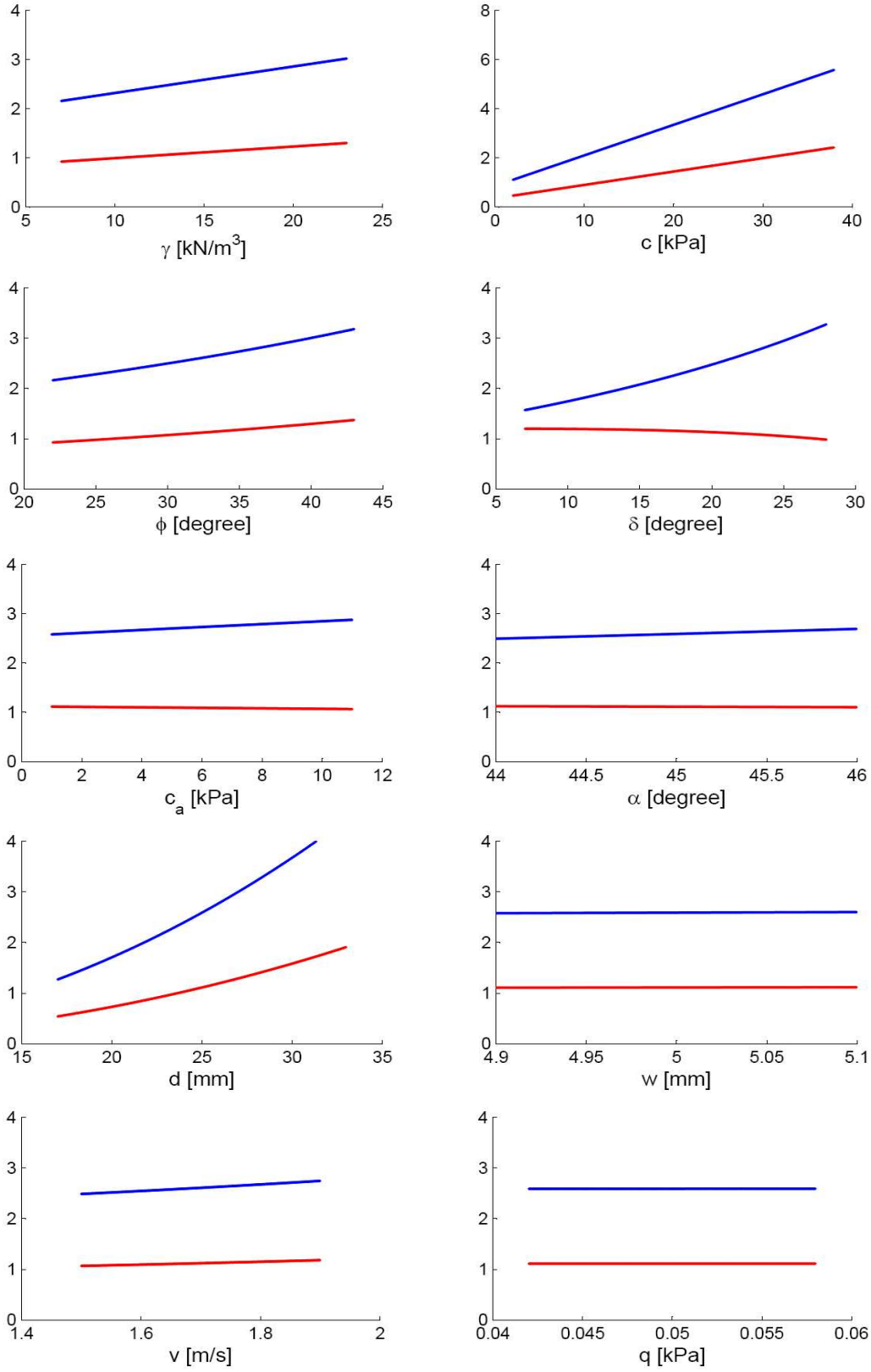

– Horizontal force [kN] – Vertical force [kN]

Tillage forces-tillage system parameters relationships

Appendix IV: Correlation analysis of soil engineering properties

The correlation coefficient between two random variables $\mathbf{Y}_1$ and $\mathbf{Y}_2$, denoted as Corr $(\mathbf{Y}_1, \mathbf{Y}_2)$ or $\rho(\mathbf{Y}_1, \mathbf{Y}_2)$, can be calculated as

$$\text{Corr}(\mathbf{Y}_1, \mathbf{Y}_2) = \rho(\mathbf{Y}_1, \mathbf{Y}_2) = \frac{\text{Cov}(\mathbf{Y}_1, \mathbf{Y}_2)}{\sqrt{\text{Var}(\mathbf{Y}_1) \times \text{Var}(\mathbf{Y}_2)}} \tag{IV.1}$$

where Cov $(\mathbf{Y}_1, \mathbf{Y}_2)$ is the covariance of two random variables which can be calculated as

$$\text{Cov}(\mathbf{Y}_1, \mathbf{Y}_2) = \text{E}[\mathbf{Y}_1, \mathbf{Y}_2] - \text{E}[\mathbf{Y}_1] \times \text{E}[\mathbf{Y}_2] \tag{IV.2}$$

$\text{E}[\mathbf{Y}_1, \mathbf{Y}_2]$ can be calculated as

$$\text{E}[\mathbf{Y}_1, \mathbf{Y}_2] = \int_{-\infty}^{+\infty} \int_{-\infty}^{+\infty} y_1 \, y_2 f_{\mathbf{Y}_1, \mathbf{Y}_2}(y_1, y_2) dy_1 dy_2 \tag{IV.3}$$

If the two random variables are statistically independent, then $\text{E}[\mathbf{Y}_1, \mathbf{Y}_2] = \text{E}[\mathbf{Y}_1] \times \text{E}[\mathbf{Y}_2]$ and the correlation coefficient $\rho(\mathbf{Y}_1, \mathbf{Y}_2)$.

The physical significance of the covariance can be inferred from Equation (IV.1). If the Corr $(\mathbf{Y}_1, \mathbf{Y}_2)$ is large and positive, the values of $\mathbf{Y}_1$and $\mathbf{Y}_2$ tend to be both large or small relative to their respective means, whereas if the Corr $(\mathbf{Y}_1, \mathbf{Y}_2)$ is large and negative, the values of $\mathbf{Y}_1$ tend to be large when the values of $\mathbf{Y}_2$ are small, and vice versa, relative to their respective means, and if the Corr $(\mathbf{Y}_1, \mathbf{Y}_2)$ is small or zero, there is little or no linear relationship between the values of $\mathbf{Y}_1$and $\mathbf{Y}_2$ (or if a strong relationship exists, it is nonlinear). The values of $\rho(\mathbf{Y}_1, \mathbf{Y}_2)$ range between -1 and +1. The correlation coefficient represents the degree of linear independence between two random variables.

For n correlated variables $\mathbf{Y}_i (i = 1,2, \dots, n)$ with mean m_i and standard deviation σ_i, the covariance matrix can be presented as

$$[\text{C}] = \begin{bmatrix} \sigma_1^2 & \text{Cov}(\mathbf{Y}_1, \mathbf{Y}_2) & \cdots & \text{Cov}(\mathbf{Y}_1, \mathbf{Y}_2) \\ \text{Cov}(\mathbf{Y}_1, \mathbf{Y}_2) & \sigma_2^2 & \dots & \text{Cov}(\mathbf{Y}_1, \mathbf{Y}_2) \\ \vdots & \vdots & \ddots & \vdots \\ \text{Cov}(\mathbf{Y}_1, \mathbf{Y}_2) & \text{Cov}(\mathbf{Y}_1, \mathbf{Y}_2) & \cdots & \sigma_n^2 \end{bmatrix} \tag{IV.4}$$

And the correlation matrix $[\acute{\text{C}}]$ can be expressed as

$$[\acute{C}] = \begin{bmatrix} 1 & \rho(\mathbf{Y}_1, \mathbf{Y}_2) & \cdots & \rho(\mathbf{Y}_1, \mathbf{Y}_2) \\ \rho(\mathbf{Y}_1, \mathbf{Y}_2) & 1 & \ldots & \rho(\mathbf{Y}_1, \mathbf{Y}_2) \\ \vdots & \vdots & \ddots & \vdots \\ \rho(\mathbf{Y}_1, \mathbf{Y}_2) & \rho(\mathbf{Y}_1, \mathbf{Y}_2) & \cdots & 1 \end{bmatrix} \quad \text{(IV.5)}$$

If the correlation coefficient needs to be calculated from the observed sample values, it is rare to obtain values of precisely zero, +1, or -1. In general, two random variables can be considered to be statistically independent if the correlation coefficient is less ± 0.3 and they can be considered to be perfectly correlated if the correlation coefficient is greater than ± 0.9 [30].

The correlation matrix of the 57 soil engineering property samples, used in this work, takes the following values.

$$\begin{bmatrix} \rho(\gamma,\gamma) & \rho(\gamma,\phi) & \rho(\gamma,\delta) & \rho(\gamma,c) & \rho(\gamma,c_a) \\ \rho(\phi,\gamma) & \rho(\phi,\phi) & \rho(\phi,\delta) & \rho(\phi,c) & \rho(\phi,c_a) \\ \rho(\delta,\gamma) & \rho(\delta,\phi) & \rho(\delta,\delta) & \rho(\delta,c) & \rho(\delta,c_a) \\ \rho(c,\gamma) & \rho(c,\phi) & \rho(c,\delta) & \rho(c,c) & \rho(c,c_a) \\ \rho(c_a,\gamma) & \rho(c_a,\phi) & \rho(c_a,\delta) & \rho(c_a,c) & \rho(c_a,c_a) \end{bmatrix} = \begin{bmatrix} 0.98 & -0.13 & -0.20 & 0.29 & -0.45 \\ -0.13 & 0.98 & 0.34 & -0.19 & -0.04 \\ -0.20 & 0.34 & 0.98 & -0.03 & 0.21 \\ 0.29 & -0.19 & -0.03 & 0.98 & 0.21 \\ -0.45 & -0.04 & 0.21 & 0.21 & 0.98 \end{bmatrix} \quad \text{(IV.5)}$$

These results do not compatible with the observations of Srivastava et al. [1], Sharifat [84] and Ayers [85]. For example, Srivastava et al. [1] found that, the value of internal friction angle increases by increasing the soil density. It means that the correlation coefficient should be positive, whereas in the correlation matrix, Equation (IV.5), $\rho(\gamma, \phi) = -0.13$.

The inaccuracy of these results may be caused by the insufficient of data points. No work in literature recommends the minimum number of data points to get an accurate estimation of the correlation coefficient between random variables. Therefore, the following example is considered to demonstrate the relationship between the correlation coefficient and the number of data points.

Let $\mathbf{Y}_1$and $\mathbf{Y}_2$ to be two independent random variables. $\mathbf{Y}_1$ is a normal variable with $m = 6$ and $\sigma = 2$ and $\mathbf{Y}_2$ is a lognormal variable with $\lambda = 2.5$ and $\xi = 0.5$. And let$\mathbf{Z}_1$, $\mathbf{Z}_2$ and $\mathbf{Z}_3$ to be three correlated random variables. The relationships between the independent variables$\mathbf{Y}_1$, $\mathbf{Y}_2$ and correlated variables $\mathbf{Z}_1$, $\mathbf{Z}_2$, $\mathbf{Z}_3$ are:

$$\begin{aligned} \mathbf{Z}_1 &= \mathbf{Y}_1^2 - 2 \times \mathbf{Y}_2^2 + 2 \times \mathbf{Y}_1 \times \mathbf{Y}_2 \\ \mathbf{Z}_2 &= 6 \times \mathbf{Y}_1^2 + 2 \times \mathbf{Y}_1 \times \mathbf{Y}_2 + 3 \times \mathbf{Y}_2 \\ \mathbf{Z}_3 &= 2 \times \mathbf{Y}_2^2 + \mathbf{Y}_1 \times \mathbf{Y}_2 + 6 \times \mathbf{Y}_1 \end{aligned} \quad \text{(IV.2)}$$

Correlation coefficient values for different values of data point numbers are given in Table IV.1 and presented in Figure IV.1. It is observed that the correlation coefficients converge for 50.000 data point numbers.

n	$\rho(Z_1, Z_2)$	$\rho(Z_1, Z_3)$	$\rho(Z_2, Z_3)$
10	-0.550	-0.881	0.678
25	-0.057	-0.889	0.409
50	-0.308	-0.902	0.645
75	-0.464	-0.967	0.623
100	-0.312	-0.965	0.507
125	-0.402	-0.964	0.599
150	-0.044	-0.962	0.486
200	-0.128	-0.967	0.346
300	-0.314	-0.965	0.535
400	-0.143	-0.953	0.418
500	-0.315	-0.966	0.537
1000	-0.364	-0.982	0.519
2000	-0.335	-0.976	0.524
3000	-0.277	-0.973	0.483
4000	-0.325	-0.978	0.504
5000	-0.284	-0.976	0.478
10000	-0.315	-0.974	0.513
20000	-0.309	-0.972	0.515
30000	-0.296	-0.973	0.500
40000	-0.296	-0.975	0.491
50000	-0.295	-0.974	0.496

Table IV.1 : Correlation coefficient-number of data points relationship

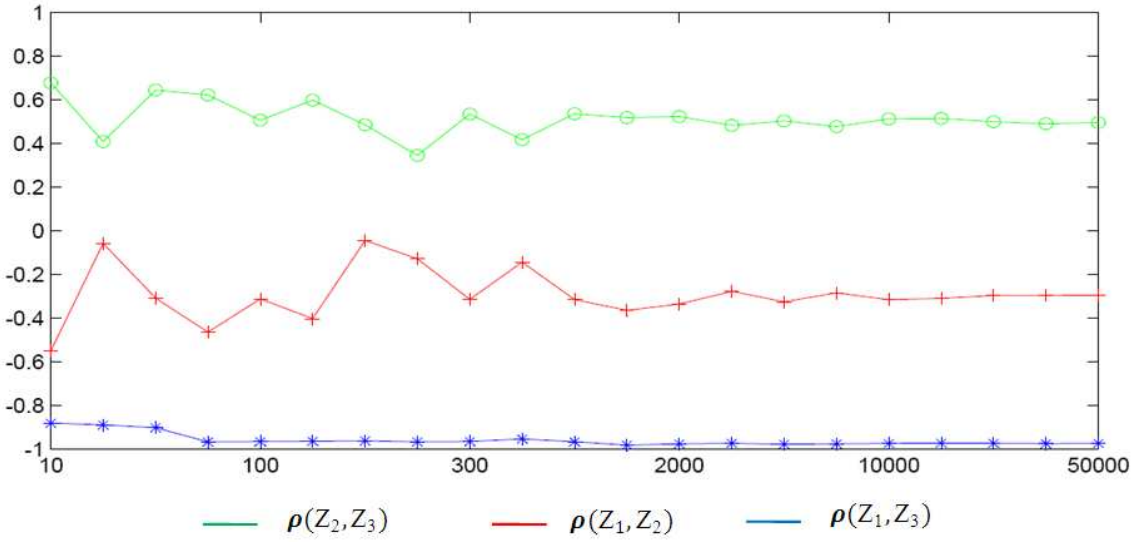

Figure IV.1 : Correlation coefficient-number of data points relationship

Appendix V: Samples of soil engineering properties

The following table presents the samples of soil engineering properties (soil density γ, soil cohesion c, angle of internal friction ϕ, angle of soil-tool friction δ, soil-tool adhesion c_a), collected from the literature, used in this work.

N°	$\gamma\ (kN/m^3)$	$c\ (kPa)$	ϕ (°)	δ (°)	$c_a\ (kPa)$	Source
1	14.70	4.60	37.5	22.0	0.00	[7]
2	10.80	0.00	34.0	22.0	0.00	[7]
3	14.61	8.90	23.3	18.8	0.00	[9]
4	15.01	2.26	35.0	23.0	0.00	[14]
5	15.70	3.63	35.0	23.0	0.00	[14]
6	14.70	4.60	35.0	23.0	0.00	[14]
7	15.30	10.5	30.8	24.0	0.00	[17]
8	19.00	31.7	42.0	24.0	0.00	[17]
9	16.38	6.00	32.0	24.0	0.00	[19]
10	14.02	23.0	22.0	22.0	8.00	[19]
11	18.05	20.4	34.0	25.0	0.00	[20]
12	16.98	15.5	31.8	23.0	0.00	[20]
13	15.79	15.3	30.3	22.0	0.00	[20]
14	16.98	15.5	31.8	23.0	0.00	[21]
15	14.34	7.19	34.5	23.5	3.29	[24]
16	11.50	33.5	37.3	27.3	9.40	[24]
17	11.00	35.3	29.8	25.2	8.10	[24]
18	14.50	6.30	36.0	23.3	2.20	[24]
19	13.20	11.9	33.1	22.1	2.70	[24]
20	14.70	2.00	30.0	15.2	7.66	[26]
21	14.12	6.00	35.0	20.0	0.00	[86]
22	16.38	6.00	32.0	24.0	0.00	[86]
23	13.73	9.00	35.0	29.0	0.00	[86]
24	14.02	23.0	22.0	22.0	8.00	[86]
25	13.23	9.23	29.0	22.0	0.00	[87]
26	14.71	12.1	30.2	22.3	0.18	[88]
27	14.91	13.3	29.6	23.6	0.21	[88]
28	15.30	24.5	36.5	24.7	0.29	[88]
29	15.01	22.6	34.5	23.1	0.35	[88]

30	14.62	20.5	32.2	24.0	0.31	[88]
31	13.05	6.70	39.3	23.8	0.60	[89]
32	14.22	11.7	36.8	24.0	8.30	[89]
33	12.50	5.00	35.0	24.5	3.25	[90]
34	12.80	10.2	38.0	22.0	5.27	[90]
35	13.50	11.0	32.5	24.8	3.22	[90]
36	12.50	5.00	35.0	24.5	3.21	[90]
37	12.75	8.60	32.6	22.4	0.00	[91]
38	12.75	7.00	31.4	13.1	0.00	[91]
39	12.75	9.30	29.2	14.4	0.00	[91]
40	14.72	22.7	29.3	16.0	0.00	[91]
41	14.72	17.0	30.6	18.9	0.00	[91]
42	14.72	16.0	30.9	15.6	0.00	[91]
43	14.72	11.7	30.8	25.0	0.00	[91]
44	14.72	8.10	31.4	19.8	0.00	[91]
45	14.72	9.20	30.8	18.3	0.00	[91]
46	16.19	19.5	37.6	11.9	0.00	[91]
47	16.19	30.7	26.6	13.3	0.00	[91]
48	16.19	20.3	30.8	24.0	0.00	[91]
49	16.19	18.6	27.4	24.1	0.00	[91]
50	16.19	13.2	28.4	21.6	0.00	[91]
51	16.19	13.9	29.1	20.9	0.00	[91]
52	17.66	16.7	33.5	23.0	0.00	[91]
53	17.66	22.0	29.2	15.9	0.00	[91]
54	17.66	12.8	29.8	17.2	0.00	[91]
55	17.66	11.6	30.9	18.8	0.00	[91]
56	19.62	29.9	28.8	19.9	0.00	[91]
57	19.62	21.3	27.1	14.8	0.00	[91]

Appendix VI: Results of goodness-of-fit tests

1- Soil density:

The mean and variance values for the samples of soil density are $E(\gamma) = 15.01[kN/m^3]$ and $Var(\gamma) = 3.84[(kN/m^3)^2$. The histogram of soil density is presented in Figure VI.1.

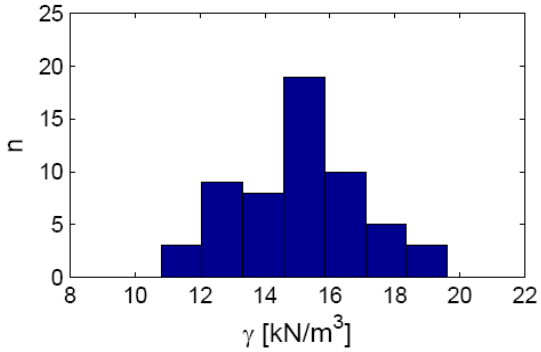

Figure VI.1 : Histogram of soil density

According to the shape of the histogram of soil density, two hypothesized distributions are selected, namely the normal distribution with $(m = 15.01, \sigma = 1.96)$ and the lognormal distribution with $(\xi = 0.13, \mu = 2.7)$. The results of Chi-Square and K-S testes are given in Table VI.1.

Goodness-of-fit test	Normal distribution	Lognormal distribution
Chi-Square	3.976	4.183
K-S	0.120	0.094

Table VI.1 : Results of goodness-of-fit tests for soil density samples

For the significance level of $\alpha = 5\%$, the corresponding $c_{0.95,5}$ and $D_{57}^{0.05}$ (from Appendix II) are found to be 9.488 and 0.180, respectively, which are greater than the results of Chi-Square and K-S testes. Thus, both the normal and lognormal distributions are acceptable with a 5% significance level. However, it can be seen that the lognormal distribution is slightly better than the normal distribution. Therefore, the probability density function of the soil density can be expressed in Equation VI.1 and shown in Figure VI.2.

$$f(\gamma) = \frac{1}{0.33 \times \gamma} \exp\left[-\frac{1}{2}\left(\frac{\ln(\gamma) - 2.7}{0.13}\right)^2\right] \qquad 0 < \gamma < +\infty \tag{VI.1}$$

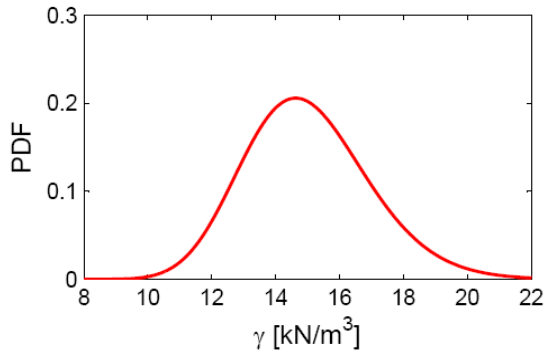

Figure VI.2 : Probability density function of soil density

2- Soil cohesion:

The values of mean and variance for these data are $E(c) = 13.93[kP]$ and $Var(c) = 71.23[(kP)^2]$. According to the shape of the soil cohesion histogram, presented in Figure VI.3. It can be found that both the lognormal distribution with $(\xi = 0.56, \mu = 2.48)$ and the Weibull distribution with $(k = 15.51, \lambda = 1.66)$ can be model these data. Table VI.2 gives the results of the Chi-Square and K-S tests for these two hypothesized distributions.

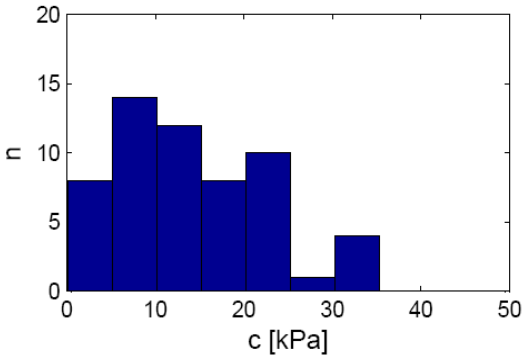

Figure VI.3 : Histogram of soil cohesion

Goodness-of-fit test	Lognormal distribution	Weibull distribution
Chi-Square	14.997	5.135
K-S	0.083	0.041

Table VI.2 : Results of goodness-of-fit tests for soil internal cohesion samples

The results of the Chi-Square test show that two distributions are acceptable with a 5% significance level. Conversely, the K-S test shows that only the Weibull distribution is acceptable for the same significance level. As a result, the Weibull distribution is selected

to model these data. Figure VI.4 shows the probability density function for the soil cohesion, which have the following formula:

$$f(\mathrm{c}) = 0.107\left(\frac{\mathrm{c}}{15.51}\right)^{0.66} \times \exp\left[-\left(\frac{\mathrm{c}}{15.51}\right)^{1.66}\right] \qquad \mathrm{c} \geq 0 \tag{VI.2}$$

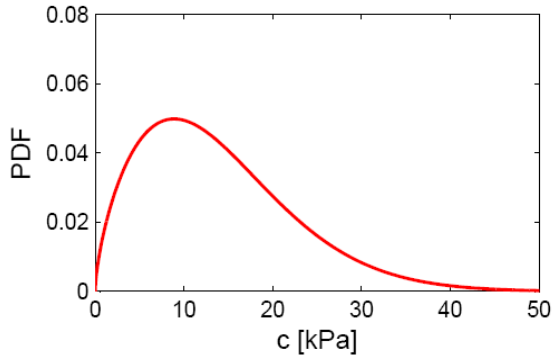

Figure VI.4 : Probability density function of soil cohesion

3- Internal friction angle:

These samples have the following mean and variance values $E(\emptyset) = 32[°]$ and $Var(\emptyset) = 715.64[(°)^2]$. The histogram of internal friction angle is presented in Figure VI.5 and two hypothesized distributions are selected for modeling the variability of internal friction angle, namely the normal distribution with $(m = 32, \sigma = 3.96)$ and the lognormal distribution with $(\xi = 0.12, \mu = 3.46)$. Table VI.3 presents the results of the Chi-Square and K-S testes.

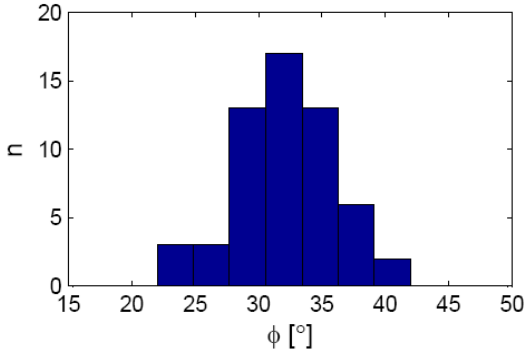

Figure VI.5 : Histogram of internal friction angle

From the above results, it can be seen that the normal distribution is better than the lognormal distribution. Thus it is used to model the variability in the internal friction angle, and its probability density function can be expressed in Equation VI.3 and illustrated in Figure VI.6.

Goodness-of-fit test	Normal distribution	Lognormal distribution
Chi-Square	1.9996	4.4015
K-S	0.0692	0.0733

Table VI.3 : Results of goodness-of-fit tests for internal friction angle samples

$$f(\emptyset) = \frac{1}{9.93}\exp\left[-\frac{1}{2}\left(\frac{\emptyset - 32}{3.96}\right)^2\right] \qquad -\infty < \emptyset < +\infty \tag{VI.3}$$

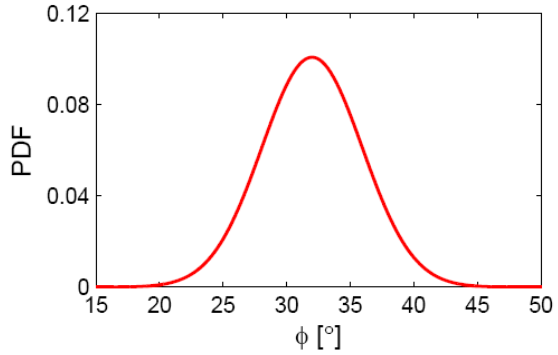

Figure VI.6 : Probability density function of internal friction angle

4- Soil-tool friction angle:

The mean and variance values for the samples of soil-tool friction angle are $E(\delta) = 21.32[°]$ and $Var(\delta) = 17.25[(°)^2]$. Its histogram is plotted in Figure VI.7.

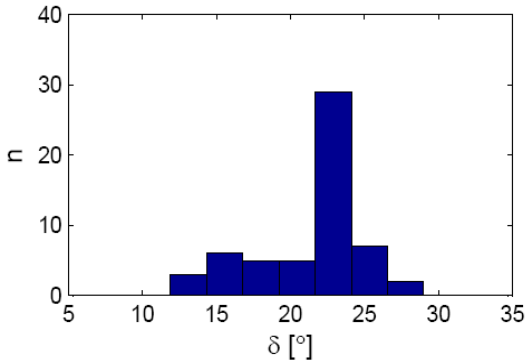

Figure VI.7 : Histogram of external friction angle

The probability distributions which can be used to model these samples are:

- Normal distribution with $m = 21.32$ and $\sigma = 3.71$.
- Lognormal distribution with $\mu = 3.04$ and $\xi = 0.19$.
- Weibull distribution with $k = 5.96$ and $\lambda = 22.99$.

- Weibull distribution with $\varepsilon = -64.08$, $k = 87.14$ and $\lambda = 31.52$.

From the results in Table VI.4, it can be noted that only the Weibull distribution with two and three parameters guarantees a 5% significance level for the K-S test. No probability distribution can be guaranteed this significance level for the Chi-Square tests. However, the Weibull distribution with three parameters is better than the others distributions. Therefore, it can be used to model the variability in the external friction angle.

Goodness-of-fit test	Normal distribution	Lognormal distribution	Weibull distribution (2P)	Weibull distribution (3P)
Chi-Square	32.117	45.141	23.187	19.759
K-S	0.208	0.236	0.171	0.150

Table VI.4 : Results of goodness-of-fit tests for external friction angle samples

The Weibull distribution with three parameters has the following probability density function. This equation is plotted in Figure VI.8.

$$f(\delta) = 0.36\left(\frac{\delta + 64.07}{87.14}\right)^{30.52} \times \exp\left[-\left(\frac{\delta + 64.07}{87.14}\right)^{31.52}\right] \quad \delta \geq 0 \qquad \text{(VI.4)}$$

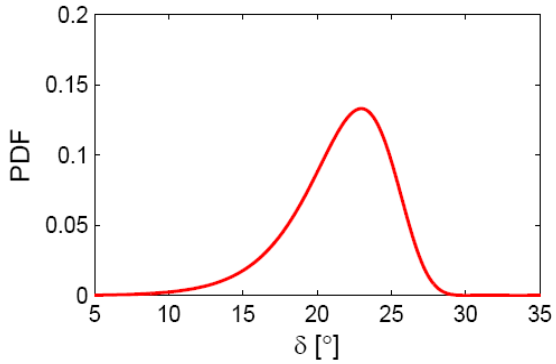

Figure VI.8 : Probability density function of external friction angle

5- Soil-tool adhesion:

The mean and variance values for the samples of soil-tool adhesion are $E(c_a) = 1.31[kP]$ and $Var(c_a) = 7.03[(kP)^2]$. The histogram of soil-tool adhesion is plotted in Figure VI.9.

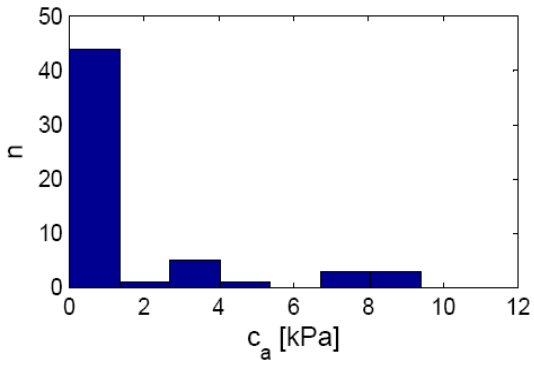

Figure VI.9 : Histogram of soil-tool adhesion

It is noted that three probability distributions can be consistent with the 57 samples of soil-tool adhesion: the lognormal distribution with $\mu = -2.83$ and $\xi = 2.65$, the Weibull distribution with $k = 0.24$ and $\lambda = 0.35$ and the exponential distribution with $\eta = 0.76$. The results of the goodness-of-fit tests for these three probability distributions are presented in Table VI.5. Only the exponential distribution respects a 5% significance level for the Chi-Square test. Therefore, it is applied to model these data.

Goodness-of-fit test	Lognormal distribution	Weibull distribution	Exponential distribution
Chi-Square	0.667	0.667	0.999
K-S	41.254	25.249	5.677

Table VI.5 : Results of goodness-of-fit tests soil-tool adhesion samples

The probability density function of the exponential distribution, presented in Figure VI.10, is written as the flowing form:

(VI.5)

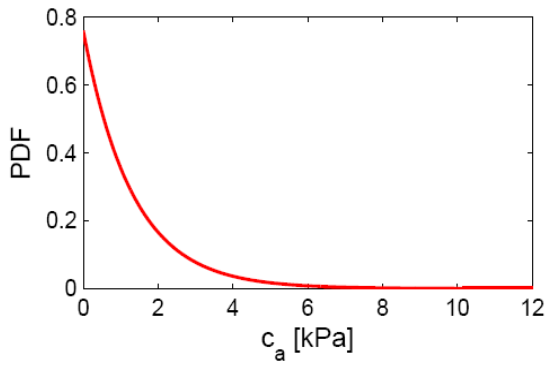

Figure VI.10 : Probability density function of soil-tool adhesion